SLAC-PUB-2876
SCIPP-82-9
January 1982
(T/E)

HEAVY FLAVOR PRODUCTION FROM PHOTONS AND HADRONS*

Clemens A. Heusch

Santa Cruz Institute for Particle Physics
University of California
Santa Cruz, California 95064

and

Stanford Linear Accelerator Center
Stanford University, Stanford, California 94305

Lectures Presented at the
Summer Institute on Particle Physics
Stanford Linear Accelerator Center
July 27 to August 7, 1981

* Work supported in part by the Department of Energy, contracts DE-AM03-76SF00034 (SCIPP) and DE-AC03-76SF00515 (SLAC).

1. Introduction

In these lectures, I will cover the present state of the production and observation of hadrons containing heavy quarks or antiquarks as valence constituents, in reactions initiated by real and (space-like) virtual photon or by hadron beams. I will not discuss "heavy flavor" production in e^+e^- annihilation, which is well covered in a number of recent review papers[1]; similarly, neutrino production will be omitted due to the different (flavor-changing) mechanisms that are involved in those reactions.[2]

What flavors denote heavy quarks? Is strangeness a heavy flavor? Certainly, its massiveness is attested to by the rest masses of K, η, ϕ mesons vs. those of π, ρ, ω; moreover, it is unstable under the weak interaction. The Zweig-rule breaking diagrams involved in the decay of the $s\bar{s}$ component of the η and in ϕ decay foreshadow features that were explained only by mechanisms studied in connection with $c\bar{c}$ decays. We could further argue that any quark that is not a valence constituent of a target nucleon be considered on an equal footing, thus throwing the s quark in a bag with c, b, ... Still, remember that $m(K) < m(\rho)$; that diffractive reaction indications favor similar "sizes" for ρ, ω, and ϕ.

In contrast, the masses of charmed and bottom quarks are considerably higher,

$$m_c > m_p$$

$$m_b >> m_p;$$

the $(c\bar{c})$ and $(b\bar{b})$ bound states permitted the development of highly plausible non-relativistic potential models that successfully describe their spectroscopy. Let us therefore take a semantic lead from lepton physics where a "heavy fermion" has

$$m_f > m_p \qquad (f = \tau, \ldots)$$

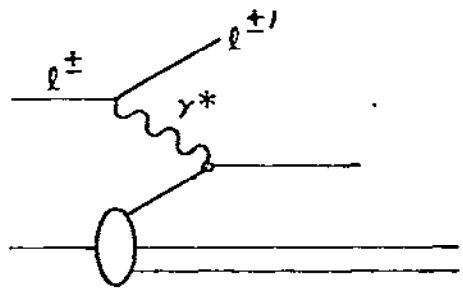

Figure 1. Basic diagram for virtual photoproduction. The $Q^2 < o$ photon acts as a local probe.

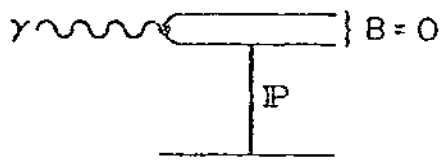

Figure 2. Basic ideas for heavy flavor production by real photons: a) diffraction dissociation of the photon.

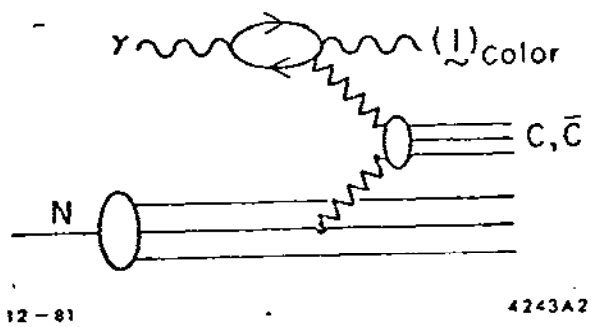

Figure 2. b) representative QCD diagram (GGF).

and an associated lifetime $\tau_f < 10^{-10}$ sec. More to the point, maybe, this permits us to define as heavy quarks those that have masses that clearly meet the condition $m(Q) >> \Lambda$, when Λ is the QCD scale parameter. We will then denote heavy quarks and antiquarks as $Q,\bar{Q}$, so that q=u,d,s; Q=c,b,.... While the available experimental evidence limits us to charm and, to a much lesser extent, bottom production, we expect that any insight gained from it will be inherently applicable to heavier quark systems, notably to those that may contain the postulated sixth ("top") quark.

What can we hope to extract from available data? Heavy quarks are not a-priori valence constituents of stable matter available as reaction targets or beams. Starting with the simplest case, Fig. 1 shows the classic diagram for electroproduction: the space-like photon acts as a structureless, local probe for the nucleon content. We know the success of the formalism involving parton distribution and fragmentation functions from light-flavor hadron production experiments. Will we discover a sea of charmed partons at low fractional momenta? Are there other heavy component parts of the nucleon wave function that a local probe will uncover? Section 2 will investigate this question.

Next, we admit a probe with some structure of its own: Fig. 2 shows two ways in which a real photon produces heavy flavors when interacting with a nucleon: we expect soft interactions to lead to diffractive dissociation of the photon's hadronic component, telling us about the symmetry structure of the photon (2a); hard interactions allow gluons to interact with the nucleon field, with all attendant QCD implications (2b). Section 3 will examine to what extent vector meson dominance ideas can accommodate the observed phenomena.

Finally, heavy flavor production in hadron-hadron collisions brings all appropriate degrees of freedom into the picture. From the

simple-minded Drell-Yan graph (Fig. 3a) to gluo-excitation of an existing $Q\bar{Q}$ component (3b) to gluon-gluon fusion (3c), quark and gluon distributions inside the hadrons are needed to parameterize the process. Section 4 will show to what extent the data obtained both in fixed target experiments and in storage rings amplify the information gleaned from simpler systems (Sections 2,3).

In each case, the basic question can be formulated naively: does the current find or create quarks? Is the established theoretical framework--parton field theory, vector-dominance, QCD--capable of describing the data in a quantitative, or at least qualitatively acceptable, way?

Our experimental review will principally comprise the production of hadronic systems containing c and b quarks. What are, then, the observables?

Charm: $c\bar{c}$ States, "charmonia", gave the first indications of Q production and still provide valuable insights into decay mechanisms as well as quark potentials. Their spectroscopy is well-defined, with the ψ, χ, and η, states described in reference 3.

$c\bar{q}$, $\bar{c}q$ states: there is a 16-plet of 0^- states, another for 1^-, etc., as expected from SU(4) decomposition. Each of these contains six open-charm states with $C = \pm 1$, as shown in Fig. 4a. Of the pseudoscalars, all but--possibly--the F^+ ($\bar{F}^-$) states have been observed, mostly in e^+e^- annihilations. Of the vector states, there is good evidence for D* production. No higher meson states with overt charm have been seen.

cqq states: Fig. 4b shows that we expect a sextet and a triplet with $J^P = \frac{1+}{2}$, $C = +1$, and a triplet with $C = 2$. Evidence for baryon production is presently limited to the $C = 1$, $J^P = \frac{1+}{2}$ state usually called

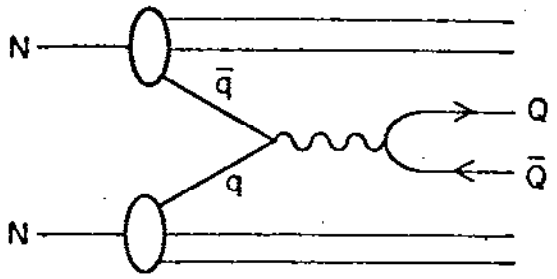

Figure 3. Basic ideas for heavy flavor production in NN Collisions: a) quark fusion

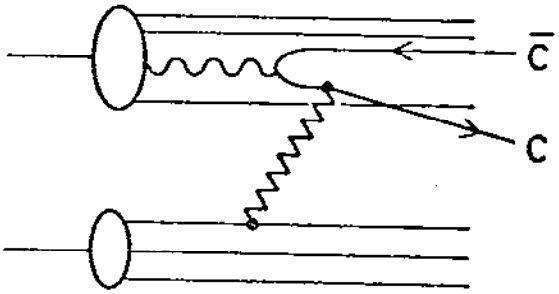

4243A3

Figure 3. b) flavor excitation

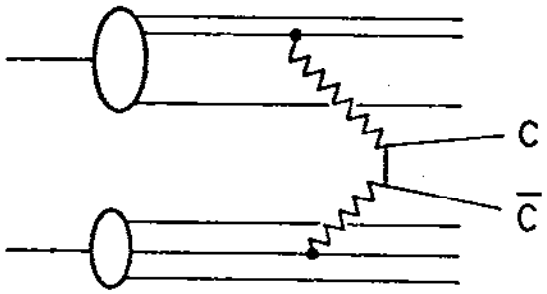

12-81

Figure 3. c) gluon-gluon fusion (GGF).

Table 1-1 $1/2^+$ baryon states with charm quarks.

Name	Quark content	SU(3)	I, I_3	Strangeness	Charm
C_1^{++} or Σ_c^{++}	cuu	6	1, 1	0	1
C_1^{+} or Σ_c^{+}	$c(ud)_{sym}$	6	1, 0	0	1
C_1^{o} or Σ_c^{o}	cdd	6	1,-1	0	1
Ξ^+	$c(us)_{sym}$	6	1/2, 1/2	-1	1
Ξ^o	$c(ds)_{sym}$	6	1/2,-1/2	-1	1
Υ^o	css	6	0, 0	-2	1
C_o^+ or Λ_c^+	$c(ud)_{anti}$	$\bar{3}$	0, 0	0	1
A^+	$c(us)_{anti}$	$\bar{3}$	1/2, 1/2	-1	1
A^o	$c(ds)_{anti}$	$\bar{3}$	1/2,-1/2	-1	1
X_u^{++}	ccu	3	1/2, 1/2	0	2
X_d^+	ccd	3	1/2,-1/2	0	2
X_s^+	ccs	3	0, 0	-1	2

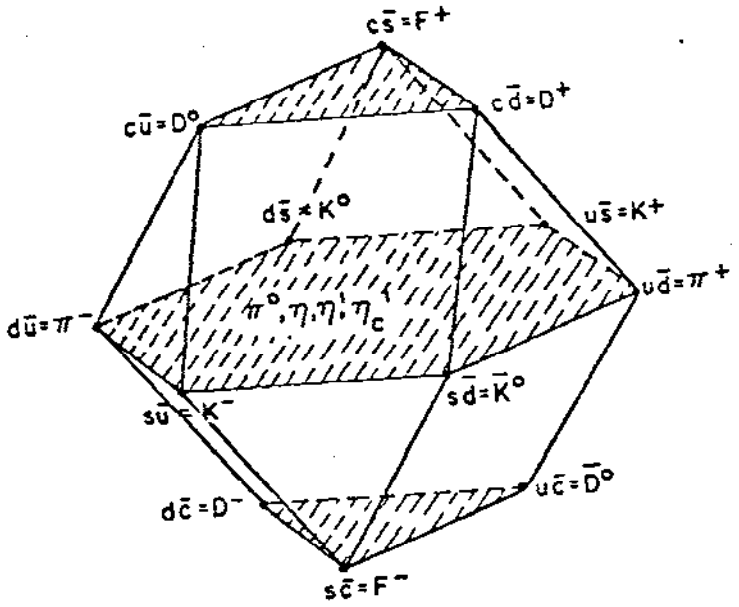

Figure 4. Charmed hadron spectroscopy.
a) 16 meson states ($J^P = 0^-, 1^-, \ldots$) with $C > -1, 0, +1$.

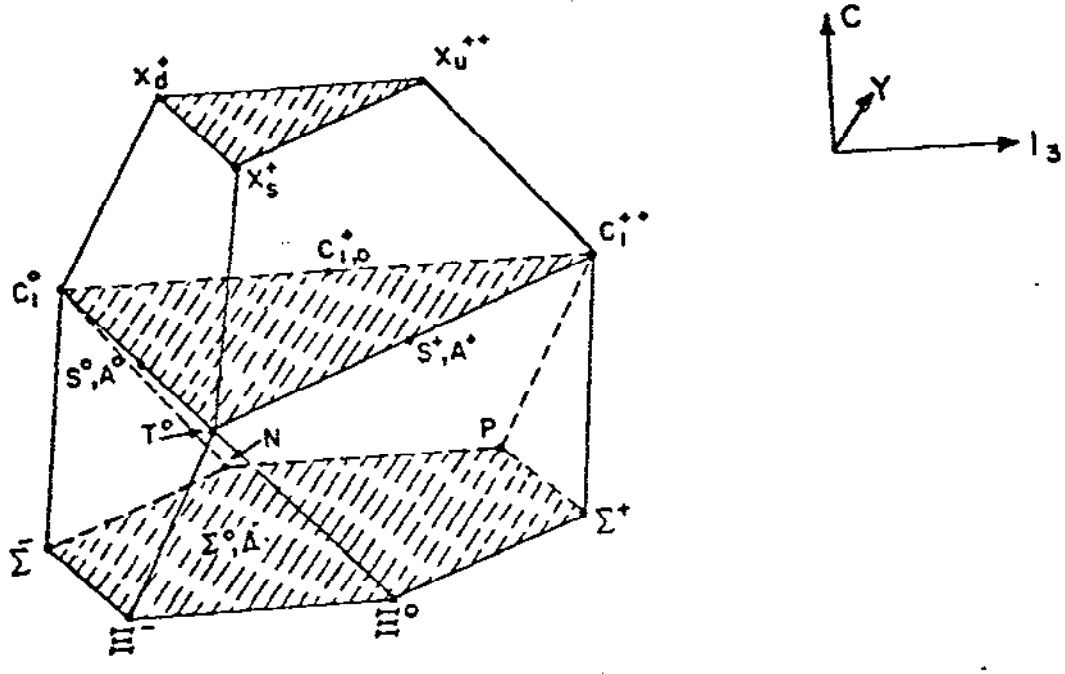

Figure 4. b) 20 baryon ($J^P = \frac{1}{2}^+$) states with $C > 0, 1, 2$.

Λ_c (or $[c(ud)_a]$). Table 1-1 shows the full set of low-lying states we may observe for the $J^P = \frac{1+}{2}$ systems alone; corresponding heavier states are likely to decay strongly and thus elude observation at the present time, for the most part.

Beauty (Bottom): Hidden-beauty "bottomonium" states are well established in e^+e^- reactions, but evidence from photon or hadron-induced collisions has not significantly reached beyond the remarkable set of experiments which first established their existence.[4]

Open-beauty mesons are expected, in the standard six-quark model, to show up as indicated in Fig. 5a for the lowest-lying states, in triplets and singlets. $J^P = \frac{1+}{2}$ baryons are similarly expected in sextets, triplets, and singlets, as shown in Fig. 5b. Higher states again are expected to cascade strongly into these. Only one exclusive state has been claimed to date for experimental detection.

Clearly a very large amount of spectroscopy remains to be explored. Cross-sections for e^+e^- production of hadrons decrease with energy, so that photo- and hadroproduction may well provide our best hope to provide the luminosities needed for an exploration of many detailed features. As will be seen below, the experimental obstacles may be formidable. But if recent ideas are borne out, nature may play into our hands by providing an intrinsic, "long-lived" heavy-quark component which can be isolated in phase-space. This conjecture will be a focus of the discussions to follow.

How do we observe heavy flavors in the final states?

Hidden flavors: $J^P = 1^-$ states have a well-understood spectroscopy (ψ, ψ', ...; Υ, Υ', ...); production from P states (χ, ...) with

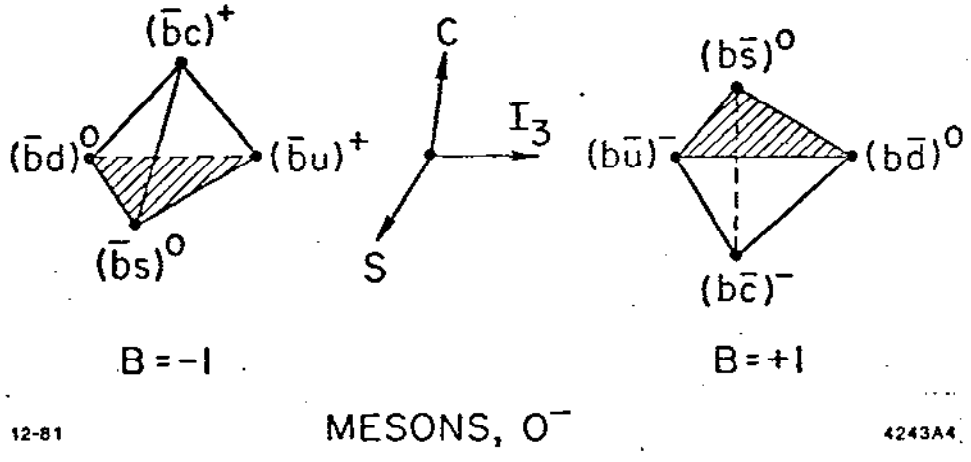

Figure 5. Open-beauty hadron spectroscopy according to the standard 6-quark model:
a) Mesons: one $\underline{4}$ with B = -1, one $\underline{4}$ with B = +1 ($J^P = 0^-, 1^-, \ldots$)

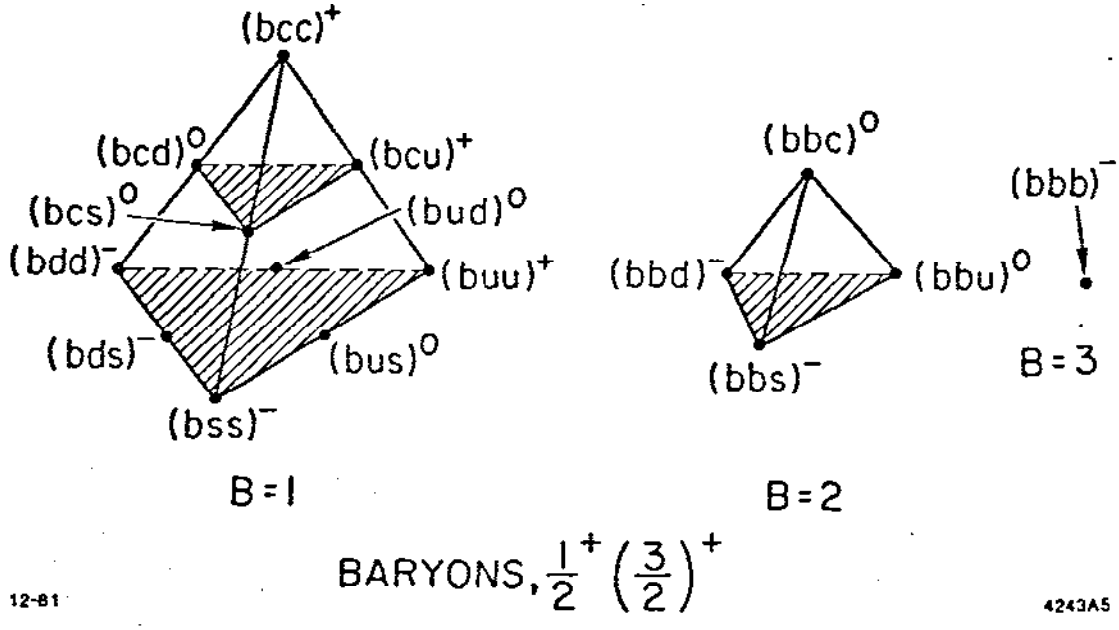

Figure 5. b) Baryons: one $\underline{10}$ with B = 1, one $\underline{4}$ with B = 2, one singlet with B = 3 ($J^P = \frac{1}{2}^+, \frac{3}{2}^+$).

subsequent radiative decay can give valuable information on production mechanisms. Dilepton final states are easy to detect and provide polarization analysis (mainly for ground states of vectors).

Open charm, open beauty:

The principal decay diagram for the heavy quark involves W emission and flavor change (Fig. 6); decay probabilities of the W bosons into fermion pairs are calculable. A choice of lepton (or quark) flavor in the final state, together with that of a particular kinematic region (say, high $p_\perp$) will tag an enriched sample. We can then follow the recipe favored by these features:

a) low lying levels have sharply defined masses, well predicted by models; they tend to decay weakly;

b) characteristic hadronic decay modes are Cabibbo-favored or - suppressed;

c) semileptonic decays yield prompt leptons for tagging, may be characterized by missing (ν) momentum;

d) lifetimes may well be in a detectable range. High-s experiments and new high-resolution detection techniques make this an important feature.

Experimentally, the difficulties are legion, as will be seen below: production cross-sections are small, decay branching fractions for any given final-state channel are often minuscule. Together with the large multiplicities, this often leads to forbidding combinatorics.

New developments for high-flux beams and high-luminosity storage devices, for precise vertex detectors, for large-solid-angle detectors, for clever triggers and microprocessor event selectors mitigate these problems to some extent; clearly, the experimentalist needs to mobilize

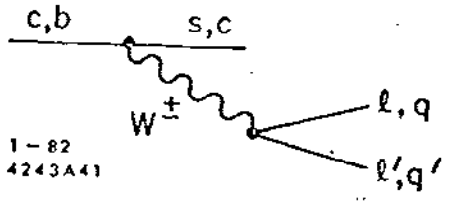

Figure 6. Basic Q weak decay graph, hadronic or semi-leptonic.

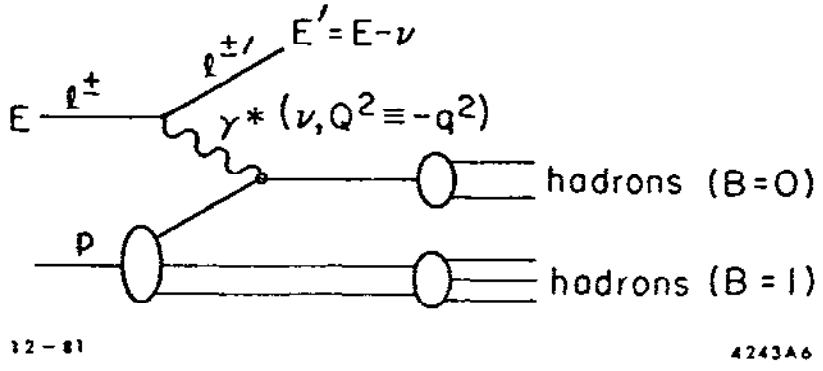

Figure 7. This is a repeat of Figure 1, electroproduction graph. Here it is in the usual quark-parton picture.

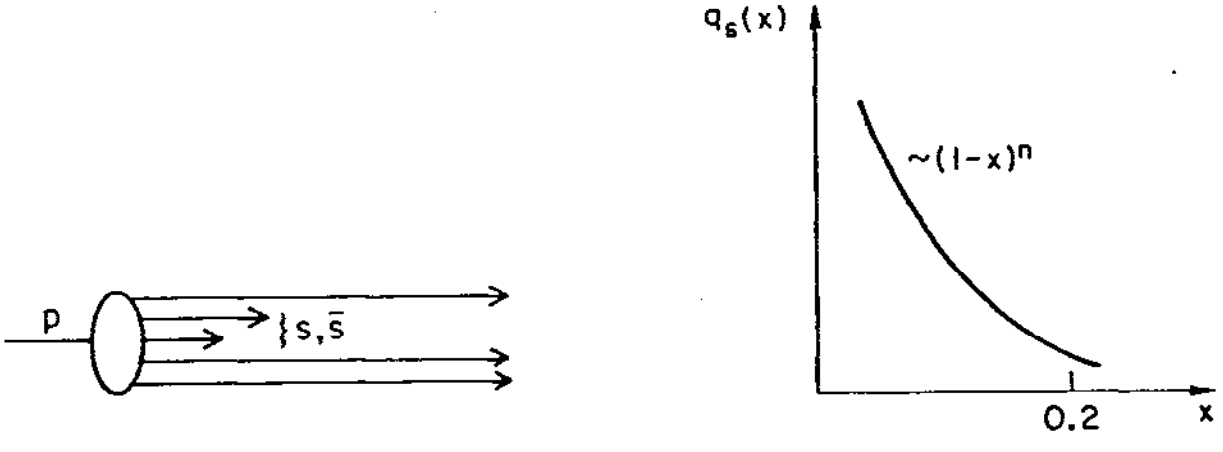

Figure 8. a) Longitudinal momentum distribution for "wee-partons" b) for the strange quark case.

all his resources to make sense of the available information: detection efficiencies and accuracies for identified γ, e, μ, π, K, p, ... have to be optimized; this has to be accomplished over a large solid angle.

The following sections will establish how far this art has carried our knowledge, to what extent the ensuing phenomenology is compatible with theory, and where present evidence puts our understanding of where we find heavy quarks, or how we produce them.

2. Heavy Flavors from Spacelike Photons

2.1 Basic Notions:

In this section, we investigate heavy quark production by spacelike photons, denoted by mass squared values

$$q^2 \equiv - Q^2 < 0.$$

We recall that the collision of such photons γ^* with hadrons in the so-called deeply inelastic régime gave the decisive impetus to the parton picture,[5] and that hadron production in such collisions led to the quark interpretation of the parton. Fig. 7 recapitulates the basic diagram and notation. Note that Q^2 as defined above is also to be interpreted as the momentum transfer (squared) from charged lepton to hadron system: the "size" of the space-time region of interest is then

$$d \sim (Q^2)^{-1/2} .$$

For $Q^2 >> m_p^2$, we can then regard γ^* as a point-like probe of the target nucleon system. In this approximation, we will regard the spacelike photons not as potential sources of heavy quarks, but only as local probes for what is already there: we "look" at the target--valence, sea, and glue components. This is the simplest case studied in these lectures.

2.2 Principal Models

2.2.1 The Parton Model:

The elementary process is a hard elastic scatter of γ^* off $q_i(x)$, where $q_i(x)$ is a parton of quark flavor i and fractional longitudinal momentum x ($-1 \leq x \leq 1$). All other quarks are regarded as spectators.

This simple-minded notion needs information:

a. the parton distribution inside the target N

$$q_i^N(x,k_\perp^2)$$

which, for the time being, we will reduce to

$$q_i^N(x) = \int dk_\perp^2 q_i^N(x,k_\perp^2)$$

b. the parton fragmentation functions into final hadron of type h of fractional energy z in units of E_q:
($0 \leq z \leq 1$).

$$D_{q_i}^h(z)$$

At this level, we are ignoring $p_\perp$.

Let us now assume that the subprocesses factorize; we can then formulate an inclusive lepto-production cross-section of hadrons h in this fashion:

$$\sigma(\ell^\pm N \to \ell^\pm h + \ldots) \sim \sum_i q_i(x)\sigma(\gamma^* q_i)D_{q_i}^h(z) \ .$$

Note that this formulation applies to charged lepto-production; for ν production, $W^\pm q_i$ scattering may change the quark flavor, so that

$$\sigma(\nu N \to \ell^{\overset{+}{-}} h + \ldots) \sim \sum_{i,j} q_i(x)\sigma(Jq_i \to q_j)D_{q_j}^h(z)$$

where J denotes the appropriate current. For $J_{e.m.}$, the photon couples to the quark charge Z_i, and the process becomes calculable if indeed the $q_i^N(x)$ and $D_{q_i}^h$ are universal. They can be extracted from electro-production and inclusive $e^+e^- \to q_i\bar{q}_i \to + \ldots$ data, respectively, while

$\sigma(\gamma^* q_i)$ is given by Dirac. As an example, take the production of negative hadrons h^- off protons. Their multiplicity n^- is given by

$$\frac{dn^-}{dz} = \frac{\Sigma_i Z_i^2 \, q_i^p(x) \, D_{q_i}^{h^-}(z)}{\Sigma_i Z_i^2 \, q_i^p(x)} .$$

Sum over the three valence quarks u, u, d and find with the electric charges $Z_u = \frac{2}{3}e$, $Z_d = -\frac{1}{3}e$,

$$\frac{d}{dz} n^-(z) = \frac{4u(x) \, D_u^{h^-}(z) + d(x) \, D_d^{h^-}(z)}{4u(x) + d(x)} .$$

Now assume that u, d quarks have equal x distributions so that

$$u(x) \simeq 2 \, d(x) \qquad (x \gtrsim 0.2)$$

and expect

$$\frac{d}{dz} n^-(z) \simeq \frac{1}{9} \{8 \, D_u^{h^-}(z) + D_d^{h^-}(z)\},$$

a negative hadron distribution independent of x! This checks out well with experiment. The model has a good basis in available data, for low- to moderate Q^2 values. If we use it similarly to determine, from measurements of $\frac{d}{dz}(\ell^{\pm} n \to K + \ldots)$, the strangeness content of the proton, we find (Fig's. 8 a,b) the functions $q_s(x)$, $\bar{q}_s(x)$: obviously, the s, $\bar{s}$ are concentrated at small values of x ("wee partons"); their distribution is parameterized by $q_s(x) \sim (1-x)^n$, with n = 5.
Will -- at high Q^2, where we might expect an SU(4) symmetric sea -- inclusive charm electroproduction yield similar results for the c, b quark seas?

2.2.2 Lowest-order QCD: The "Photon-Gluon Fusion" Model

At this point, the heavy quark masses introduce a new element; the mass scale $m_c \simeq 1.5$, $m_b \simeq 5$ GeV/c^2 indicates highly local probes: clearly, QCD is likely to be applicable here, possibly in its perturbative formulation. This introduces new graphs (Fig. 9). Remember that a comparison of Feynman's parton model with data had led to the conclusion that some 50% of a hadron's momentum is carried by gluons (Fig. 9a). This initial state thus leads to the lowest-order QCD graph (Fig. 9b) called the $\gamma^* g$ fusion graph. It clearly does not probe the flavor content of the nucleon wave function. To the same order in α_s, Figs. 9c, d show the incipient Q^2 evolution of the simple parton model in a way which still does probe the flavor content.

The photon-gluon fusion graph has been calculated in detail. To do so successfully, simplifying assumptions have to be made:

a) It must be assumed that the color-octet gluon turns into the color-singlet $Q\bar{Q}$ system by subsequent soft-gluon exchanges, without further noticeable effects ("automatic color bookkeeping").

b) "Semilocal duality" is invoked to connect $Q\bar{Q}$ production below and above "open-Q" threshold, e.g., $4\,m_c^2 \leq s \leq 4\,m_D^2$ and $s > 4\,m_D^2$.

c) The strong coupling is fixed by, e.g., the appropriate quark mass:

$$\alpha_s = \frac{1.5}{\ell n\, m^2_{c\bar{c}}\, \Lambda^{-2}}$$

d) The basic parton model calculation can be used for the process $\gamma^* q_i \to c\bar{c}X$ (as above);

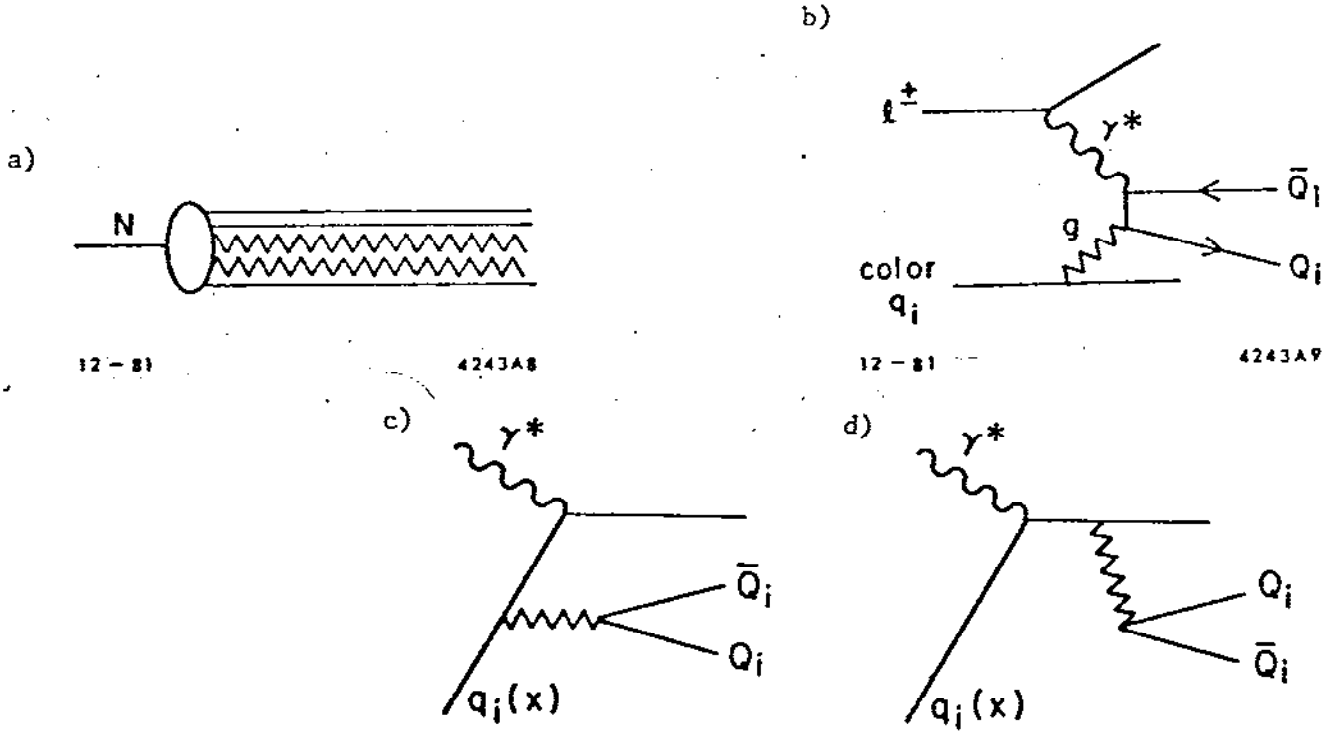

Figure 9. QCD inspired graphs: a) gluons carry ~ 50% of the nucleon momentum. b-d) lowest-order QCD graphs for $Q\bar{Q}$ production: photon-gluon fusion, gluon bremsstrahlung.

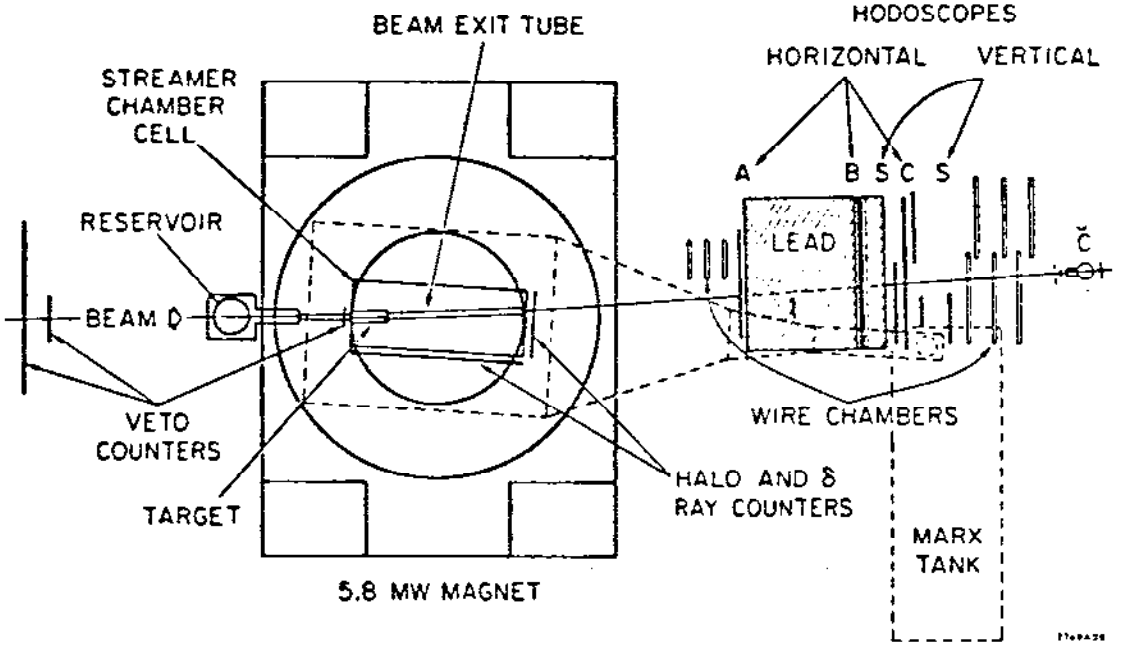

Figure 10. Experimental setup for Santa Cruz/SLAC streamer chamber search. Scattered μ penetrates the lead wall, all charged secondaries leave tracks in chamber.

e) The production process is presumed unaffected by subsequent fragmentation $q_i \rightarrow h$.

In addition, we have to fix certain input data: the mass of the heavy quark, the form of the gluon distribution (usually $a \cdot x^{-1}(1-x)^b$); note that it proves useful to redefine

$$x = \frac{Q^2 + m^2_{c\bar{c}}}{2M\nu} ;$$

and the t dependence, which is not predicted by the model. To connect the results to observables, we further glean the form of $D^h_{q_i}(z)$ from e^+e^- annihilation, typically

$$D(z) = (1-z)^\alpha$$

with

$$z = \frac{2E_D}{m_{c\bar{c}}} .$$

We can now calculate predictions from this first order QCD calculation,[6] for both hidden and open heavy flavors:

inclusive $Q\bar{Q}$ production as a function of E (or of ν);

the charm (beauty) contribution to $\nu W_2 = F_2(x)$;

the azimuthal dependence

$$\frac{d\sigma}{d\phi} = \sigma_0 \ (1 + a_2 \cos 2\phi)$$

(this is a feature endemic to the $\gamma^* g$ fusion model due to parity invariance and $Q\bar{Q}$ interchangeability: the model predicts $a_2 = a_2(p_\perp)$);

the transverse momentum dependence of $\sigma(Q\bar{Q})$.

In an obvious departure from the parton model, the parton fragmentation functions will now have to take the basic graph (Fig. 9 b) into

account, which lets both forward q, $\bar{q}$ share the transferred four-momentum: The function $D_g(z)$ is symmetric about $z_a = 0.5$; there will usually be two jets:

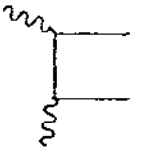

2.2.3 QCD Evolution

The other real novelty, going beyond the first-order QCD graph, is the Q^2 evolution of the fragmentation functions. Once these points are understood, another calculable quantity will be the structure function F_2: the production cross sections as a function of $m_{c\bar{c}}$ will predict

$$F_2^{\psi} \text{ (for } 4\, m_c^2 \leq s \leq 4\, m_D^2),$$

$$F_2^{c\bar{c}} \text{ (for } s \geq 4\, m_D^2).$$

These quantities clearly enter into the phenomenology of scale breaking, as will be discussed below. Recall then that, in principle, all scaling violations are described, in QCD terms, by the Altarelli-Parisi[8] equations. Starting from renormalization group concepts, we maintain factorization as in the simple parton model, but give up the concept of point cross sections: Contributions from all orders in α_s are, in principle, included. For an SU_N gauge theory, with m flavors, the couplings are characterized by

$$\alpha_s = \frac{g^2_s}{4\pi} = \frac{6\pi}{(11N - 2m)\, \ell n\, Q\Lambda^{-1}} ,$$

and determine the evolution of the quark and gluon content with Q^2 (or, in the usual nomenclature) with

$$t \equiv \ell n \ Q^2/Q_0{}^2.$$

Call y the fractional quark or gluon momentum inside the target nucleon; we can then write, for each flavor i:

$$\frac{d}{dt} q_i(x,t) = \frac{\alpha_s(t)}{2\pi} \int_x^1 \frac{dy}{y} \{q_i(y,t) \ P_{qq}(\tfrac{x}{y}) + g(y,t) \ P_{qg}(\tfrac{x}{y})\}$$

$$= \int \quad \text{---}\sim\text{---} + \sim\!\!< \quad + \ldots$$

Similarly, the gluon evolution can be written by a sum over all flavors:

$$\frac{d}{dt} g \ (x,t) = \frac{\alpha_s(t)}{2\pi} \int_x^1 \frac{dy}{y} \{\Sigma_i \ q_i(y,t) \ P_{gq_i}(\tfrac{x}{y}) + g(y,t) \ P_{gg}(\tfrac{x}{y})\}$$

$$= \int \quad \text{---}\sim\text{---} + \sim\!\!\sim\!\!\sim \quad + \ldots \ ,$$

where the meaning of the probability functions P_{qq} etc. should be clear from the graphs below each term. To calculate these integrals, assume flavor independence of the functions P(z), which would be fully justified for $m_{q_i} \to 0$). It is immediately visible that, by subtraction, we can compute the Q^2 evolution of the non-singlet densities

$$\Delta_{ij}(x,t) \equiv q_i(x,t) - q_j(x,t)$$

$$\frac{d}{dt} \Delta_{ij}(x,t) = \frac{\alpha_s(t)}{2\pi} \int_x^1 \frac{dy}{d} \Delta_{ij}(y,t) \ P_{qq}(\tfrac{x}{y}) + \ldots$$

It also becomes quite clear that our capability to measure specific heavy flavor production will shed light on the effects of the evolution function P_{Qg}, and will tell them apart from the effects of any possible intrinsic heavy quark component in the target.

2.3 Experimental Evidence

How do we look for heavy flavor production from virtual photons? The optimal case might be given by a visual detector: incoming and outgoing lepton tracks fix all parameters of the virtual photon, all charged secondaries can be measured.

The first experiment to make an attempt after this recipe was the SLAC/Santa Cruz Streamer Chamber Collaboration:[9] a high-$p_\perp$ muon trigger selected muons scattered deeply out of a 14 GeV μ^+ beam (Fig. 10). Their final momenta were measured together with those of all other charged particles emerging from a liquid hydrogen target. The experiment had a sensitivity of about 50 events per nano-barn of cross-section. Working close to threshold for the process

$$\mu^+ N \to \Lambda_c \bar{D} + \ldots + \mu^+,$$

it had the advantage of seeing all charged secondaries close to the vertex, being sensitive to K^o_s and Λ decays, and fully defining the virtual photon kinematics. The experimenters searched for the Cabibbo-favored Λ_c, D decays into final states containing strange particles, by looking for invariant-mass peaks in systems containing identified $K^o \to \pi^+\pi^-$, $\Lambda^o \to p\pi^-$ decays. The absence of a threshold enhancement in $c\bar{c}$ electroproduction and the smallness of individual branching ratios did not allow a signal to be observed above background: the result was an upper limit

$$\sigma(\gamma^* p \to \Lambda_c \bar{D}) \times \Pi \text{ (B.R.s into } K^o, \Lambda^o \text{ modes)}$$

$$\times \text{ detection efficiency} < 20 \text{ nb.}$$

An upcoming run of the European Muon Collaboration (EMC) will, at much higher energy and with considerably increased luminosity, do a similar

search at CERN, using a Munich (M.P.I.) built streamer chamber for hadron recognition in the final state.

In the meantime, considerable data have been collected by three major experiments at FNAL and CERN, employing much cruder detectors to search for heavy quark decay muons as a key to $c\bar{c}$, $b\bar{b}$ production mechanisms and cross-sections:

Berkeley/Fermilab/Princeton (BFP) used a beam of 209 GeV (± 2%) muons at Fermilab (where the beam setup permits targeting of 1.4×10^{-7} μ per primary 400 p). Their detection equipment, shown schematically in Fig. 11, is basically a heavily instrumented magnetized steel calorimeter. It contains 475 tons of steel magnetized to ~19.7 k Gauss; scintillator hodoscopes permit triggering, proportional and drift chamber systems allow track reconstruction.

$$\text{total exposure:} \quad \sim 1.4 \times 10^{11}\ \mu^+$$
$$\sim 2.9 \times 10^{11}\ \mu^-$$
$$\text{acceptance:} \quad 0 \leq Q^2 \leq 50\ (\text{GeV/c})^2$$
$$50 \leq \nu \leq 200\ \text{GeV}$$

Just as other heavy-target experiments, the measurement of heavy flavor production proceeds only via multi-μ final states. Data evaluation then involves a long sequence of production model assumptions, acceptance modelling by Monte Carlo techniques, and the evaluation of backgrounds from meson decays and trident production

$$\pi \rightarrow \mu + \ldots ,$$
$$K \rightarrow \mu + \ldots ,$$
$$\mu Z \rightarrow \mu\mu\mu Z .$$

Using appropriate cuts on highly contaminated samples, the observed cross-

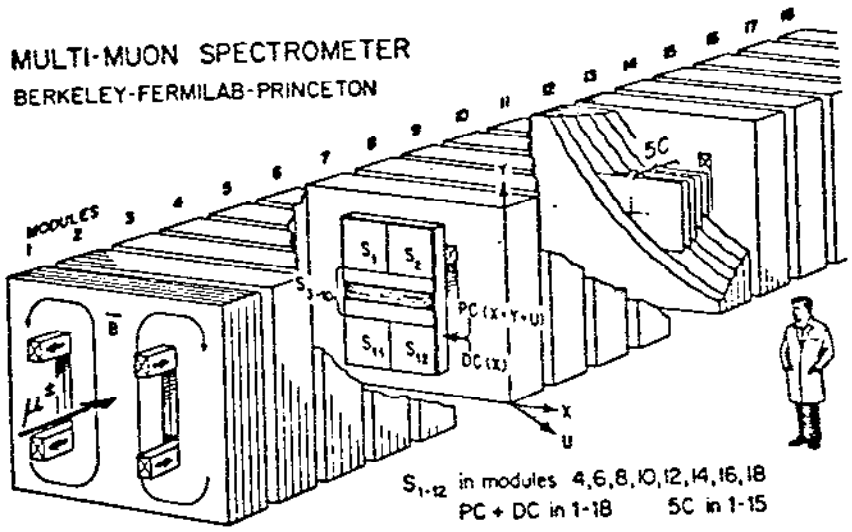

Figure 11. Modular thick-target detector of BFP Collaboration at Fermilab.

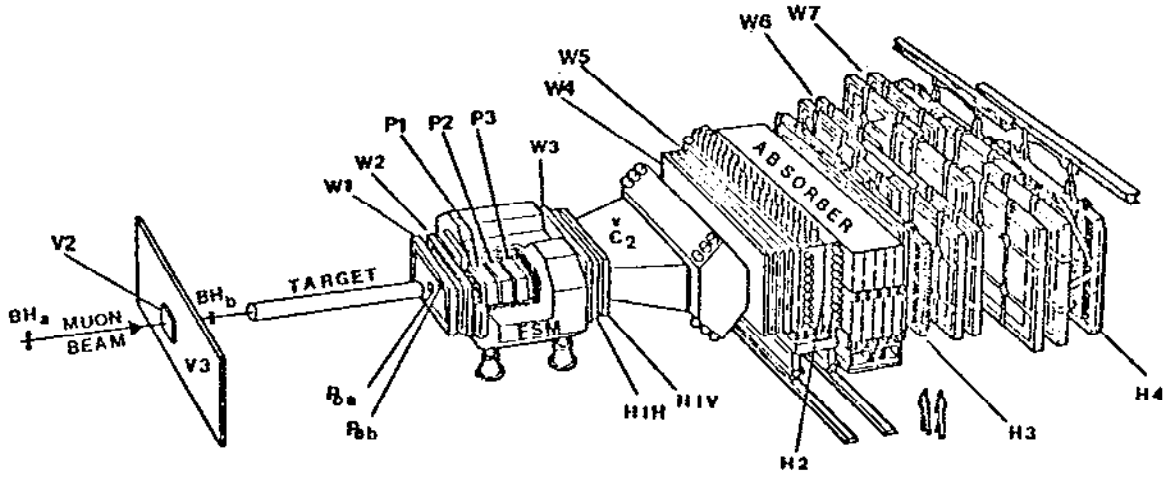

Figure 12. European Muon Collaboration detector: target can be thick or "thin" (LH_2); has been surrounded by a Streamer Chamber.

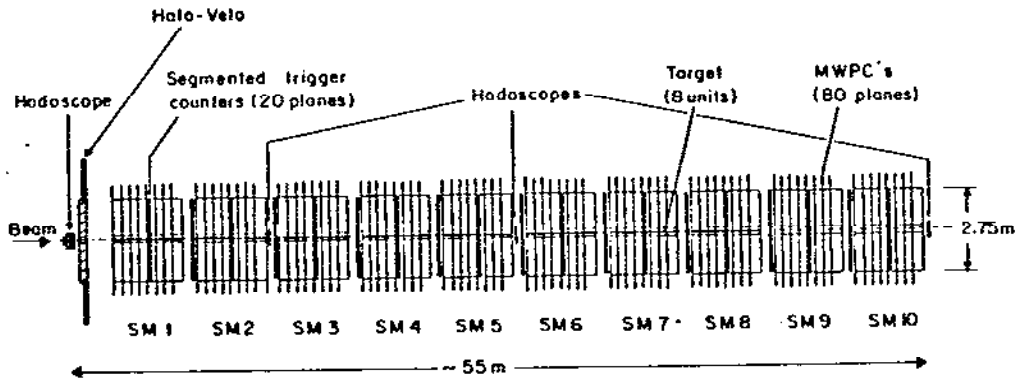

Figure 13. Modular thick-target detector of NA-4 Collaboration at CERN, concentrating on high-Q^2 secondaries.

sections will then still have to be reduced from μZ (e.g., μFe) to μN scattering.

The European Muon Collaboration (EMC) makes use of an SPS muon beam (unlike BFP above, the experiment is still in progress) which at 280 GeV momentum (± 5%) yields $1.6 \times 10^{-6} \mu^+$ per 400 GeV proton incident on a primary Be target. The apparatus,[12] shown in Fig. 12, is somewhat more ambitious than BPF's: it incorporates both a 6 m long LH_2 target and a heavy Fe-scintillator target, 4.75 m long. Downstream, there are Cherenkov counters for particle identification in addition to trajectory-defining devices and calorimeter modules. Their more recent data set, to which we will refer below, is based on a 250 GeV sample with

exposure	4×10^{11}	μ^+
cut on	$\theta_{\mu\mu'}$	> 15 mrad
energy loss	ν	> 136 GeV.

Bologna-CERN-Dubna-Munich-Saclay (BCDMS). Lastly, in Fig. 13 we show the modular detector of the NA-4 Collaboration.[13] Its basic aim is sensitivity to inclusive high-Q^2 events; a long Fe toroid surrounds a 40m carbon target with a field that is designed to scatter deflected μ's back toward the axis. The central "hole" clearly presents problems for the low-Q^2 secondaries, but μ's within the aperture are well measured by appropriate hodoscopes. The beam is shared with the EMC experiment.

2.3.1 Hidden-Charm (ψ) Production

ψ's are detected via their 2μ decay mode: all experiments first identify the scattered μ from all bona-fide 3μ events, then impose cuts on the observed energy to tell elastic from inelastic events. Fig. 14 shows dimuon mass plots from the EMC to illustrate the point. Subtractions tend to be straightforward. The resulting elastic ψ pro-

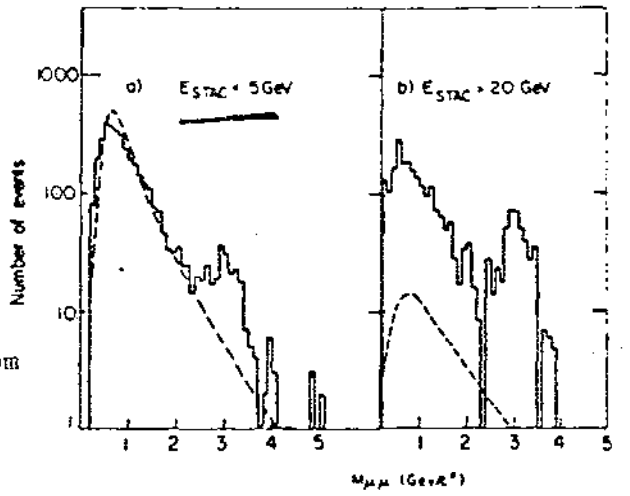

Figure 14. Di-muon invariant mass plots from EMC
a) elastic ψ signal (hadronic energy deposit small);
b) inelastic ψ signal.

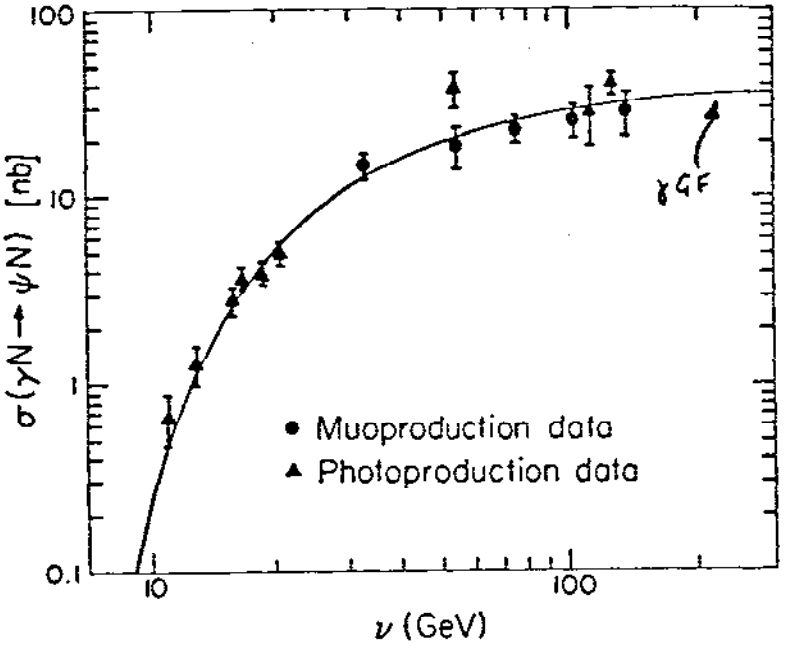

Figure 15. Comparison of ψ muoproduction energy dependence with photon-gluon fusion model (γGF). Data from BFP. Photoproduction points for comparison.

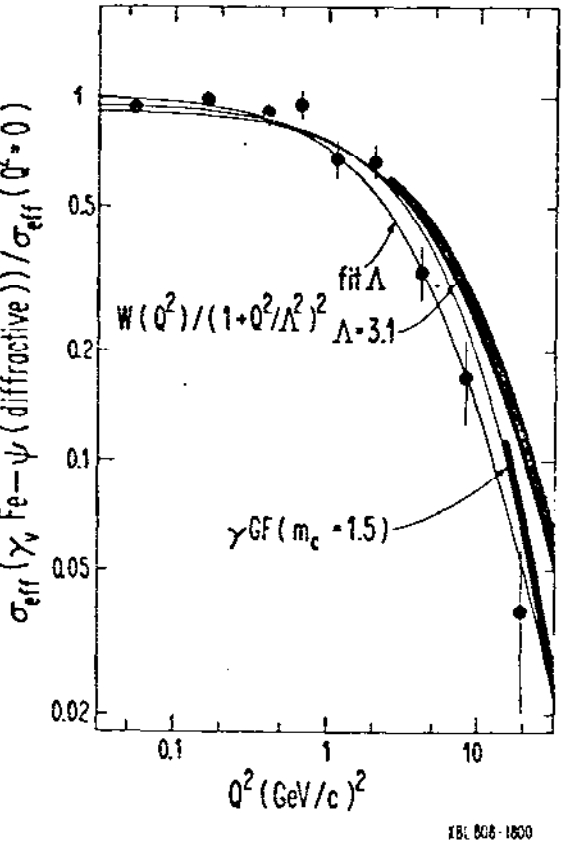

Figure 16. Q^2 dependence of ψ muoproduction: neither vector dominance (VDM) propagator fit nor γGF fit are satisfactory.

duction cross-section is shown, for the BFP data, in Fig. 15, as a function of energy. Note that, with an appropriate choice for the gluon distribution inside the target nucleon,

$$g(x) = \frac{3}{x}\,(1 - x)^5,$$

the photon-gluon fusion model (γGF) predicts,[14] for

$$2m_c \leq m_{c\bar{c}} \leq m_{D\bar{D}}\ ,$$

the curve indicated in Fig. 15, which contains an appropriately normalized comparison of photo-production and muoproduction data on elastic ψ production. The Q^2-distribution, shown in Fig. 16, is predicted by the vector dominance model through the transverse ψ propagator term

$$\sigma_{el}\ (\mu N \to \psi N) \propto \frac{W(Q^2)}{(1 + Q^2\Lambda_0^{-2})^2}\ .$$

The data, however, indicate that the VDM term is not quantitatively satisfactory either at small Q^2 values (say, at $0.3 > Q^2$) or in the high-Q^2 range: the γGF cross section with a charmed quark mass of 1.5 GeV/c^2 is reasonably close at larger Q^2, but the VDM fit for the Λ parameter leads to 2.08 GeV (instead of $\Lambda = m_\psi = 3.1$ GeV!). The t-dependence, not predicted by γGF, clearly shows the hadronic character of the ψ by the presence of a coherent component

$$\frac{d\sigma}{dt}\ (\gamma^*Fe \to \psi x) = \frac{d\sigma}{dt}\Big|_{t=o}\ (A_e^2 e^{\alpha t} + A_e \varepsilon e^{\beta t})$$

with the "shadowing factor" $A_e \simeq 0.9$, and coherent slope $\alpha = 150\ (\mathrm{GeV/c})^{-2}$; β is the well-known measure for the small size of ψ's: $\beta = 2(\mathrm{GeV/c})^{-2}$. Remember that, in contrast, ρ^o muoproduction leads to $\beta(\rho^o) \simeq 6(\mathrm{GeV/c})^{-2}$!

An interesting feature explored by BFP is the ψ polarization, "self-analyzed" in the 2μ decay.[15] Of 3 measurable angles, γGF makes a distinctive prediction that the production cross-section depend on the angle

ϕ_{21} between μ scattering plane, $\vec{n}_1$, and $\gamma^* - \psi$ diffraction, $\vec{n}_2$. Fig. 17 demonstrates that there is no indication for the predicted characteristic effect.[16] For the other two angles, (with $\vec{n}_3$ = normal of the ψ decay plane) $\phi = \cos^{-1}(\vec{n}_3 \cdot \vec{n}_2) - \cos^{-1}(\vec{n}_2 \cdot \vec{n}_1)$, and θ_1, the polar angle for the $\psi \to 2\mu$ decay, s-channel helicity conservation and the vector dominance model predict a trend

$$\sigma(\theta,\phi) \propto 1 + \cos\theta + \varepsilon(2R - \eta \cos 2\phi) \sin^2\theta.$$

Here, $\varepsilon = \frac{\gamma_L}{\gamma_T}$ and $R = \frac{\sigma_L}{\sigma_T}$ are the usual longitudinal-to-transverse ratios of virtual photon flux and cross-section. The "muon polarization" term in cos 2ϕ, is established by the data with a weight factor η of about unity•γGF has no prediction, since color neutralization demands multiple gluon exchange.

2.3.2 Hidden-Beauty (Υ) Production

In precisely the same manner that we discussed for the extraction of ψ production data, BFP looked for Υ muoproduction among the tri-muon candidate sample. From over 10^5 trimuon events, which contain ~6,700 ψ's, no serious signal could be gleaned, as indicated in Fig. 18. As a result, only an upper limit is given[17]

$$\sigma(\mu N \to \mu\Upsilon + \ldots) \times BR\ (\Upsilon \to \mu\mu) < 2.2 \times 20^{-38}\text{cm}^2$$

with 90% confidence. The branching ratio is known to be

$$\frac{\Gamma(\Upsilon \to \mu\mu)}{\Gamma(\Upsilon \to \text{all})} = (3.1 \pm 0.9)\%$$

so that

$$\sigma(\mu N \to \mu\Upsilon + \ldots) \leq 0.79 \times 10^{-36}\text{cm}^2.$$

Figure 17. Dependence of ψ production on angle between two scattering planes: γGF prediction (dashed line) is not supported by the data.

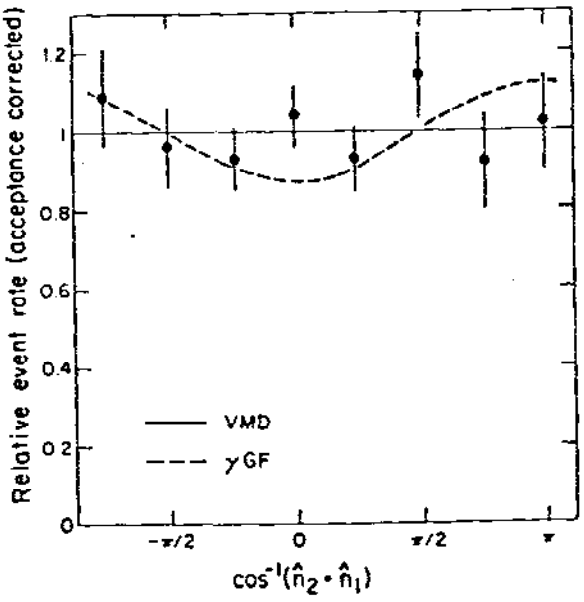

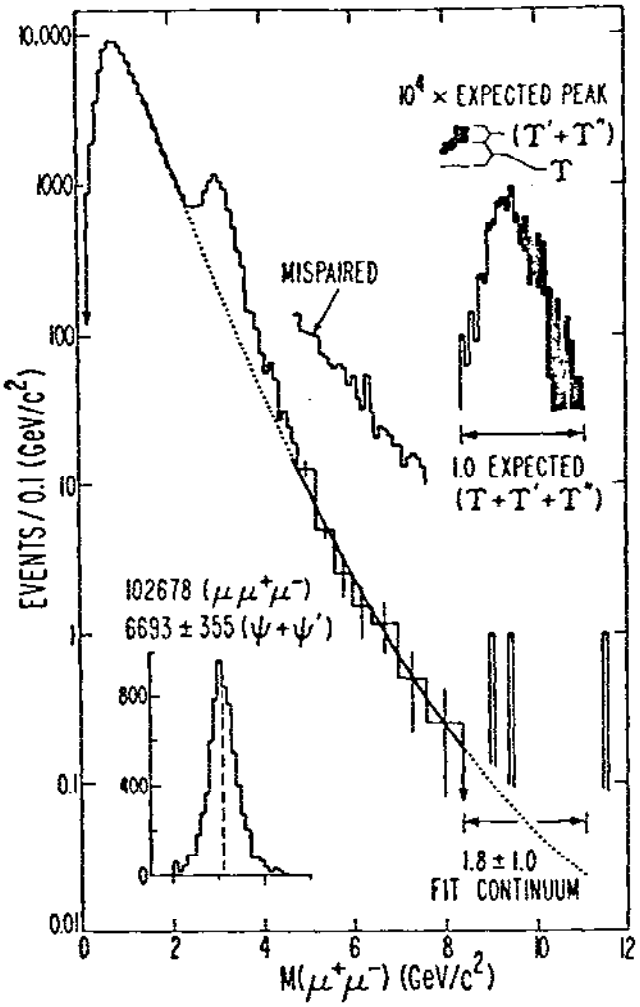

Figure 18.

Dimuon spectrum from BFP: there is a clean ψ signal, but no indication of T production. Inset: enlarged shape of T + T' + T'' expected effect.

This value is above both the VDM and the γGF expectations, so that a more stringent test is needed.

2.3.3 Open-Charm Production

Information concerning the associated production of charmed hadrons

$$\gamma^*N \to c\bar{c} + \ldots$$

comes from muoproduction experiments with either one or two "prompt muons" detected in addition to the scattered beam muon. Production graphs now admit an important new possibility: the excitation of "intrinsic charm" -- be that a low-x charmed quark (antiquark) from the "sea" or a possible valence component of the target nucleon. The first will lead to "central production" of charmed hadrons, the second may lead to "leading" charmed final-state particles. (Fig. 19).

The analysis involves initial γGF modelling as before, then looking for a possible excess of the data. We now demand $m^2_{c\bar{c}} > 4m^2_D$ and assume the gluon distribution

$$g(x) = \frac{3}{x}(1-x)^5$$

with

$$x = \frac{m^2_{c\bar{c}} + Q^2}{2M\nu} \quad (\neq x_{B_j}) \ .$$

A typical experimental signature is, for trimuons:

$$\mu_{Beam} + \mu^+\mu^- \ ,$$

missing energy > 10 GeV (unseen ν's),

$$E_{\mu^+,\mu^-} > 10 \text{ GeV}.$$

Backgrounds will creep into this signature from such processes as μ tridents (calculable by QED), vector meson decays $V^o \to \mu^+\mu^-$ ($V^o = \rho^o$, ω^o, ...), decay muons from τ leptons and heavier quarks, and the decays of K's and π's.

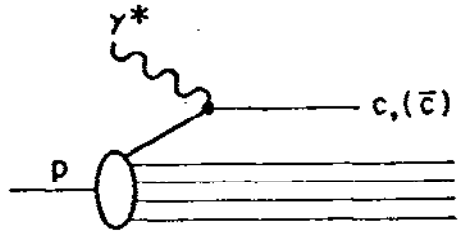

Figure 19. General graph for excitation of intrinsic $Q(\bar{Q})$ component of nucleon wavefunction: can imply "leading" heavy-flavored hadrons.

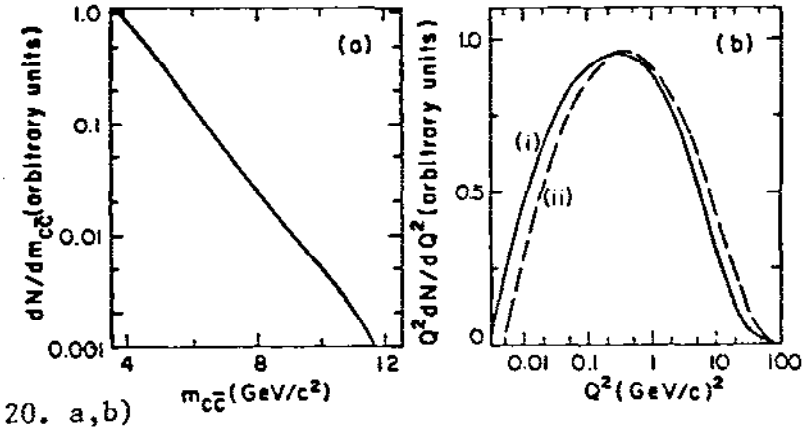

Figure 20. a,b)

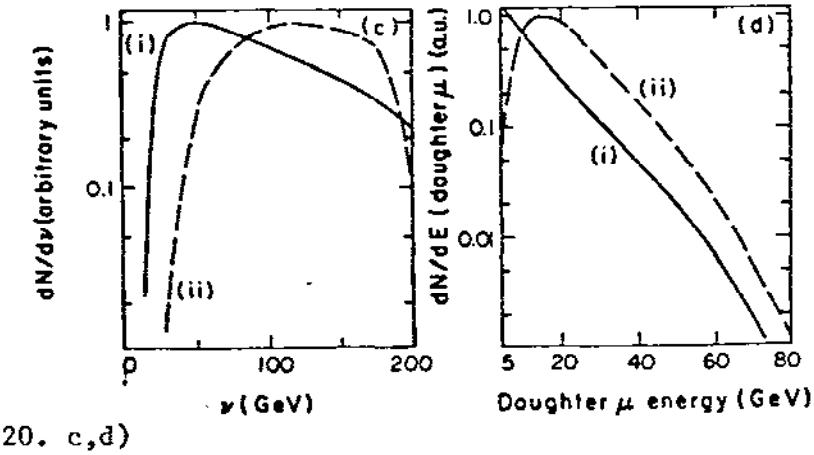

Figure 20. c,d)

Acceptance modelling for open charm, BFP setup. For the spectrum in (a), Q^2 (b), ν (c), and decay lepton (d) acceptances are reasonably matched.

Acceptance models[18] first use the γGF model, with a strong coupling $\alpha_s = 1.5/\ell n\ (4m^2_{c\bar{c}}) \approx \frac{3}{8}$, to generate the invariant mass spectrum $m_{c\bar{c}}$ shown in Fig. 20a. The t dependence is taken from ψ production (see above). The $c\bar{c}$ pair is assumed to absorb all allowable γ* energy, then to fragment into D^o and $D^{\pm}$ by a ratio of 2:1, taken from SPEAR results. Inserting appropriate semileptonic branching ratios which allow final-state decay muons to trigger the event criteria, Fig. 20b shows that the generated spectrum in Q^2 is almost uniformly accepted (dashed line). Fig's. 20c,d similarly display the generated and the accepted spectra in ν and in the energy of the decay muon.

Similar generation and acceptance modelling for the background processes clearly is a major task; systematic uncertainties are due to the assumed K/π ratios in the decay cascades (π, K contribute (19 ± 10%) of the dimuon signal!) and to the shape of the assumed charmed-quark fragmentation function

$$D_c^D(z) = (1 - z)^{0.4}.$$

BFP quotes them as amounting to $\{^{+28\%}_{-20\%}\}$. The resulting final data in terms of Q^2 and ν are shown in Fig's. 21 and 22 for the effective cross-section

$$\sigma_{eff} = (1 + \varepsilon R)\sigma_T$$

resulting from the general expression

$$\frac{d^2\sigma}{dQ^2 d\nu} = \gamma_T(1 + \varepsilon R)\sigma_T,$$

with the flux of transverse photons $\gamma_T = \frac{\alpha}{2\pi} \frac{(\nu^2 + Q^2)^{\frac{1}{2}}}{Q^2 E_\mu^2\ (1 - \varepsilon)}$ and the

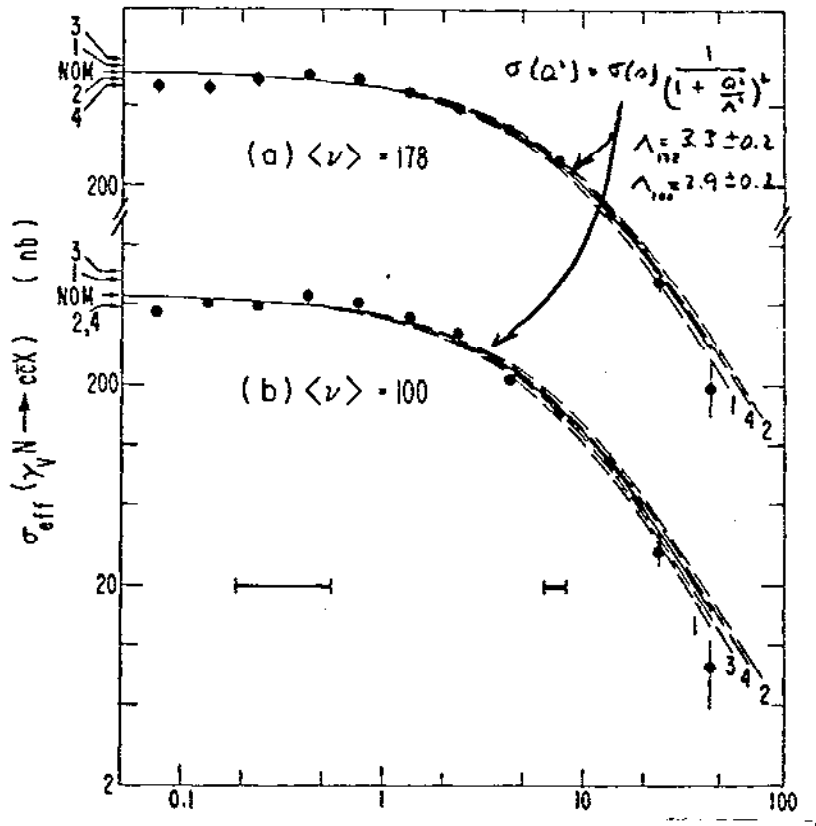

Figure 21. Q^2 dependence of open-charm data (BFP).

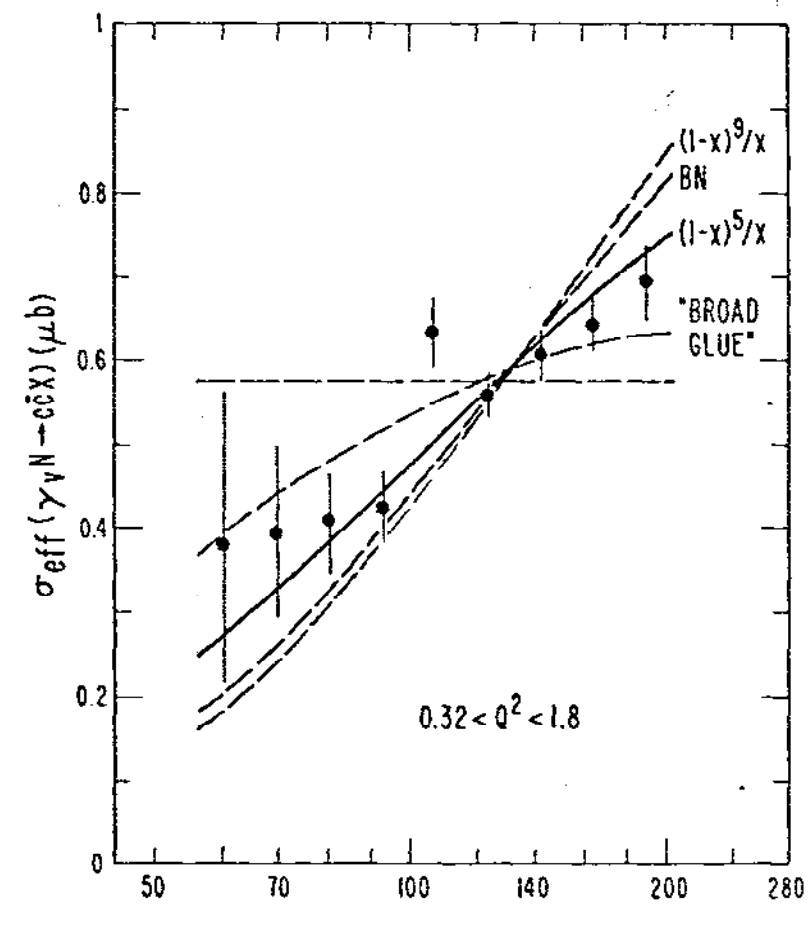

Figure 22. ν dependence of open-charm cross-section, for events in flat Q^2 region ($\lesssim$ 2 GeV/c^2), (BFP).

polarization parameter $\frac{1}{\epsilon} = 1 + \frac{2}{Q^2}(Q^2 + \nu^2)\tan^2\frac{\theta}{2}$. The Q^2 dependence (Fig. 21) can be fitted with a VDM-inspired transverse propagator term

$$\sigma(Q^2) = \sigma(0)\ (1 + \frac{Q^2}{\Lambda^2})^{-2}.$$

The resulting Λ values are (3.3 ± 0.2) GeV at $\langle\nu\rangle$ = 178 GeV, (2.9 ± 0.2) at $\langle\nu\rangle$ = 100. The ν dependence (Fig. 22) corresponds to the region where σ_{eff} is flat in Q^2, i.e., $Q^2 \lesssim 2(\text{GeV/c})^2$. The extrapolation of this Q^2 dependence to real photons, $Q^2 \leq 0$, leads to photoproduction values of

$$\sigma(\gamma N \to c\bar{c}) = \begin{cases} 560\ ^{+\ 200}_{-\ 120}\ \text{nb at 100 GeV}, \\ 750\ ^{+\ 180}_{-\ 130}\ \text{nb at 178 GeV}. \end{cases}$$

Clearly, the errors are much larger than in the ψ production case (section 2.3.1), but a γGF fit with the same g(x) parametrization as above is seen to give satisfactory agreement.

EMC data are obtained basically in a similar way, but the apparatus acceptance modelling makes use of the specific features of the setup. Backgrounds can be suppressed by a criterion that no extra track be seen in the center hodoscopes, thus discriminating against muon tridents. A new data set[19] containing ~ 10,000 dimuon events (5,6k $\mu^+\mu^+$, 4,4k $\mu^+\mu^-$) and ~ 31,000 trimuons ($\mu^+\mu^+\mu^-$) was first tested for a preferred form of the fragmentation function (flat in the center-of-mass or flat in the laboratory system). Fig. 23 shows that a flat distribution in the lab gives the better fit to 2- and 3-μ data.

Fig. 24 gives the Q^2 dependence for both data sets, for two energy bins, for both the effective virtual-photon cross-section and the resulting structure function F_2. They are seen to be well compatible with the

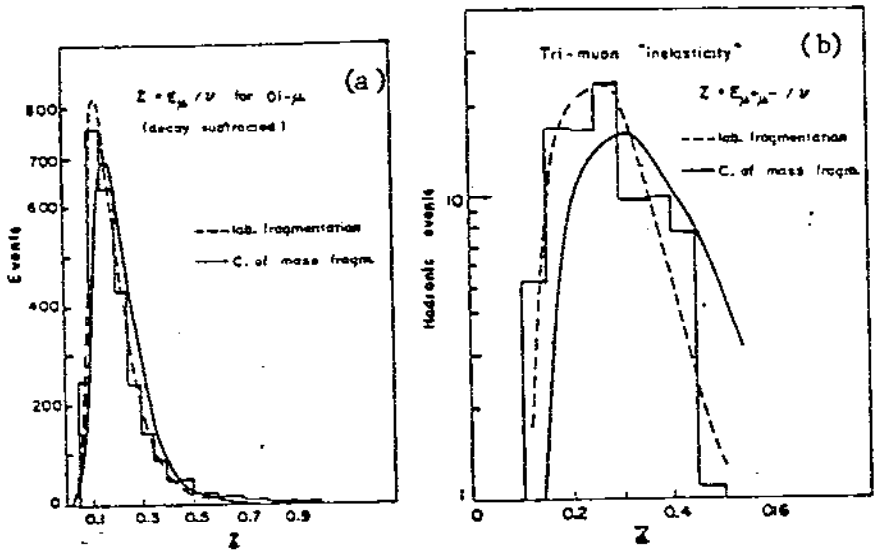

Figure 23. Acceptance modelling involves assumptions about fragmentation functions. Both for dimuons (a) and trimuons (b), fragmentation is preferred flat in the lab system (EMC).

Figure 24.

a) Q^2 dependence of effective γ^* cross-section and F_2, for dimuon data (EMC).

b) trimuon data (EMC).

γGF fit. The energy dependence is seen to again agree with the γGF expectations for a low-Q^2 and a high-Q^2 bin shown in Fig. 25. Note the difference between the two curves.

2.3.4 Open-Beauty Production

Together with the sample just described, the EMC observed wrong-sign tri-muon events. Of these, 12 have the signature $\mu^+\mu^+\mu^+$, 3 $\mu^+\mu^-\mu^-$. If these are to be candidates for $B\bar{B}$ production, we expect large missing energies for unseen neutrinos from decay chains

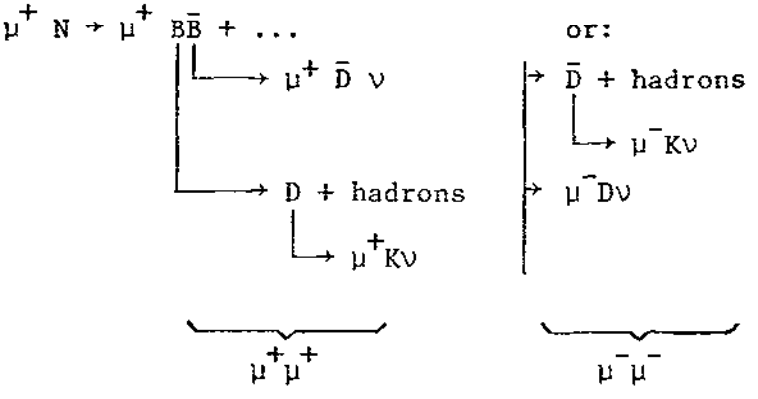

Three of the above events survive all cuts and selection criteria. If all three were due to $B\bar{B}$ decay, then,[19] assuming a semileptonic BR($b \to \mu + \ldots$) of 10%,

$$\sigma(\mu N \to \mu B\bar{B}\, x) = (5 \pm 3)10^{-36}\,\mathrm{cm}^2$$

at E_μ = 250 GeV. Some kinematic features of the events in question are described in Fig. 26.

BFP, analogously to their charm analysis, modeled acceptance for $B\bar{B}$ events using parameters $m_b = 4.7\ \mathrm{GeV/c^2}$, $Z_b = \frac{1}{3}$, $\alpha_s = 1.5\,(\ell n\ 4m_b^2)^{-1}$.

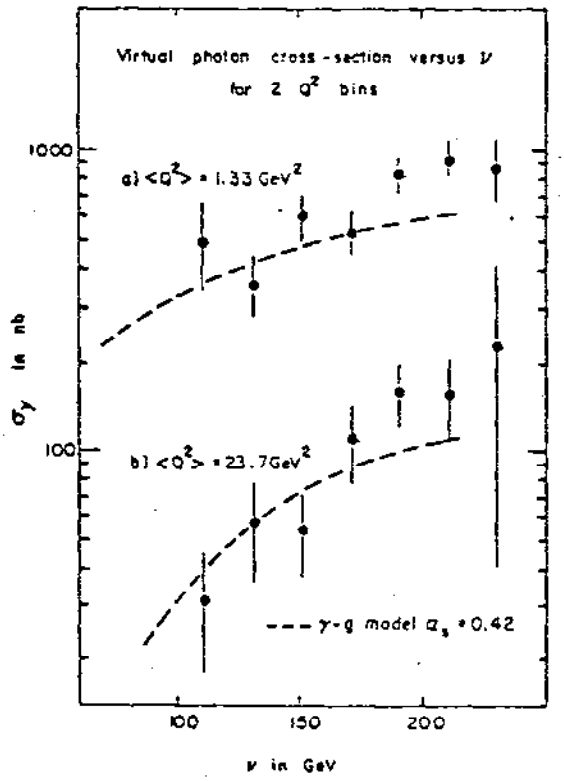

Figure 25. ν dependence of γ^* cross-section from EMC from two different Q^2 bins. Dashed curves are due to γGF model.

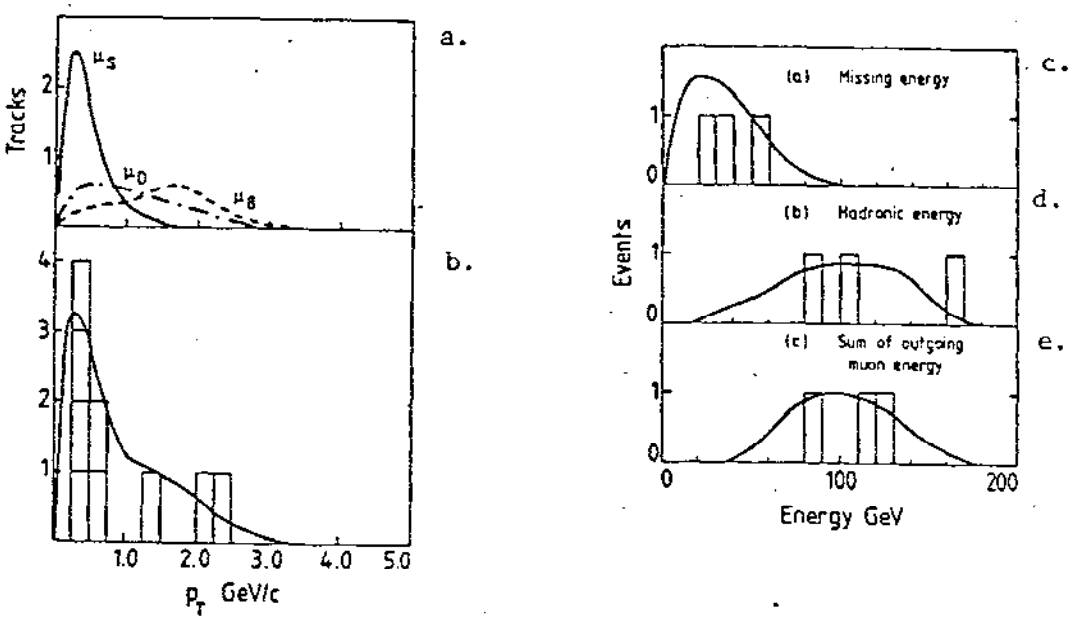

Figure 26. a) Expected p_t structure of μ daughter distribution, from s, c, b decay; b) Data from 3 exotic events (EMC); c,d,e) Energy characteristics of exotic events.

Then, for a branching fraction $B(b\bar{b} \to \mu) = 0.17$, as for $c\bar{c}$, the good agreement of the data with nothing but a weighted charm production model (Fig. 27) leaves room for[20]

$$\sigma(\mu N \to B\bar{B}\ X) < 17 \times 10^{-36} cm^2,$$

certainly compatible with the result of BFP. Without going into details, we stress that both results are not in disagreement with γGF expectations,[21] but are considerably smaller than VMD predictions.[22]

2.3.5 Heavy-Quark Production and Scale Breaking

Remember "Bjorken scaling": the structure function F_2 of inelastic lepton scattering is, for $\nu, Q^2 \to \infty$, Q^2/ν fixed, not dependent on the variables Q^2 or ν, but only on their ratio $x_{BJ} \equiv Q^2(2M\nu)^{-1}$. We have seen, however, how QCD evolution (Section 2.2.3) makes more quarks share the momenta available: this will lead to an increase of F_2 (and the inelastic scattering cross section) at small x, a decrease at large x, with Q^2. A recent compilation of scale breaking data, shown in Fig. 28, clearly supports this notion.[23] The appearance of new quark thresholds will, predictably, have an impact on $F_2(Q^2)$ which can be separately determined. Such a contribution cannot scale!

Use the definition of the structure function $F_2(\nu, Q^2)$ through the inelastic scattering cross section

$$\frac{d^2\sigma}{d\nu dQ^2} = \frac{4\pi\alpha^2}{\nu Q^4}\left[1 - y + \frac{y^2}{2(1 + R\ (x, Q^2))}\right] F_2(\nu, Q^2)$$

with $y \equiv \nu E^{-1}$ to define, in strict analogy,

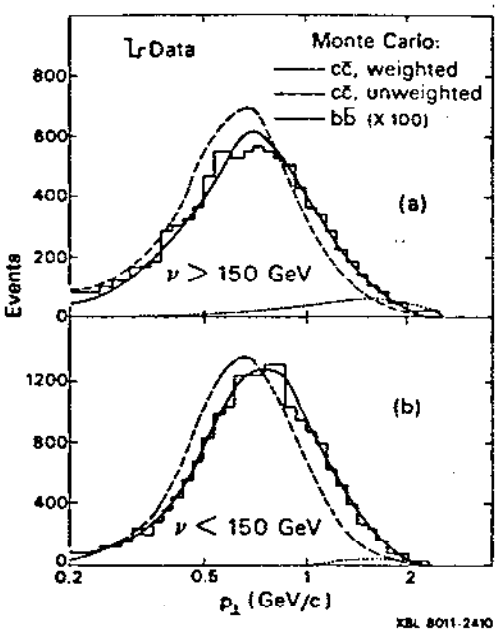

Figure 27. Characteristic $p_\perp$ behavior of open-behavior of open-b daughter muons (dotted line) together with data. Any admixture would have to be tiny.

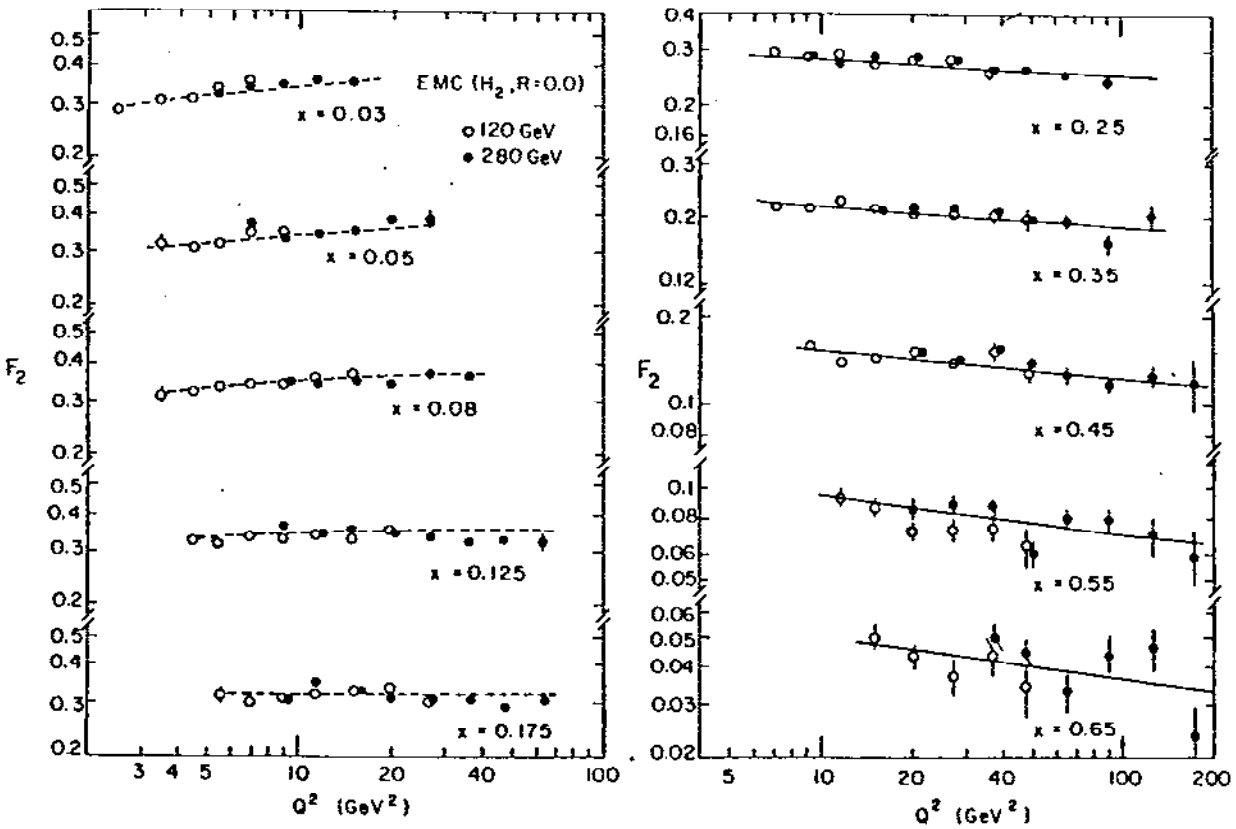

Figure 28. $F_2(Q^2)$ for 10 different x bins (EMC, hydrogen target data). Scale breaking displays characteristic QCD behavior.

$$F_2^{c\bar{c}}(\nu, Q^2) = \frac{\nu Q^4}{4\pi\alpha}\left[1 - y + \frac{y^2}{2(1+R)}\right]^{-1} \frac{d^2\sigma(c\bar{c})}{d\nu\, dQ^2} .$$

Using the BFP data from Section 2.3.3, Fig. 29[24] shows the strong Q^2 dependence of $F_2^{c\bar{c}}$ for two different energy (ν) bins. An insert in the figure, with different scale, shows that, by comparison, the Q^2 trend of the total F_2 is not remotely as strong. Now we plot these data for fixed x bins: there are only two points for the Q^2 dependence of each x bin, but the trend (Fig. 30a) is clearly strongly scale breaking:

Remember, for a scaling $F_2^{c\bar{c}}$ function, each pair of F_2 points would have to be equal within errors. A remarkable result is to be gleaned from the dash-dotted lines of Fig. 30a: if the Q^2 trend were as strong as they indicate, all scale breaking observed for F_2 could be ascribed to $c\bar{c}$ production. As it were, $F_2^{c\bar{c}}$ explains approximately one-third of the observed scale breaking of $F_2^{\mu p}$.

Lastly, Fig. 30b shows similar data due to the EMC. γGF calculations are in clear accord with the data from both collaborations.

2.4 What Have We Learned From Virtual Photoproduction of $Q\bar{Q}$?

We conclude Section 2 by a checklist of results we obtained, results that eluded us, explanations that work, models that don't, and questions which will weigh on our minds as we advance to more complicated systems in the coming sections:

a. No exclusive hadronic final state has been observed to date. All information comes from inclusive decay lepton data; its interpretation hinges on the validity of models for production and decay mechanisms.

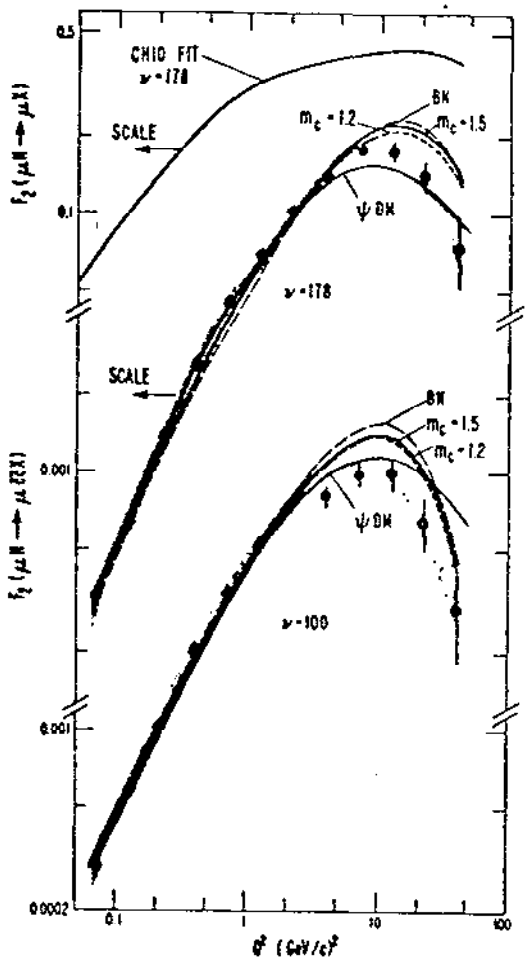

Figure 29. Comparison of F_2^{charm} with $F_2^{\mu N}(Q^2)$. Steeper dependence for charm part is obvious (BFP).

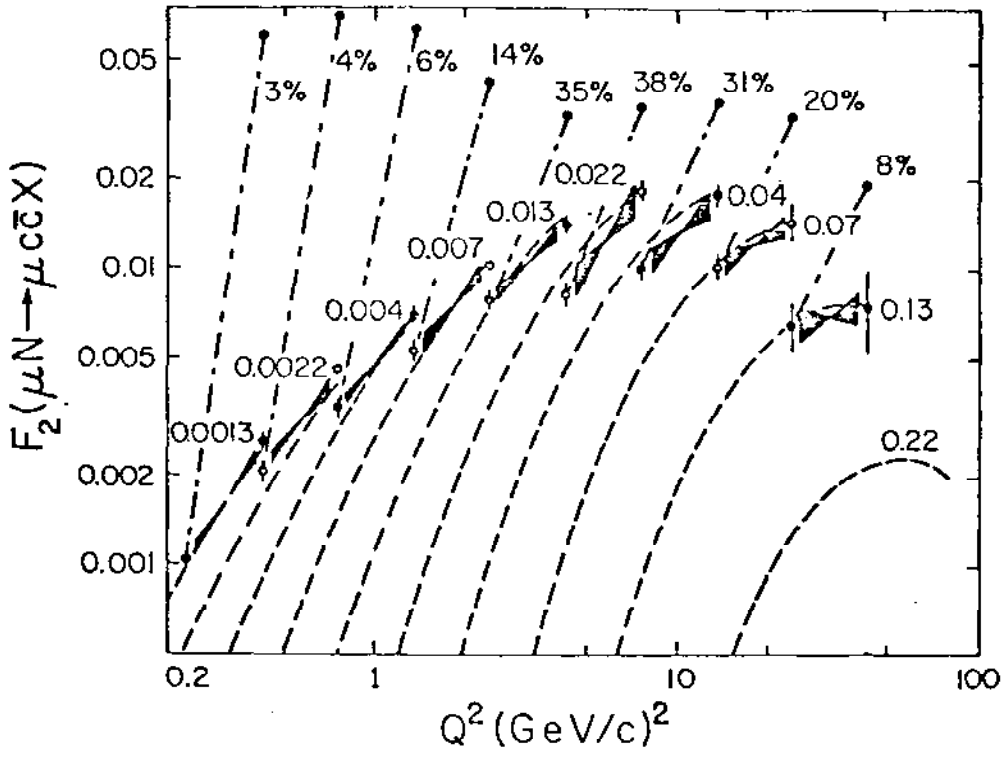

Figure 30. a) F_2^{charm} vs. Q^2 for separate x bins with γGF fits (dashed lines), with typical data errors. Dashed-dotted lines: what it would take for F_2^{charm} to explain all scale-breaking (BFP).

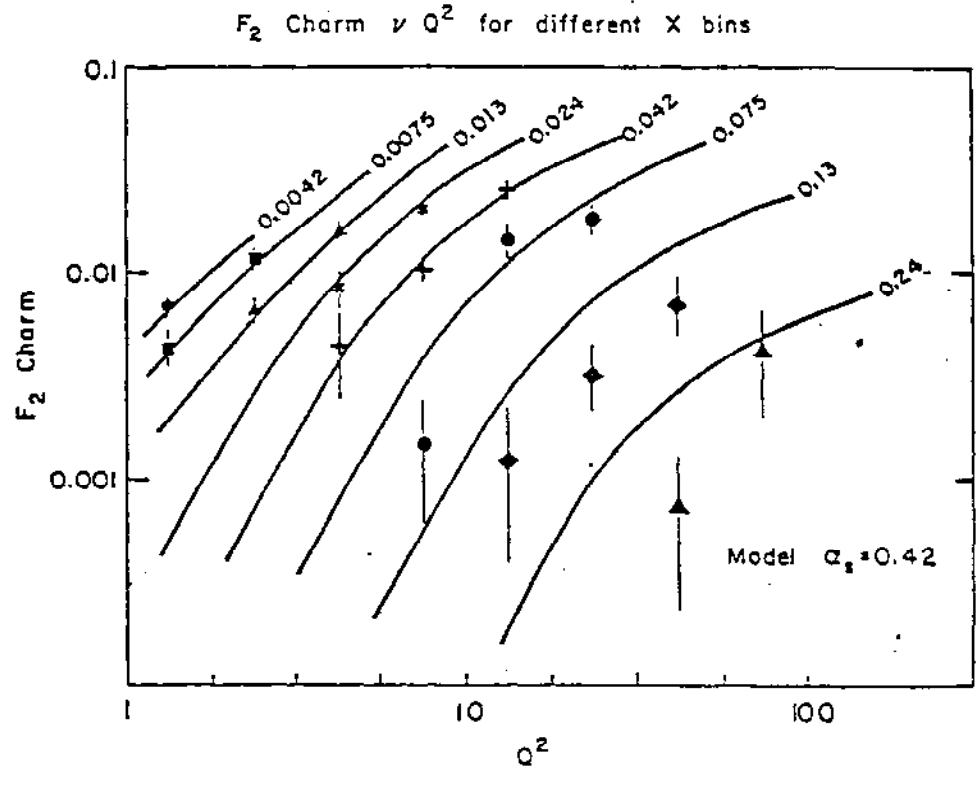

Figure 30. b) Similar data from EMC.

b. The simple parton model does not explain the observed features of heavy-quark production.

c. Similarly, the vector-meson dominance model does not give quantitative agreement, but it gives useful approximate ideas, particularly on production and decay of heavy $Q\bar{Q}$ systems.

d. The lowest-order QCD graph, corresponding to the Bethe-Heitler graph in quantum electrodynamics, gives an adequate description of $c\bar{c}$ production if appropriate parameters are chosen:

$$m_c = 1.5 \text{ GeV}/c^2,$$
$$g(x) = \frac{3}{x}(1-x)^5,$$
$$\alpha_s(Q^2) = 1.5\,[\ell n\, m^2(c\bar{c})]^{-1}.$$

It must be stressed that this so-called photon-gluon fusion model contains somewhat arbitrary scale factors. Its success is mainly sensitive to the form chosen for the gluon distribution.

e. Heavy-quark (mainly $c\bar{c}$) production is responsible for about one-third of the observed scaling violations of $F_2^{\mu N}$.

f. There is no compelling signal yet for $b\bar{b}$ production from space-like photons.

g. The extrapolation of the data shown here to $Q^2 = 0$ will have to be compared to $Q\bar{Q}$ production from real photons.

h. At this stage, there is no need to postulate the existence of an intrinsic, long-lived $Q\bar{Q}$ component in the nucleon wave function.

What do we expect from the next generation of muoproduction experiments? Above all, we need to gain access to detailed features of primary reaction fragments and their decays: we need to see interaction and decay

vertices, construct invariant-mass plots, and observe decay lengths of heavy hadrons. Moreover, a fuller exploration of Q^2 and ϕ dependence should tell us more about the merit of vector dominance concepts in the spacelike domain.

3. Heavy Flavors From Real Photons

3.1 Basic Notions:

As we take a step from the "point-like" probe of the nucleon force field, as which we have viewed the spacelike photon, to the light-like photon, it is worthwhile to think seven years back, when the first $Q\bar{Q}$ system was observed. Those observations were open to various interpretations at the time, as every wished-for phenomenon was tentatively identified with the revolutionary discovery: was the J/ψ indeed a heavy quark-antiquark system? Was it a deeply bound baryon-antibaryon state, the intermediate vector boson, a gluonium? At that time, a splendid confirmation came from the wide-band photon beam at Fermilab, that indeed the new state was hadronic in character: the invariant-mass spectrum of dimuons produced in a Be target showed[25] (Fig. 31a) not only a clear mass peak at the ψ mass, but a coherent forward production peak (Fig. 31b); the first confirmed a direct coupling of the new state to the real photon, just like ρ^0, ω, ϕ; the second gave a remarkably small diffractive production slope off nucleons:

$$\frac{d\sigma}{dt}\,(\gamma N \to \psi N) \sim e^{bt}, \text{ with } b \simeq 2(\text{GeV/c})^{-2},$$

indicating a very small hadronic system. The coherent peak, finally, established the hadronic character of the new state.

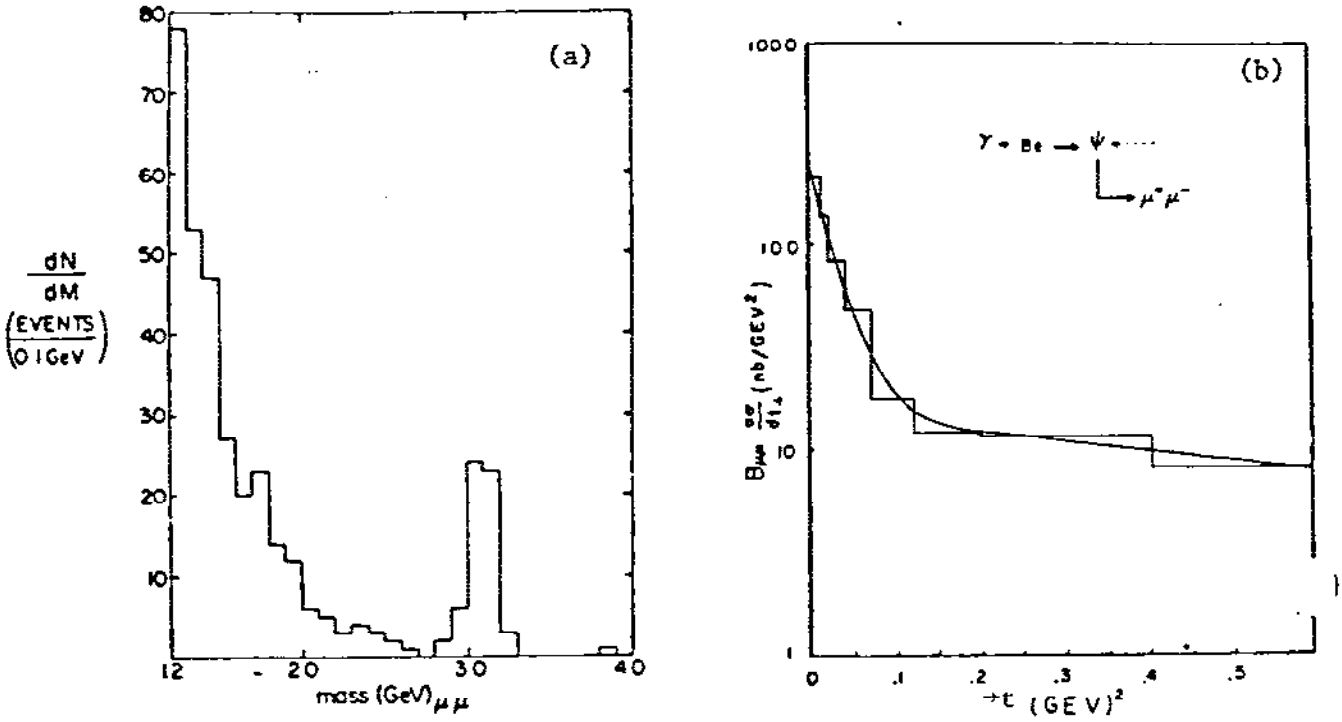

Figure 31. Production of μ pairs in wide-band photon beam at FNAL. a) mass distribution with ψ peak; b) t dependence of peak, with two characteristic slopes.

Today, we take it for granted that ψ and Υ (plus their radial excitation states) take their place among the vector hadron states that share all quantum numbers with the real photon; normal notions on unitary symmetry are then expected to tell us about the photon coupling to the new $Q\bar{Q}$ vector states.

How then do we expect heavy flavors to manifest themselves in γN collisions? The same experiment that so unexpectedly observed them in the $\mu\mu$ final state also quickly found out[26] that photoproduction is not an easy panacea for spectroscopists and invariant-mass bump hunters. Where appropriate kinematics conditions prevail, we will look for signals due to the heavy $Q\bar{Q}$ component of the hadronic photon in the total hadronic cross-section $\sigma^{tot}(\gamma p)$, in the structure of the elastic diffraction peak; we will investigate elastic and inclusive production of charmonia and "bottomonia," and finally the production of open-charm states. The neutral incoming beam opens this latter field up to cumulative but highly resolving visual techniques, where decay vertices can be separately studied.

3.2 Principal Models

How does our model approach change as we move from spacelike to lightlike photons? The point-like component is always present,[27] but will reveal itself mostly in large-transverse-momentum processes. As kinematic régimes open up, there will be an evolution

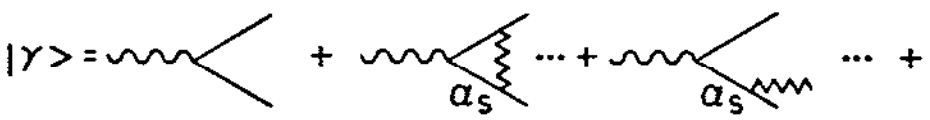

(point) soft part: vecto-hadron vector hadron plus gluon

3.2.1 Vector Dominance

With appropriate loops in the second and third terms, we have the vector dominance picture

which[28] views the hadronic photon interaction as a sum over neutral vector interactions weighted by couplings that are dictated by unitary symmetry and kinematical considerations:

$$\sigma(\gamma p) = \sum_{V^0} \frac{4\pi}{\gamma_V^2} \sigma(V^0 p).$$

The application of these ideas, so successful for soft processes involving light-quark states, is not obvious for $Q\bar{Q}$ systems the masses of which make the real photon much farther removed from their respective poles.

The first experiment to test these notions was the total hadronic cross-section measurement at Fermilab.[29] While its normalization to lower-energy data was problematical, it established the possibility of an increase in $\sigma_{tot}(\gamma p)$ above charm threshold by up to 6 μb. Fig. 32 shows that, in this context

$$2 \leq \Delta\sigma_{tot}(\gamma p) \leq 6\mu b,$$

where we would then add, $\sigma_{Q\bar{Q}} \leq \Delta\sigma_{tot}$. The upper limit given here corresponds to a sizeable heavy-vector contribution which, if in fact present, is the first "intrinsic" heavy flavor we are encountering: it should show up in diffraction and fragmentation.

Letus look at elastic photon proton scattering first: it is well established that, at low energies, the elastic diffraction peaks for

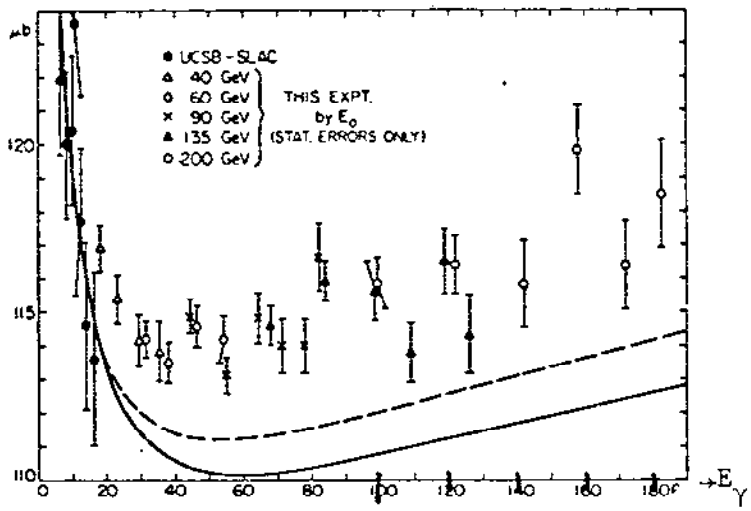

100

Figure 32. Total hadronic photon scattering cross-section at high energies (FNAL Exp. 25). Lines indicate smooth fitting to low-energy data. Excess ~ 2-6 μb.

$\gamma p \to \gamma p$ and the quasi-elastic peaks for $\gamma p \to \rho^0 p$, $\gamma p \to \omega^0 p$ have the same slopes, whereas we saw in Fig. 31a that, for a $c\bar{c}$ system, the slope parameter is $b_\psi \simeq 2(\mathrm{GeV/c})^{-1}$. A recent proton Compton scattering experiment showed that (Fig. 33) the double exponential fits to this process, measured by the Santa Cruz group in the tagged photon beam at Fermilab[30] are remarkably close to those describing quasi-elastic ω^0 photoproduction measured in the same experiment, although these data span (well-defined) photon energies in the 100 GeV region. For soft processes, we then have to resort to explicit hadronic final states to reveal the $Q\bar{Q}$ component of the photon. For the diagram Fig. 34, we expect, in the SU(4) limit, a coupling ratio

$$\frac{1}{\gamma^2_{\gamma\phi}} : \frac{1}{\gamma^2_{\gamma\omega}} : \frac{1}{\gamma^2_{\gamma\phi}} : \frac{1}{\gamma^2_{\gamma\psi}} = 9 : 1 : 2 : 8.$$

The FNAL wide-band beam experiment[25] had already revealed that the ψ is a very small object, yielding a total scattering cross-section $\sigma(\psi p) \sim 1 - 2$ mb, and in fact, it is well established for ρ photoproduction that its importance w.r.t. the total hadronic photon cross-section decreases rapidly (Fig. 35) as the "large" lightlike photon goes to a "smaller size" in the space-like region.

3.2.2 QCD Evolution

To what extent is photon "evolution" parallel to the gluon's evolution as seen in Section 2.2.3 above? Starting with the color singlet photon, we can define a similar sequence that differs only in the first step

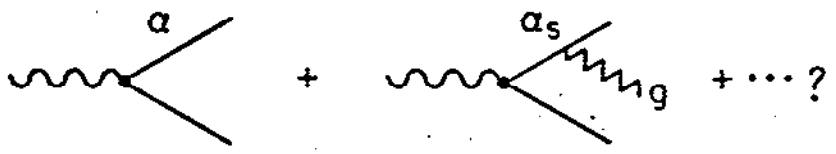

the "unveiling" of the photon state function[27] then depends on the off-shell energy ε available: in general,

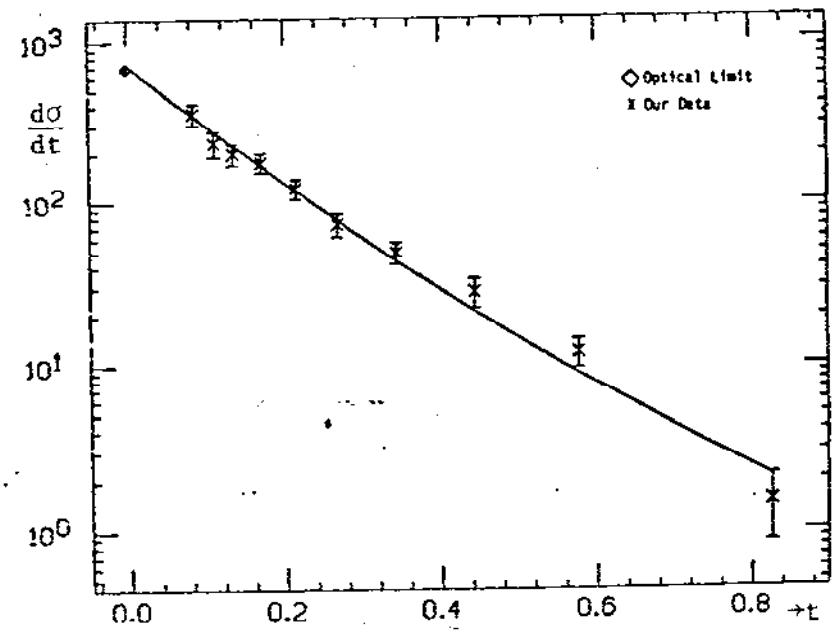

Figure 33. Elastic scattering of tagged photons (FNAL Exp. 152), t distribution. Double exponential fit is characteristic of light-quark component of photon.

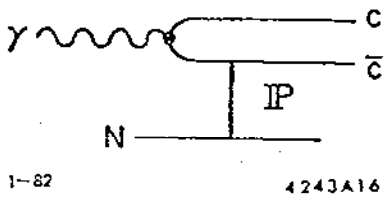

Figure 34. Diffractive photoproduction of heavy vector states.

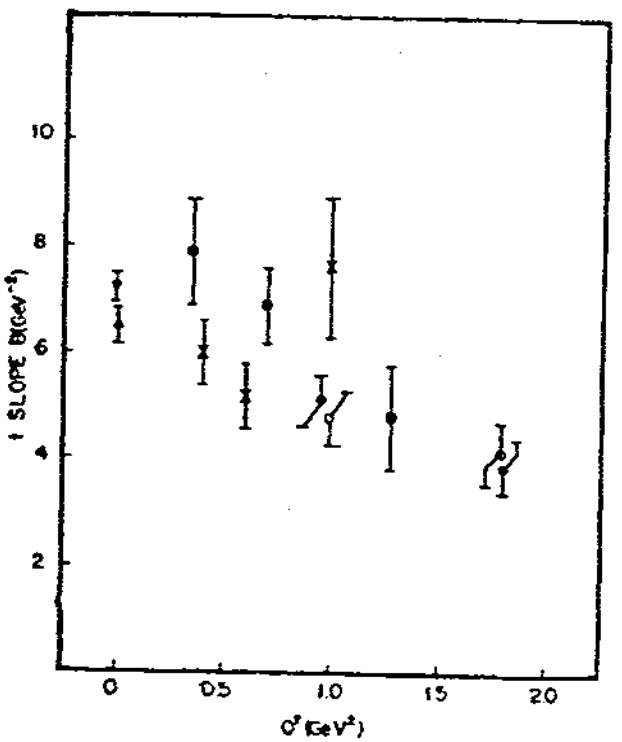

Figure 35. Q^2 dependence of diffraction peak slope for ρ^0 electroproduction data from various groups.

$$\varepsilon = m^2 - \Sigma(k_\perp^2 + m_Q^2)x^{-1}.$$

For the real photon, $m^2 = 0$; the second term denotes the "binding energy." The distance to be probed then clearly is $d = \varepsilon^{-1}$. Here is an important hint to the experimentalist: If, for given ε, you want to probe for higher masses m_Q or larger $k_\perp$, do it at $x \to 1$! For small x, the effect will be correspondingly small.

The lowest-order QCD graph is, as in the electroproduction case (section 2.2.2) the γGF model (strong Bethe-Heitler)

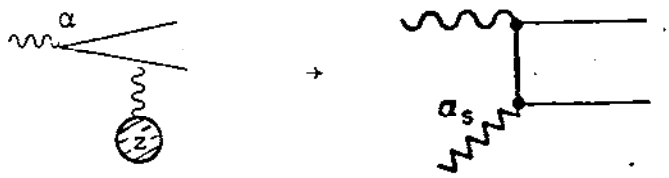

which, here, probes the gluon content of the target, g(x). For $Q^2 = 0$, it is straightforward to write down the cross section

$$\frac{d\sigma}{dM^2_{Q\bar{Q}}} = \frac{1}{s}\ \sigma_o\ (M^2)\ g(x) \qquad \text{with } x = \frac{M^2}{s}\ ,$$

where σ_o is the total cross-section for the subprocess $\gamma g \to Q\bar{Q}$,

$$\sigma_o = \sigma_{BH} \cdot \frac{1}{2} Z_Q^2 \frac{\alpha_s}{\alpha}$$

(the factor $\frac{1}{2}$ is due to color averaging). We then obtain

$$\sigma_o(M^2_{c\bar{c}}) = \frac{1}{2} Z_Q^2\ \alpha\alpha_s\ \frac{4\pi}{M^2}\ \{(1 + \frac{4m_Q^2}{M^2} - \frac{8m_Q^4}{M^4})\ \ln\frac{M^2}{2m_Q^2}\ (1 + \ldots)\}\ .$$

A glance at these formulae points up these features:

a) it will be peaked at small values M^2_{QQ};

b) it has a large lab rapidity;

c) the recoiling B = 1 system will be dominated by the proton.

3.3 Experimental Evidence

3.3.1 Neutral Vectors: Quasi-Elastic Production

In addition to the Fermilab wide-band beam data (section 3.1), early SLAC photoproduction results[31] revealed clear spectrometer data for $\psi \to e^+e^-$ and $\psi \to \mu^+\mu^-$. A strong energy dependence was observed at these low energies ($E_\gamma \lesssim 20$ GeV) by a combination of the two large spectrometers in Endstation A (Fig. 36a). A diffraction peak with slope parameter b = 2.9 was observed (Fig. 31b) (somewhat larger than the high-energy value); it may well be due to the presence of an inelastic component. Data were taken with Deuterium, Be, and Fe targets, yielding the energy dependence of the $\gamma N \to \psi N$ cross section (Fig. 31c). The small value of $\sigma_{\gamma p}$ is less astonishing than the energy trend: it is strongly reminiscent of the γGF energy trend: the vector dominance picture, which does not predict an energy trend at all, describes the high-energy régime at best!

Efforts to separate elastic events from inelastic ones are presently under way using FNAL data. That will provide an important firming up of these data.

3.3.2 D-Meson Photoproduction:

In contrast to muoproduction, photoproduction of charmed (or heavier-Q) particles is best studied with a highly instrumented spectrometer close to (or surrounding) a thin target. Detailed track fitting then becomes feasible. The most interesting results come from a prolonged study using the Omega spectrometer at CERN in an intermediate-energy tagged photon beam. Remember, however, that it took a long time to identify D meson production from e^+e^- annihilations at SPEAR despite the fact masses and decay properties had been relatively closely predicted -- and in that case, there were no fragmentation products from a nucleon target to confuse the final state!

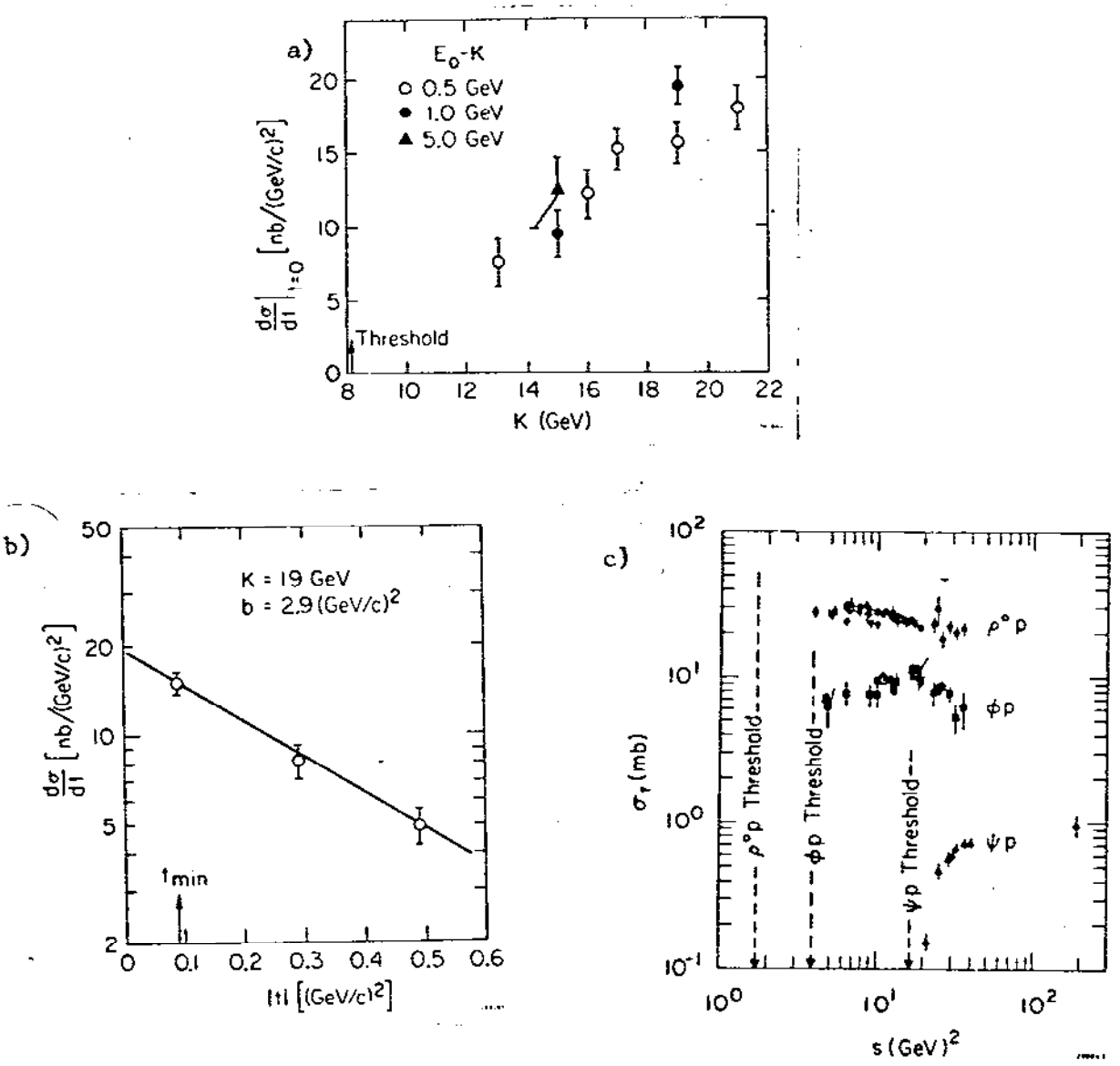

Figure 36. ψ photoproduction at SLAC energies: a) energy trend; b) same, comparison with ρ^0,ϕ^0 production; c) t dependence.

The beam provided 2 χ 20^5 tagged γ's per spill with $E_\gamma < 80$ GeV. The apparatus is schematically drawn in Fig. 37: it is seen that particle identification is incorporated as well as final state shower detection. The WA-11 Collaboration found[32] small but consistent signals for

$$\bar{D}^o \to K^+\pi^- ,$$
$$\to K^+\pi^-\pi^o ,$$
$$\to K^o_s\pi^+\pi^- .$$

These signals, shown in Fig. 38, have small statistical significance: about 3 S.D.'s (If there were no lines to guide your eye and you had never heard of D's, you might not be so convinced).

Note there is no evidence for D^o production--an important point, because it indicates associated production with a baryon -- as we would expect from a process close to threshold:

$$\gamma N \to \bar{D}\Lambda_c + \ldots$$

but not $$\to D\bar{D}_N + \ldots$$

The extraction of a cross-section involves a guess as to the x_D distribution: it is taken to be flat in p. A resulting cross-section is quoted to be

$$\sigma(\gamma N \to \bar{D}^0 + \ldots) = 525 \pm 160 \text{ nb.}$$

From Fermilab, there are published data on both D and D* production from the wide-band beam. This beam, while more intense than the tagged photon beam, has not only no energy definition, but also some unavoidable K^o and neutron backgrounds. The experiment (Fig. 39) incorporates some particle identification in addition to charged-particle momentum analysis, notably K/π separation for the range 6 - 20 GeV. Fig. 40 shows how hard this approach is:[33]

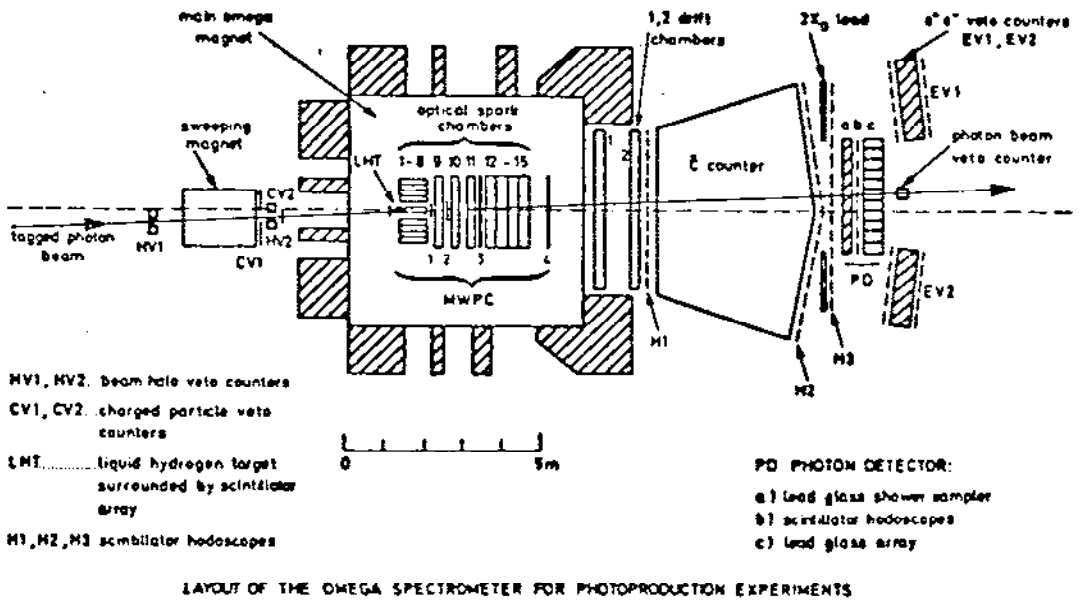

LAYOUT OF THE OMEGA SPECTROMETER FOR PHOTOPRODUCTION EXPERIMENTS

Figure 37. The Ω spectrometer in its photoproduction guise. Tagged photon beam was limited to < 80 GeV.

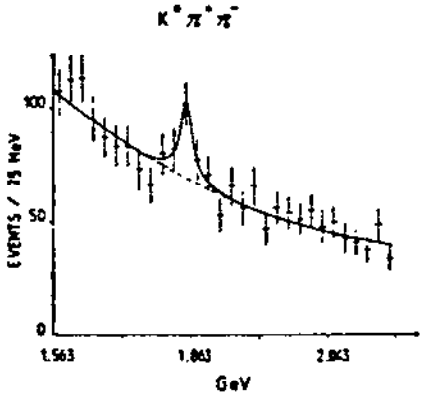

Figure 38. Various mass plots for Kπ systems, from Ω spectrometer. D signal is seen in three different channels.

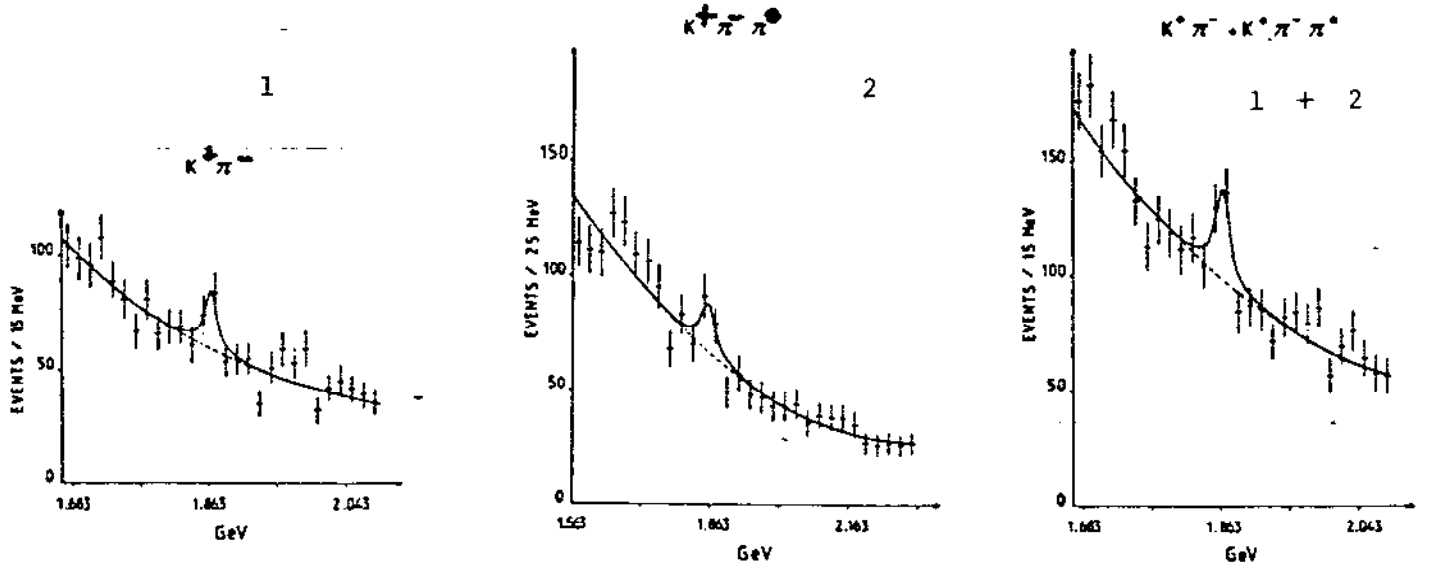

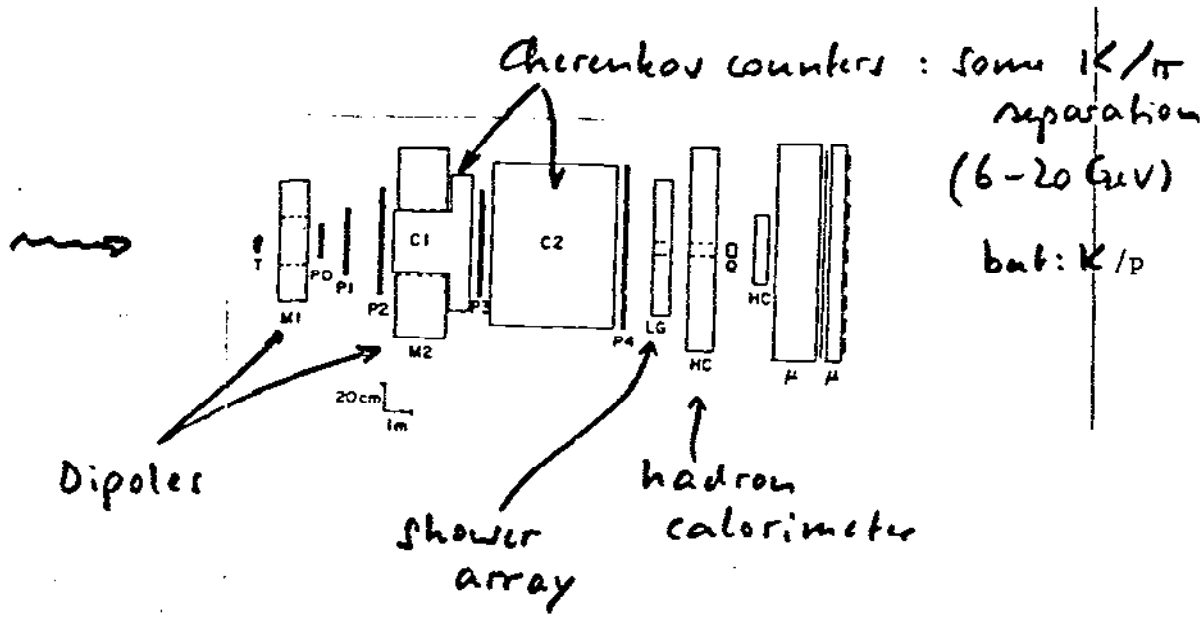

Figure 39. Photoproduction spectrometer in wide-band beam at FNAL. An all-purpose array.

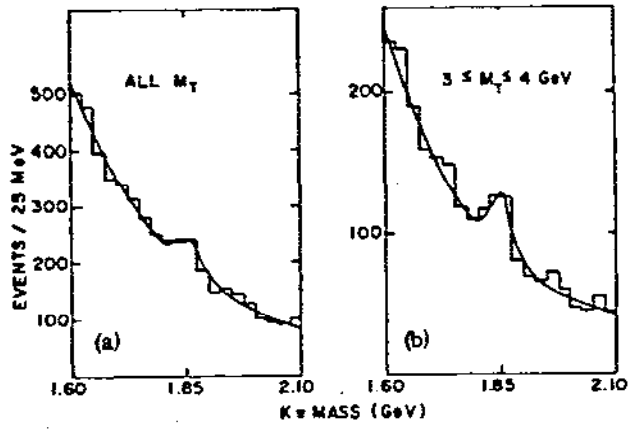

Figure 40. K mass distribution from FNAL Exp. 87. Transverse mass selection enriches signal (b).

a bump at the D mass for both the $K^-\pi^+$ and $K^+\pi^-$ systems appears only after the data, due to beam energies from 50 to 200 GeV, are cut on a number of criteria, including (Fig. 40b) the total invariant mass of the event. Even so, the authors[33] estimate that 75% of the entries in the plot are induced by the K^O component of the beam. Acceptance modelling assumes <u>pair</u> production and would indicate

$$\sigma(\gamma p \to D^O\bar{D}^O + \ldots) = 720 \pm 290 \text{ nb};$$

no signal was found in any other channel ($K2\pi$, $K3\pi$).

From the same experiment, an analysis[34] searching for D* photoproduction with subsequent decay $D^* \to D^O\pi^\pm$ started from all $(K\pi\pi)^\pm$ systems, then checked on the mass difference Δm between the $K\pi\pi$ and $K\pi$ systems. Only for the $K\pi$ band $m \sim m(D)$ was there an enhancement at $\Delta m \simeq m_\pi$ (Fig. 41). Cuts based on this observation produced a signal (Fig. 42a) in the $(K\pi)^O$ signal, which could also be seen in an event sample allowing for $D^O \to K^O_S\pi^+\pi^-$ (Fig. 42b). An observed ratio of $D^{*+}/D^{*-} = 1.4 \pm 0.4$ indicates pair production rather than $\Lambda_c\bar{D}$ associated production. Acceptance modelling, assuming a production cross-section flat in energy for $E_\gamma > 50$ GeV, then produces the result

$$\sigma(\gamma p \to D^* + \ldots) = 118 \pm 49 \text{ nb}.$$

3.3.3 Photoproduction of F Mesons

Controversial evidence on the observation on the $(c\bar{s})$ system in e^+e^- reactions has heightened interest in identifying the F meson in other interactions. A concerted effort by the Omega Spectrometer Collaboration at CERN made use of the $(c \to s)$ decay to look for $(s\bar{s})$ systems, notably the η^0 and ϕ^0.

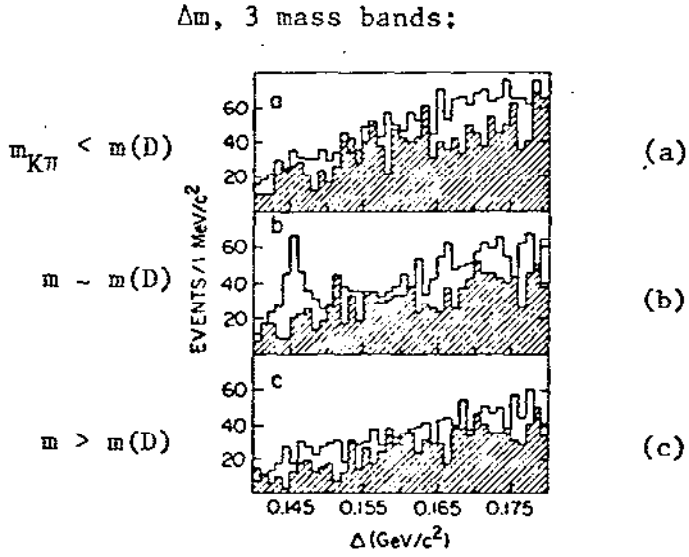

Figure 41. Mass differences $\Delta \equiv m(K^-\pi^+\pi^+) - m(K^-\pi^+)$ for three mass bands: a) below; b) at; c) above $m(K^-\pi^+) = m(D^0)$. FNAL Exp. 87.[34]

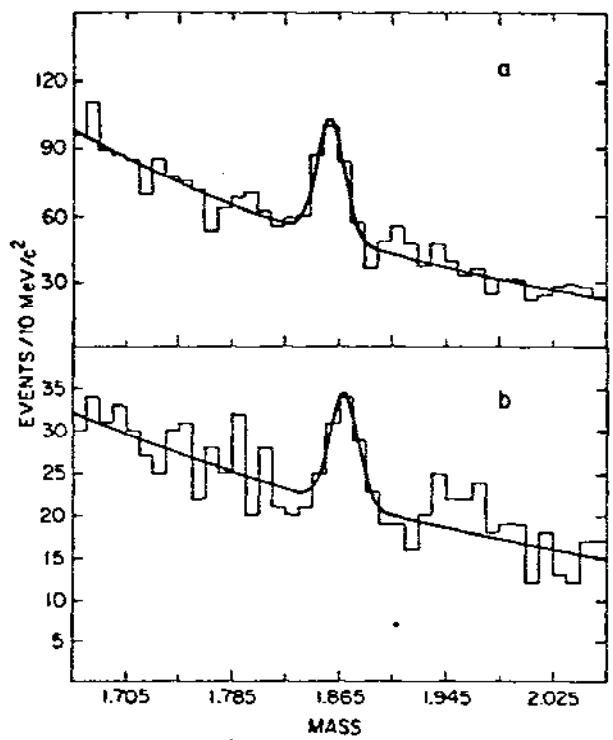

Figure 42. a) Mass plot for $K^-\pi^+$ systems with $0.1425 < \Delta < 0.148$;
b) Mass plot for $K^-\pi^+\pi^+$ systems with $0.1445 < \Delta < 0.1465$ GeV/c^2.[34]

First, a total luminosity of 110 events/nb was used[35] to cut data on the presence of $\eta(\to 2\gamma)$ in the final state. Plotting invariant mass combinations for $m(\eta + N\pi)$ with N = 1, 3, 5 then leads to the plots shown in Fig. 43. With a quoted 4 S.D. significance, a signal emerges for $m_F = 2.02 \pm 0.01$, well compatible with the predicted mass. Note that, weak as this signal may appear, it constitutes the only reasonable evidence for F production in any reaction, Acceptance modelling again involves the assumption of pair production, and leads to a photoproduction cross section of

$$\sigma(\gamma N \to F + \ldots) \times \text{B.R. } (F \to \eta + N\pi) \simeq 100 \text{ nb},$$

where the N = 1 mode contributes 27, N = 3 some 60, N = 5 (mostly due to $F \to \eta' 3\pi \to \eta 5\pi$) about 20 nb.

Second,[36] a search for F production with subsequent decay into modes containing a ϕ meson (together with 1, 2, or 3 pions) produced the result displayed in Figs. 44a,b: the $\phi\pi^{\pm}\pi^0$ mass spectrum (Fig. 44a), if cut on the F mass band, appears to show a prominent ρ component in the $(\pi^{\pm}\pi^0)$ system. Assuming then a decay $F^{\pm} \to \rho^{\pm} \phi^0$, the authors showed the same data as before after requiring $m(\pi^{\pm}\pi^0) \simeq m_\rho$. The result, as seen in Fig. 44b, is quoted as containing a 3 S.D. signal at a $(\phi\rho)$ mass slightly lighter than the F mass quoted above: $m(F \to \phi\rho) = 2.049 \pm 0.015$ GeV/c. They further quote

$$\sigma(\gamma N \to F + \ldots) \times \text{B.R. } (F \to \phi\rho) = 33 \pm 10 \text{ nb}.$$

No effect is observed in the $\phi\pi$, $\phi\pi\pi\pi$ systems (Fig. 45).

3.3.4 Photoproduction of Λ_c Baryons

Starting from a γp or γn initial state, we clearly expect associated production of $\Lambda_c \bar{D}$ to be a dominant mechanism for Λ_c photoproduction. Early indications from FNAL[37] that a large $\bar{\Lambda}_c$ signal was found with no recognizable Λ_c were therefore a bit shocking. In a recently published analysis of data from the broad-band photon beam, based on 6×10^{11} photons with $E_\gamma > 50$ GeV,

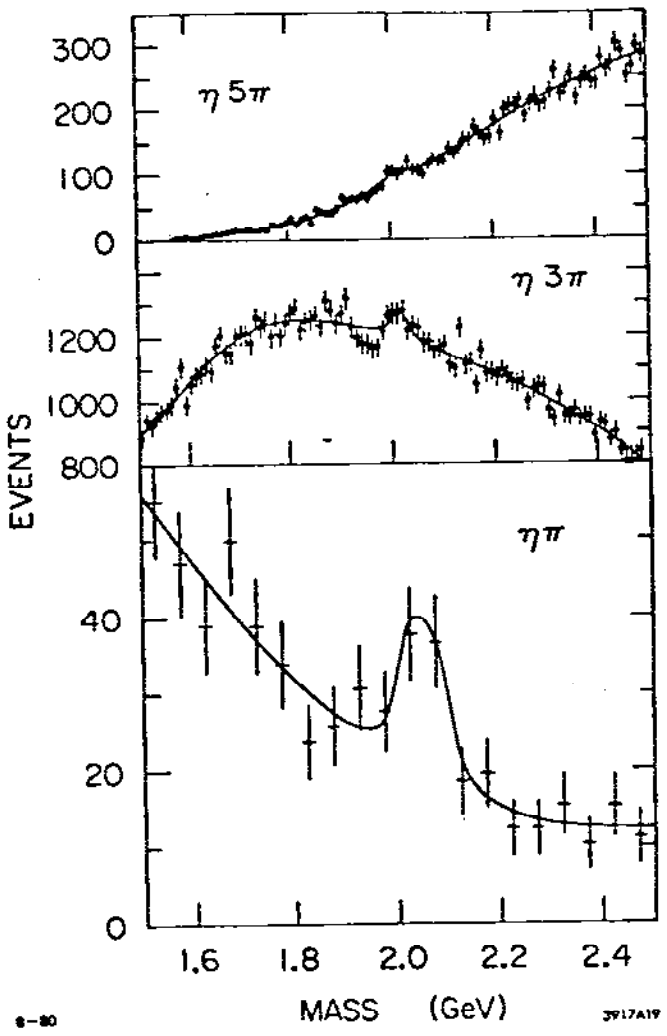

Figure 43.

Mass plots from Omega Spectrometer,[35] showing systems with an identified η plus an odd number of pions. Special selection criteria were needed to produce the signals.

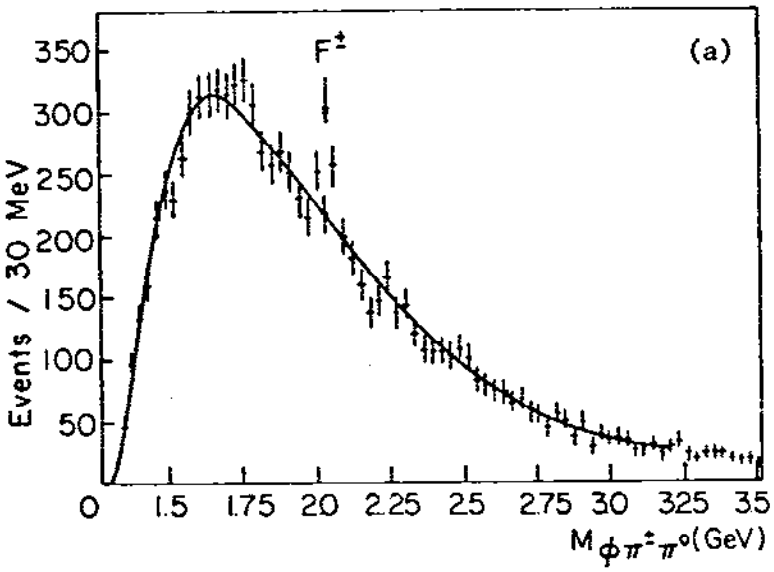

Figure 44.

a) Mass plot for $m(K^+K^-\pi^{\pm}\pi^0)$, with $m(K^+K^-) \approx m_{\phi}$

b) Same plot, but additional constraint on $m(\pi^{\pm}\pi^0) \approx m_{\rho}$.

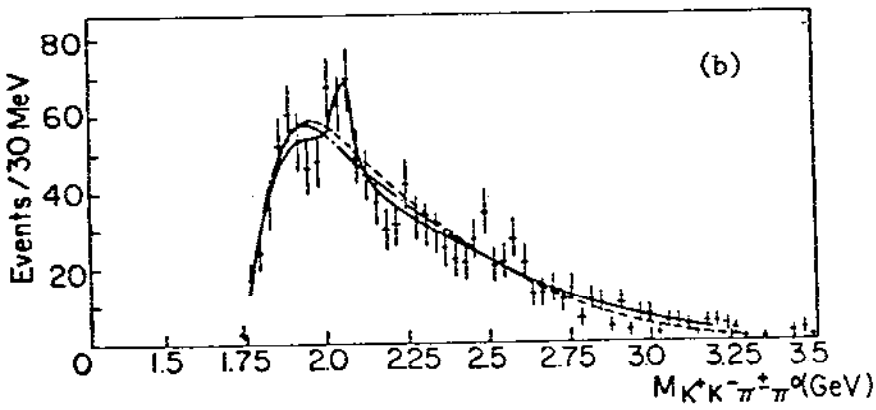

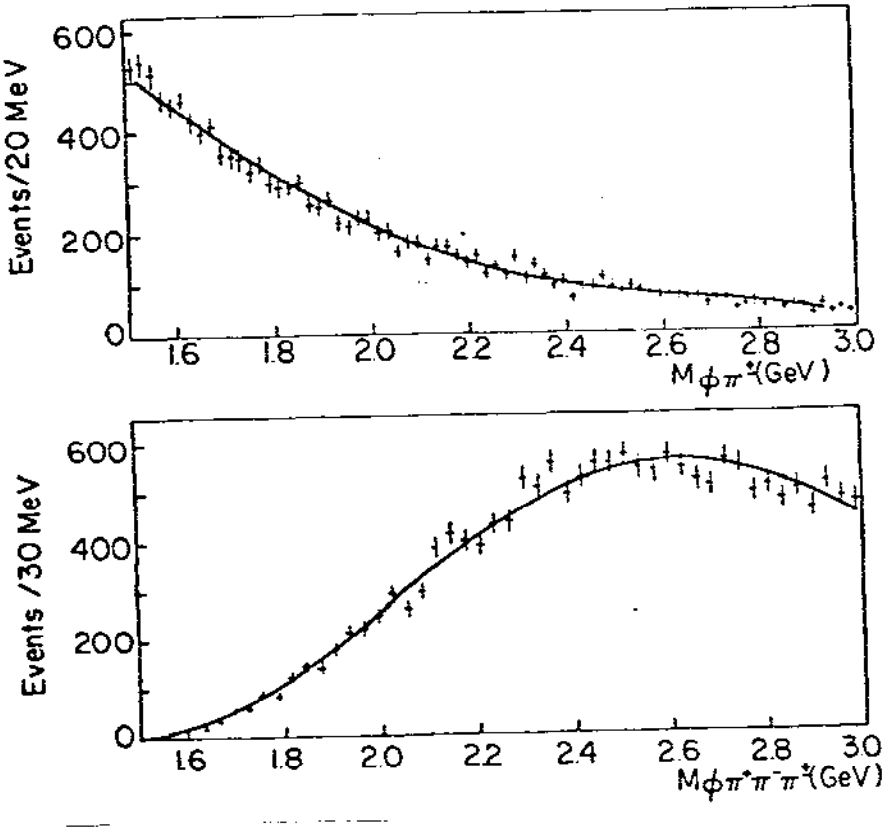

Figure 45. Mass plots for a) $\phi\pi^{\pm}$ and b) $\phi\pi^{+}\pi^{+}\pi^{-}$ systems: no signal is recognizable at F mass.[36]

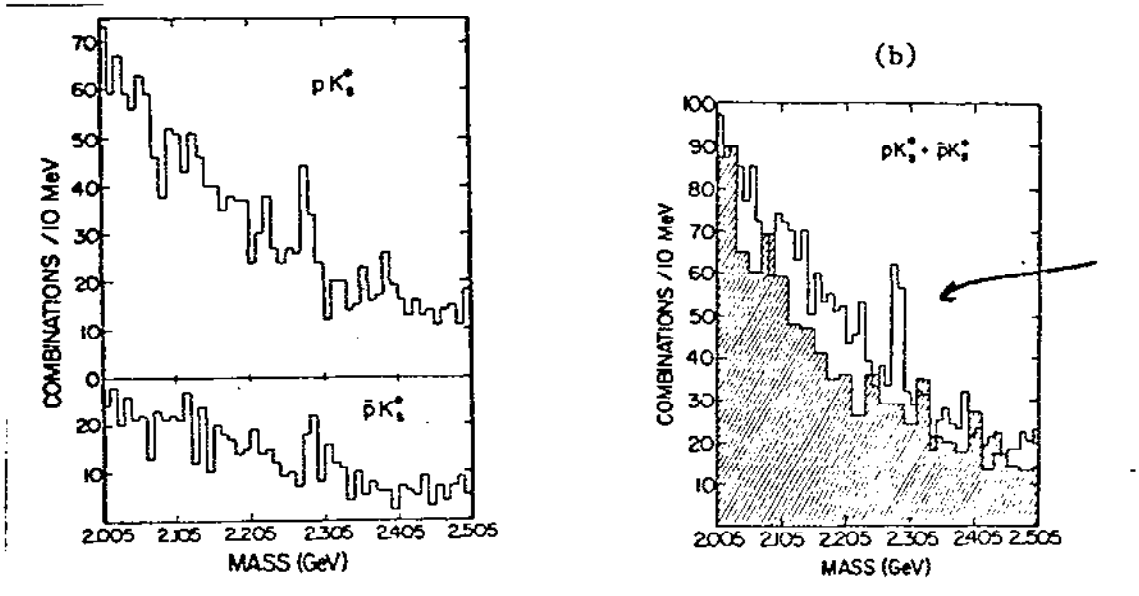

Figure 46. Search for Λ_c at FNAL:[37] a) mass plots for pK^0_S systems; b) same for $\bar{p}K^0_S$. Effect at Λ_c is comparable in size for both charge states. c) Added distribution. Shaded area: distribution after insertion of $6x^0$ of Pb in beam.

Russell et. al.[38] report on a search for Λ_c signals in Kp..., $K\bar{p}$... and $\Lambda\pi$..., $\bar{\Lambda}\pi$... systems. To eliminate some of the difficulties of the previous experiment, a data sample was taken after insertion of 6 radiation lengths of Pb into the beam line: K^o-induced events would then continue to be seen, but γ-induced reactions would be eliminated.

Fig. 46c shows the invariant-mass plot for the combined pK_s^o and $\bar{p}K_s^o$ sample. The shaded area, representing the data with Pb in the beam, does not show the indication of an enhancement at $m(pK_s^o) = 2.284 \pm 5$ GeV/c^2 exhibited by the full data sample. In Figs. 46 a,b the data are shown separately for pK_s^o and $\bar{p}K_s^o$. The authors quote a cross section, based on $\Lambda_c\bar{\Lambda}_c$ pair production, of

$$\sigma(\gamma N \to \overset{(-)}{\Lambda}_c + \ldots) \times BR(\Lambda_c \to p\bar{K}^o) = 3.0 \pm 1.2 \text{ nb/nucleon}$$

No significant signal was found in channels corresponding to $\Lambda_c \to \Lambda + \ldots$ decays, where the original photoproduction claim had been staked.[37] The branching fraction $\Lambda_c \to pK^0$ is believed to be of order 1.5%, which then leads to

$$\sigma(\gamma N \to \Lambda_c\bar{\Lambda}_c + \ldots) \simeq 200 \text{ nb/nucleon.}$$

If taken at face value, this implies, surprisingly,

$$\sigma(\gamma N \to \Lambda_c\bar{\Lambda}_c + \ldots) \simeq \sigma(\gamma N \to D\bar{D} + \ldots),$$

a result hard to believe on intuitive grounds.

3.3.5 Data From Precision Vertex Detectors: Lifetimes

A recent bonus in the $Q\bar{Q}$ photoproduction field has been the perfection of precision vertex detectors. This aspect is covered in the Topical Conference,[39,40] so that I will limit myself to a very brief mention of this important development.

We first mention an example of the emulsion technique. While an integrating device like an emulsion stack has a priori clear disadvantages of event selection, the combination of an emulsion target ("active target") with a downstream detector permits reconstruction of promising event candidates from downstream track imformation that does involve normal timing criteria.

The event shown in Fig. 47 is from CERN Exp. WA58, where the emulsion was placed upstream of the Omega Spectrometer.[41] Each emulsion particle in the experiment was exposed to ~ 10^6 photons from the tagged beam. The virtues of a visual detector with a resolution of a few μm are obvious: the event shows a convincing candidate for an associated photoproduction event

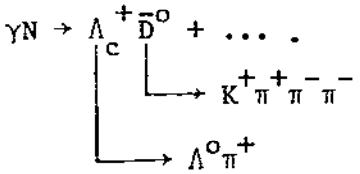

Note that all forward-emitted particles, including a Λ^0 that did not decay inside the fiducial volume of the emulsion, were identified by the Omega Spectrometer. The finite decay lengths, for Λ_c^+ and for $\bar{D}^0$, are clearly seen and yield lifetimes of order 10^{-13} sec. On the basis of few events, lifetimes for D^0 and $D^\pm$ are quoted as differing by a considerable amount:

$$\tau(D^0) = (0.58 \begin{smallmatrix} + 0.8 \\ - 0.2 \end{smallmatrix}) \ 10^{-13} \text{sec}, \ \tau(D^\pm) \approx 4.4 \times 20^{-13} \text{sec}.$$

Clearly, a triggerable device that can lead to a higher data rate will be an attractive alternative, if appropriate resolution figures can be reached. Several high-resolution bubble chambers, combined with downstream spectrometers, are taking on that challenge. In photoproduction, the SLAC Hybrid Facility[42] focuses one high-resolution camera with low field depth (6 mm) on the vertex region, while three conventional cameras take a stereo record of the entire event. The high-resolution (55 μm) camera "sees" secondary decay vertices. With selection criteria centering on a consider-

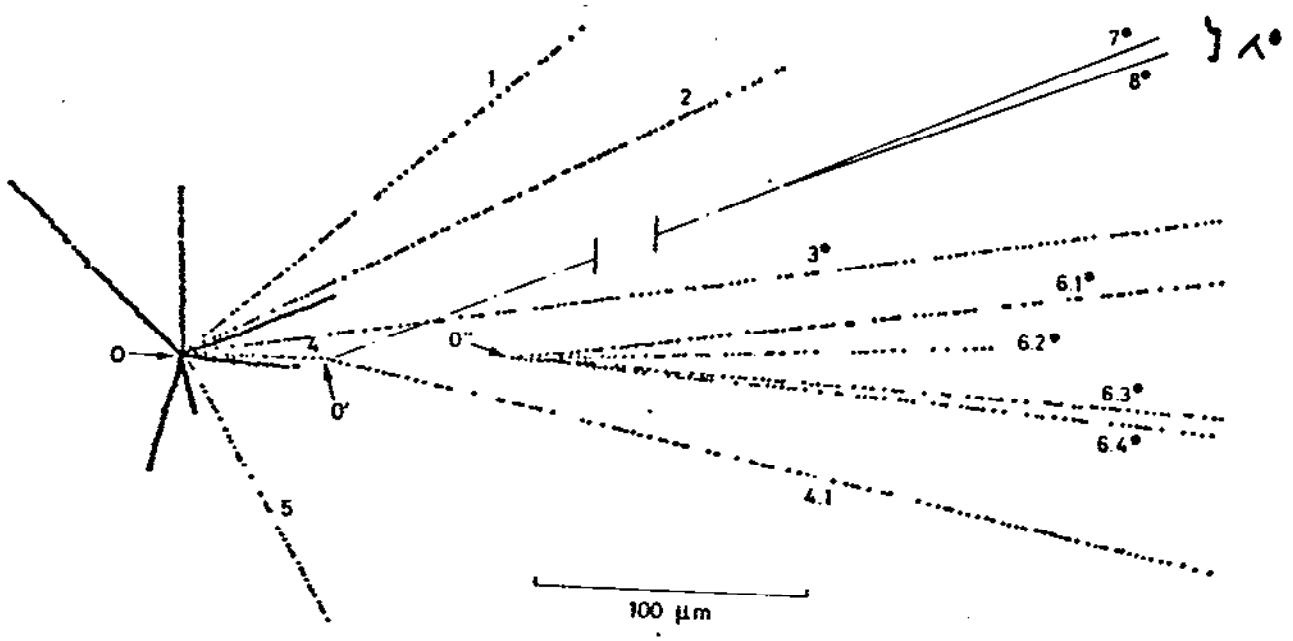

Figure 47. Emulsion event from CERN Exp. WA58. The event shows two decay vertices for $\Lambda_c \rightarrow \Lambda^0\pi^+$ and for $\bar{D}^0 \rightarrow K^+\pi^+\pi^-\pi^-$, see text.

able impact distance, 9 bona fide multiprong charm decays have been identified of these, we show an example in Fig. 48; the resulting tentative lifetimes are no longer very different for $D^{\pm}$ and D^{o}: the presently quoted numbers $(\tau_{D^{\pm}} = (5.3\ ^{+4.9}_{-1.7})10^{-13}$sec, $\tau_{D^{o}} = (2.2\ ^{+2.0}_{-0.8})10^{-13}$sec are consistent with a ratio of one.[43] The charm cross-section at the low SLAC energies is quoted as

$$\sigma(\gamma p \to c\bar{c}) \Big|_{E_\gamma = 19.5\ \text{GeV}} = (40\ ^{+40}_{-20})\text{nb};$$

3.4 What Have We Learned From Real Photoproduction of $Q\bar{Q}$ Systems?

$c\bar{c}$ production from real photons has proven valuable in several respects, but leaves important unresolved questions:

a) Diffractive photoproduction established the vector meson characteristics of the ψ. The small size of the $c\bar{c}$ system and the small value for $\sigma(\psi N)$ were determined in this channel.

b) The vector dominance model gives only very approximate notions; only a small x range close to $x \lesssim 1$ is accessible.

c) The photon-gluon fusion graph of QCD is able to account for ν dependence and for large-x processes, but does not fix the scale.

d) Spectroscopy is difficult. Most experiments are not sensitive enough, suffer from enormous combinatorics for mass plots. But: the signals for photoproduction of F mesons look suggestive and are the only such evidence anywhere.

e) Quoted cross-sections for charm photoproduction rely on uncertain assumptions ($D\bar{D}$ or $\bar{D}\Lambda_c$ production, fragmentation functions); no

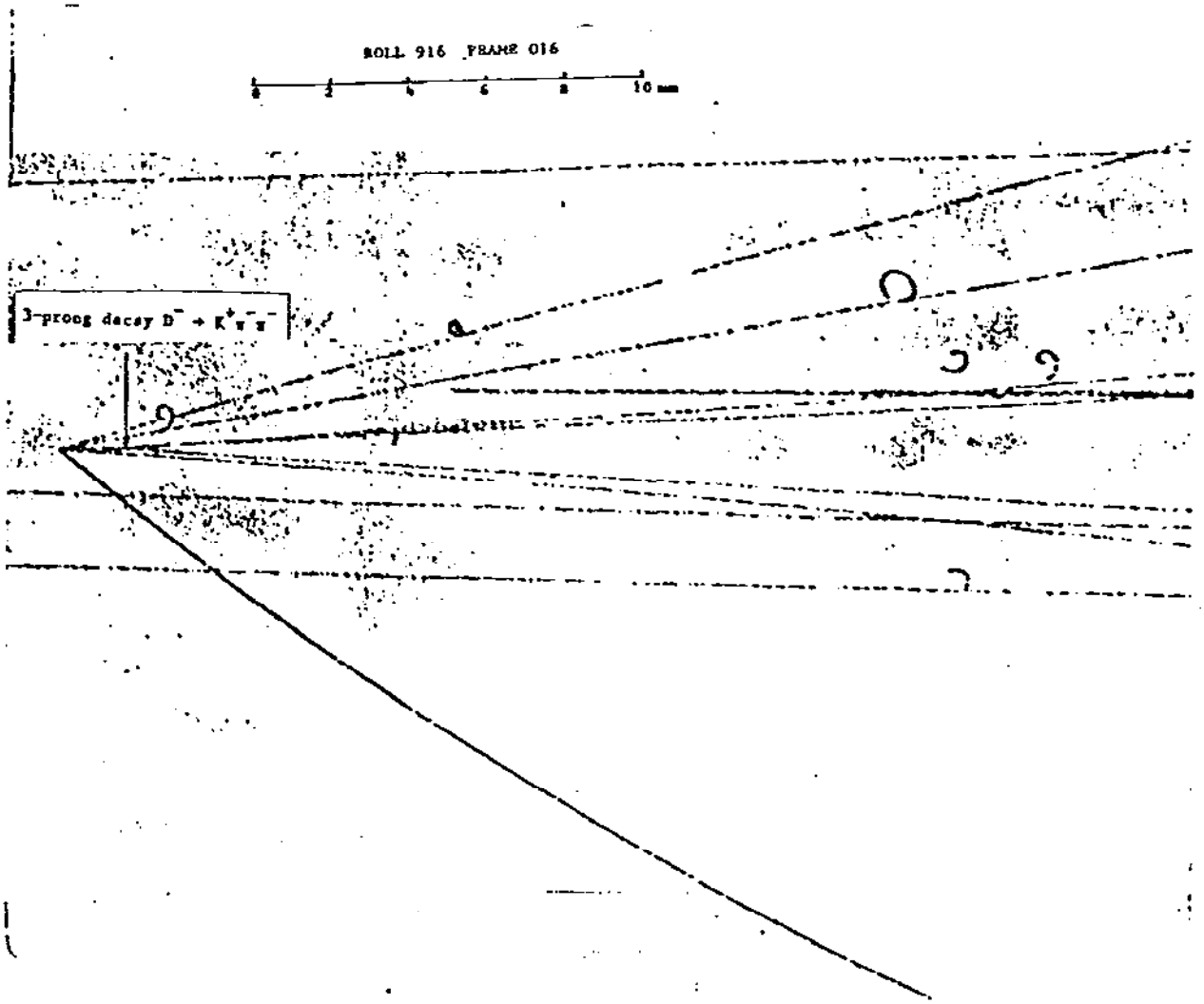

Figure 48. Event example from SLAC Hybrid Facility. Secondary vertex is indicated for $D^- \to K^+\pi^-\pi^-$ decay.[40]

individual signal is statistically compelling, but adding up published cross-sections leads to a total charm photo-production cross-section of 1-2 μb, compatible with the limit set by the $\sigma_{tot}(\gamma p)$ measurement,[29] but not saturating the "permitted" values.

f) The evidence on charmed baryon photoproduction remains problematical.

g) There is no sign of the photoproduction of $(b\bar{b})$ states, hidden or open. This may be hopeless with present luminosities.

h) Photoproduction is a very promising field for the study of decay vertices and lifetimes in high-precision detectors.

Questions raised and unanswered by our considerations include these:

VDM-inspired notions, together with suggestions of "intrinsic heavy flavors" in hadron wave functions, make us believe that the "unveiling" of the photon[27] will permit us to observe the QCD evolution of the hadronic photon. The graphs in Fig. 49 illustrate that the intrinsic $c\bar{c}$ component of a ρ-dominated hadronic photon has to be taken into account as well as the postulated[44] heavy Fock states of the target nucleon. Since soft gluon exchange may well make the vector and (pseudo-) scalar $c\bar{c}$ states comparable, some fascinating experimental signatures may be found in the target as well as the current fragmentation regions (like high-x production of η_c and negative-x ψ's). Quantitative estimates of these effects are desirable.

Photoproduction of η_c has additional virtues: Soni[45] points out its value as a probe of the gluon distributions inside the hadronic photon (Fig. 50a). Also, Primakoff graphs should be considered (50b).

Clearly, patience and hard work are needed on both the experimenter's and the theorist's side, to extract the information inherently available from photoproduction, in addition to higher luminosities and smarter selection techniques for the photoproduction facilities.

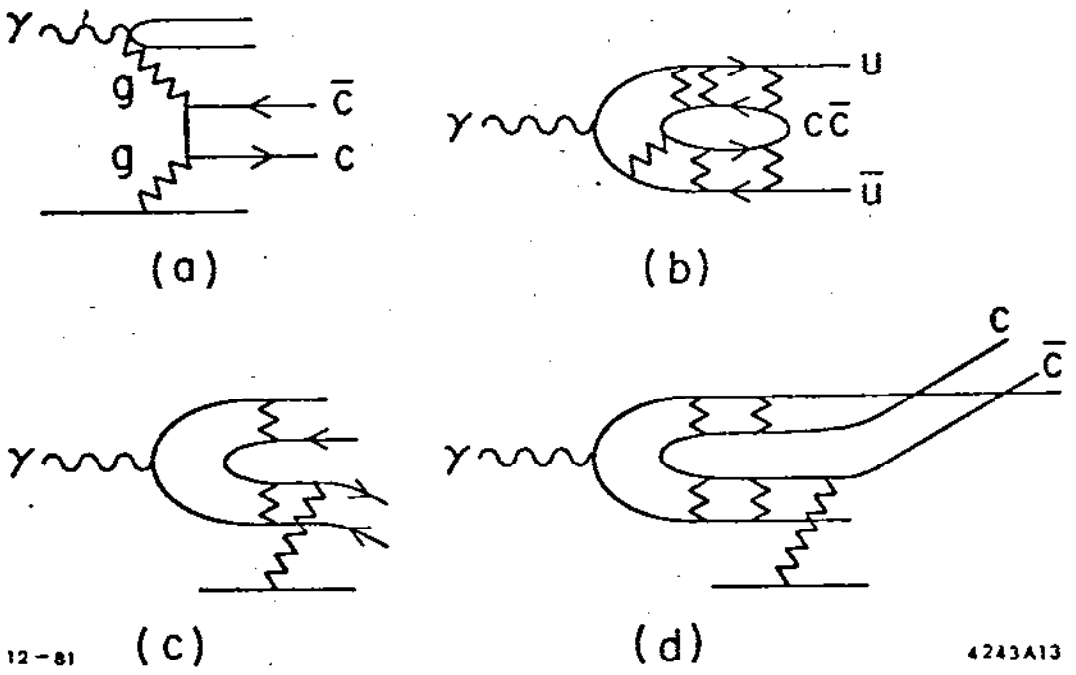

Figure 49. QCD graphs for heavy flavor production by vector-dominated photon: a) gluon-gluon fusion (GGF); b) "intrinsic heavy flavor" in ρ,ω component; c) quasi-diffractive associated charm production; d) diffractive hidden-charm production.

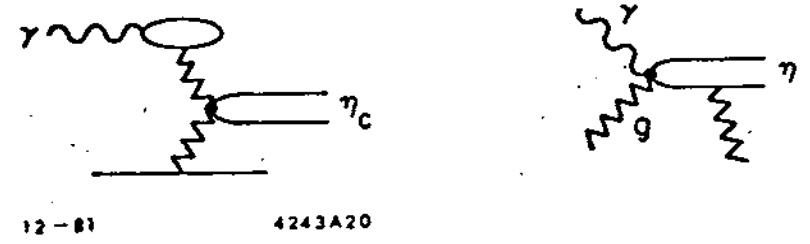

Figure 50. η_c production by a) GGF; b) Primakoff graph; second gluon in b is needed for color neutralization.

4. Heavy Flavors From Hadron-Hadron Collisions

4.1 Basic Notions:

Having graduated from the "point-like" probe (section 2) of nucleon structure to the hybrid probe that is the real photon (section 3), we now consider two sets of complicated wave-functions involving, at the very least, two or three bare valence constituents each, as mesons or (anti-) baryons interact with nucleons.

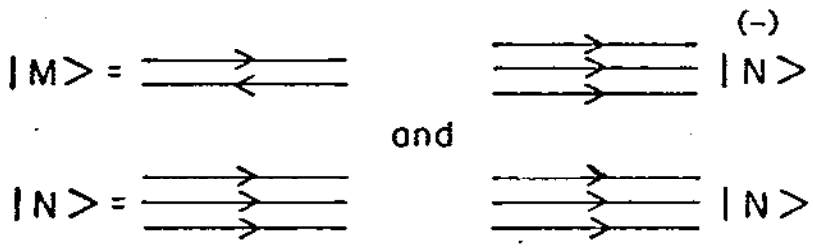

What new aspects do we expect to become available? Starting from the customary quark-parton model notions, and specializing to NN interactions for the time being, we expect, for the processes

$$NN \to c\bar{c} + \ldots$$
$$\to b\bar{b} + \ldots ,$$

contributions from the lowest-order QCD graphs shown in Fig. 51 (to order α_s^2). 51a is the gluon analogy of the Drell-Yan graph; 51b,c resemble the γGP model mentioned above if we substitute a gluon for the photon. To these gluon-gluon fusion (GGF) graphs we now have to add one (51d) due to the ggg vertex permitted in the gauge coupling. None of these graphs probe the valence constituents of the baryons. So, let us add the gluon exchange graphs(51e,f,g,h), which do directly involve the long-lived constituents of either hadron.

We can now take a serious look at a question mentioned briefly several times in the previous sections, which only at this point becomes reasonably accessible: Do we produce $Q\bar{Q}$ that were <u>made</u> in the interaction? Do we

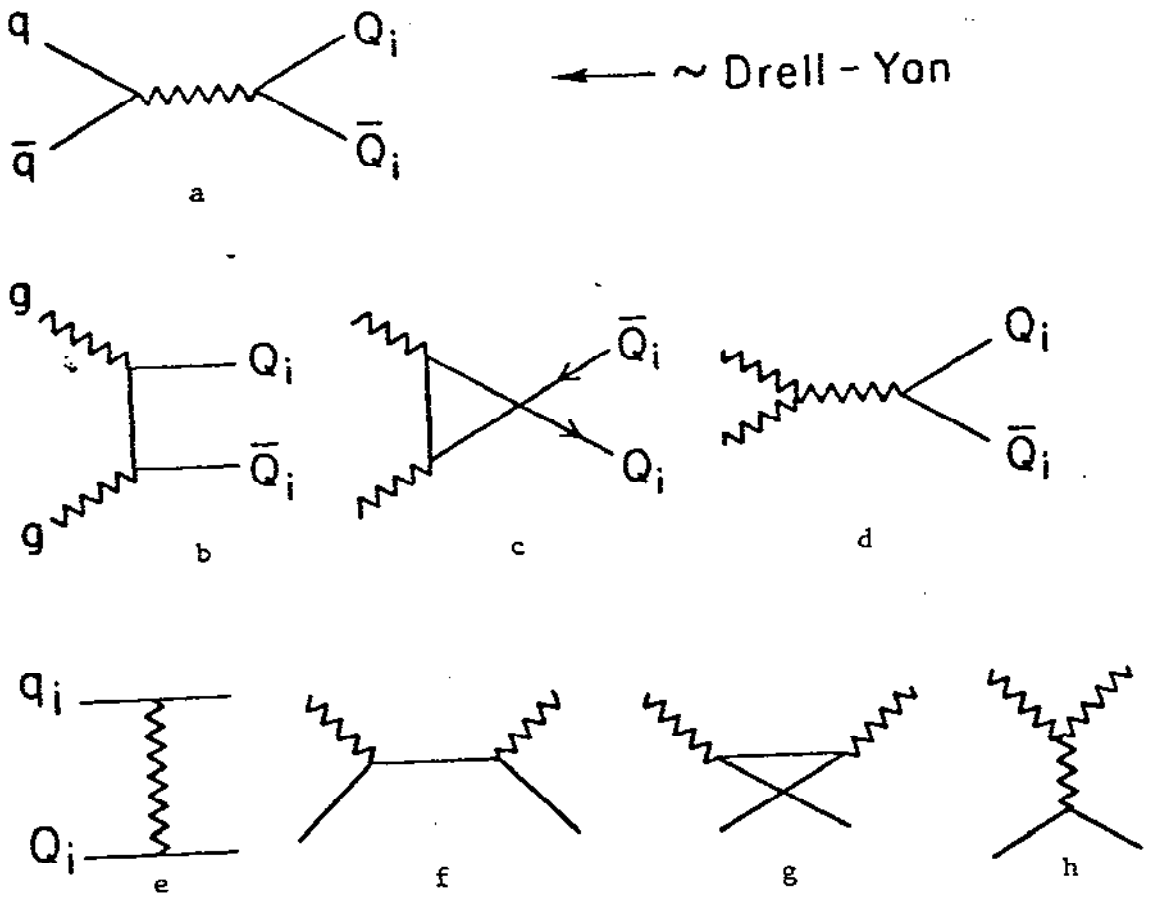

Figure 51. Heavy flavor production in hadron-hadron collisions: QCD graphs to order α_s^2: a) Drell-Yan equivalent; b-d) Gluon-gluon fusion; e-h) Gluon exchange graphs.

cunningly "unveil" an existing component of the nucleon wave function? Is there an important "intrinsic" $Q\bar{Q}$ component present on a time frame long when compared with the interaction time?

Note that this is not really a very novel idea: the vector dominance model told us to regard photon-hadron interactions in terms of just such a (relatively) long-lived set of $(q\bar{q})$ components in the photon wave function. We have known for a long time that, in fact, vector gluons are an important part of the nucleon wave function, and can in some context be regarded as quasi-free. Why then not permit them the same freedom to turn into $Q\bar{Q}$ (or $q\bar{q}$) pairs that the photon enjoys, especially since the coupling is stronger (α_s vs. α)? The principal difference is due to the color degree of freedom: a gluon always carries color, $Q\bar{Q}$ or $q\bar{q}$ never do, so that further soft gluon exchanges are indispensable; nobody knows how to treat these theoretically, but there is no harm in pursuing the analogy heuristically -- maybe a small momentum transfer will lift the vector- (or pseudo scalar-) dominated gluon on the mass shell, and into our detector.

4.2 Principal Models

4.2.1 Hard-scattering models: Drell-Yan and beyond.

The basic graph (Fig. 52) is $q\bar{q}$ annihilation. The $\bar{q}$ is expected to come from the "sea" component at small x values. If we index the annihilating particles with 1,2, their momenta are $x_1 p$ and $x_2 p$; then with $x_1 x_2 = M^2_{f\bar{f}}\, s^{-1} \equiv \tau$ ($M_{f\bar{f}}$ is the mass of the emerging fermion pairs), $x_1 - x_2 = x_f$, we have[46]

$$\frac{d^2\sigma}{d\sqrt{\tau}\, dy} = \frac{2E}{\sqrt{s}} \frac{d^2\sigma}{d\sqrt{\tau}\, dx}$$

$$= \frac{1}{3} \frac{8\pi\alpha^2}{3 M^2_{f\bar{f}} \sqrt{\tau}} F(\sqrt{\tau},\ y \text{ or } x_F),$$

where the factor $\frac{1}{3}$ is due to the color degree of freedom, and, with Z_i the charge of the parton with flavor i,

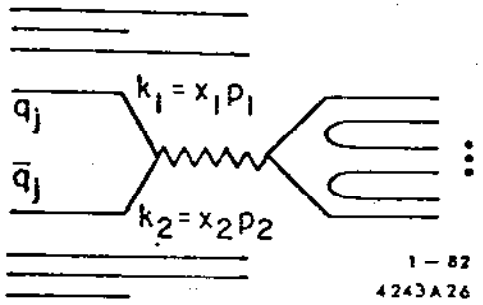

Figure 52. "Drell-Yan" graph: amalgamation of like-flavored "sea" parton and antiparton into (low-x) $Q\bar{Q}$, $q\bar{q}$, $e\bar{e}$.

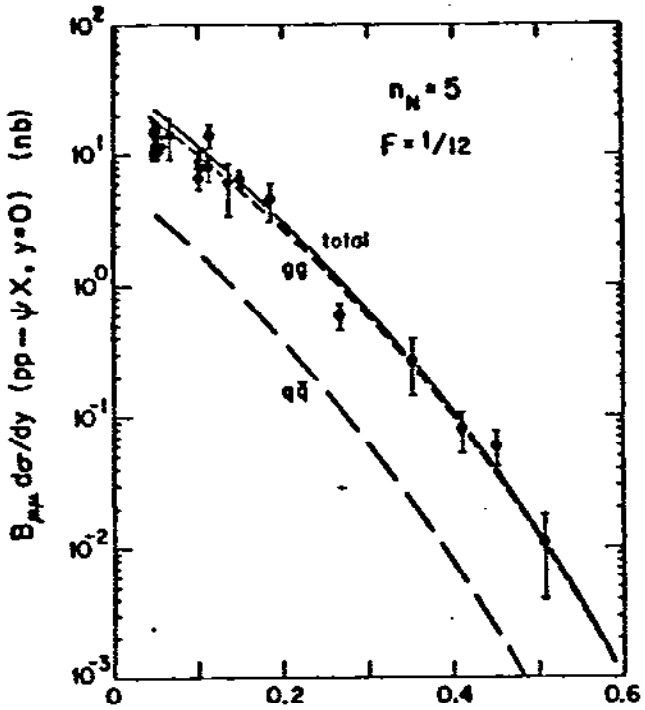

Figure 53. Calculated cross-section for Drell-Yan production of $\psi(\to\mu^+\mu^-)$ is too small to explain the data. Solid line represents gluon-gluon fusion fit with empirical factor 1/12 (see text).[55]

Figure 54. Typical energy dependence for gluon-gluon fusion process (here: $Q\bar{Q} = c\bar{c}$).

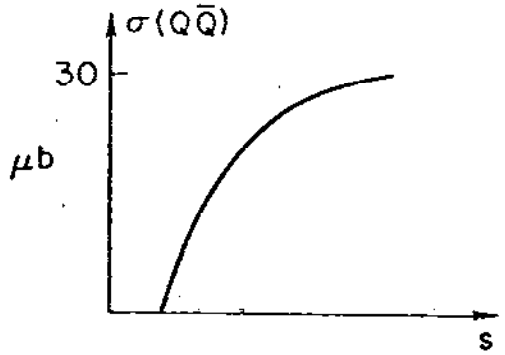

$$F = \sum_{\text{flavors } i} Z_i^2 \{q_i(x_1)\bar{q}_i(x_2) + \bar{q}_i(x_1)\, q_i(x_2)\}\,.$$

To gain information on the fragmentation of the time-like annihilation photon, we take a look at e^+e^- data or we do fragmentation modelling (cf. below). Note that the $\bar{q}_i(x)$ fields enter multiplicatively; $q_i(x)$ and $\bar{q}_i(x)$ can, however, be determined from data due to different beams ($\pi^\pm$, $K^\pm$, $\overset{(-)}{p}$, n): the presence of valence antiquarks in mesons and antinucleons is vital.

For the specific case of Drell-Yan annihilation into $\mu^+\mu^-$, Fig. 53 shows that the calculation is almost an order of magnitude below the data: a successful fit needs the addition of GGF terms.

If we ask how many fermion pairs remain bound in the case of, say, $f\bar{f} = Q\bar{Q}(c\bar{c})$, we find

$$\sigma(pp \to \psi + \ldots) = F \int_{2m_c}^{2m_D} \sigma(m_{c\bar{c}})\, dm_{c\bar{c}}\,,$$

where F is an empirical factor. In the case of γGF, where the γ is a color singlet,

$$F(\gamma g) \simeq \frac{1}{6}$$

whereas, for GGF, it is harder to make a colorless bound state, and

$$F(gg) \simeq \frac{1}{12}\,.$$

To calculate open-charm (or open-beauty) production by GGF, we look at the convolution

$$\sigma(pN \to Q\bar{Q})\,\Big|_{s} = \int_{\substack{x_1,\, x_2 \\ s>4m_D^2}} dx_1 dx_2\, \frac{F_2^{\,P}(x,Q^2) F_2^{\,N}(x,Q^2)}{x_1 x_2}\, \sigma_0(s')\,,$$

where

$$\sigma_o(s') = \sigma(gg \to Q\bar{Q})$$

is the appropriate basic cross-section at sub-energy s'. Note that, for small x, $\sigma(pN \to Q\bar{Q})$ will obviously be large: production will be strong close to threshold.

From the GGF graph, for given $m_c = 1.5$ GeV, and with g(x) taken from ep and μp data (section 2), we then predict the typical s-dependence for $Q\bar{Q}$ production (Fig. 54), leading, at $\sqrt{s} = 60$ GeV (ISR energies) to

$$\sigma^{GGF}(pp \to c\bar{c}) \Big|_{\sqrt{s} = 60 \text{ GeV}} = 20 - 30 \ \mu b$$

Moreover, this production process would suggest that the charmed daughter particles to the produced $Q,\bar{Q}$ will approximately follow the x-dependence of the parent quark. We will see that these predictions are in serious contradiction to present experimental knowledge.

Semi-perturbative fix-up by VDM:

To cure some of the contradictions, Fritzsch[47] proposed the insertion of a VDM inspired threshold factor. For the basic vertices $\gamma \to c\bar{c}$ and $g \to c\bar{c}$, with a coupling ratio $G \approx \frac{\alpha_s}{\alpha}$, we then have

$$\sigma(pp \to c\bar{c} + \ldots) = 2\,G \int_{x_{min}}^{1} dx\, g^P(x)\, \underbrace{\sigma(\gamma p \to c\bar{c} \ldots,)}_{\sigma_0(1 - \frac{s_{threshold}}{s})} .$$

This must remain an ad-hoc ansatz; as we discussed above (section 4.1), the color singlet photon and the color octet gluon will make the parallelism unclear.

Hard-scatter graphs including excitation

Hard-scattering processes involving sea partons are expected to contribute to small-x behavior. Fig. 55a shows the graph involving "extrinsic" $Q\bar{Q}$ pairs, which, for Q^2 large, will yield heavy flavors at small x values.

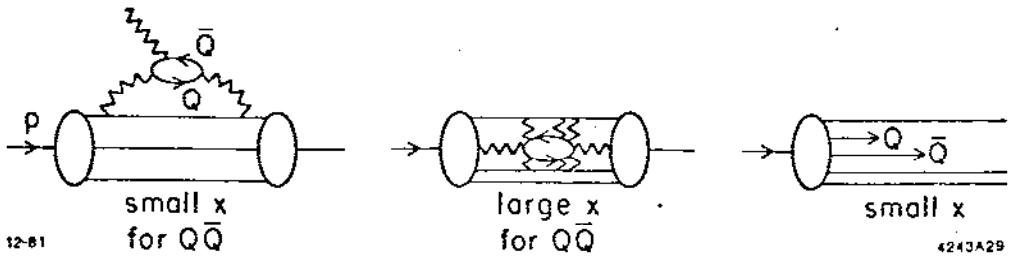

Figure 55. Heavy quarks available in the nucleon wave function for hard-scattering processes: a) "extrinsic" vacuum polarization $Q\bar{Q}$ pair (small-x); b) "intrinsic heavy flavor component (large-x); c) "sea partons" $Q,\bar{Q}$ as in the basic parton model.

(a) (b)

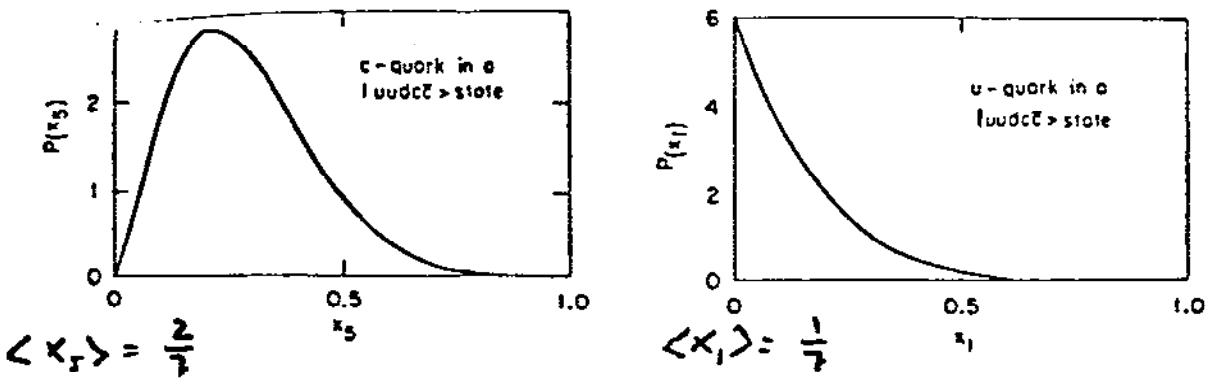

Figure 56. Longitudinal momentum distributions for intrinsic-charm hypothesis (assume $|p\rangle = |uudc\bar{c}\rangle = |12345\rangle$). a) the heavy quarks $c,\bar{c}$ have a larger average momentum than b) the light quarks u,d.

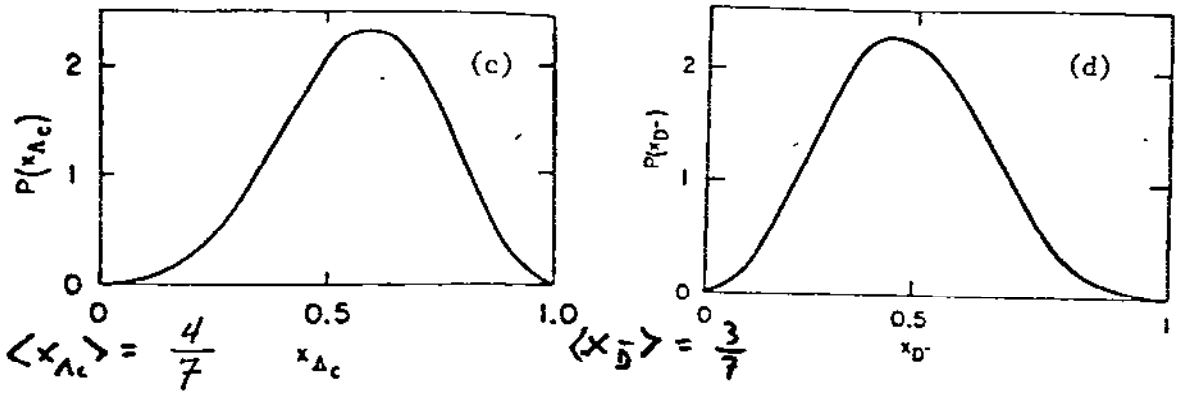

c) the resulting distribution for baryon Λ_c and;
d) for anticharmed mesons $\bar{D}$.

This is the same phenomenon as the basic "wee partons" of the original idea.[5] Brodsky and co-workers[48] have recently suggested that there may be an "intrinsic," long-lived component $Q\bar{Q}$ in the hadron wave function. This would be accessible to low-Q^2 experimentation, and would lead to large-x final state particles of heavy flavor. They look at a Fock expansion of the free proton wave function (Fig. 55b) which, for equal times, can be written as

$$|p\rangle = |uud\rangle + |uudg\rangle + |uudq\bar{q}\rangle + \ldots + |uudc\bar{c}\rangle + \ldots \ .$$

It is important that this expansion be valid on a time scale long compared to an interaction time: over such a time span, multiple gluon exchange will lead to equal velocities for the heavy components and original valence quarks.

Perturbation theory then permits us to write, in the infinite-momentum frame, the likelihood to find any specific Fock component, e.g., $|uudc\bar{c}\rangle$ (= $|12345\rangle$)

$$P(p \to uudc\bar{c}) \propto \{m_p^2 - \sum_{i=1}^{5} \frac{m_{t,i}^2}{x_i}\}^{-2}$$

with $m_{t,i}$ the "transverse mass"

$$m_{t,i} = \sqrt{m_i^2 + k_t^2} \ .$$

Simplify this by calling $m_c^2 >> m_p^2$, find

$$P(x_1 \ldots x_5) = N \frac{x_4^2 \, x_5^2}{(x_4 + x_5)^2} \ \delta(1 - \Sigma_i x_i) \ .$$

Now integrate over all other variables to find the x distributions for the charmed component (x_4, x_5) and for the valence quarks (x_1 ... x_3), in a straightforward way: the example of interest here is, for particles 4,5:

$$Q_c^{\,p}(x) = N' \; x^2\{\tfrac{1}{3}(1-x)(1 + 10x + x^2) - 2x(1 + x)\ell n \tfrac{1}{x}\} .$$

Fig. 56a shows this distribution. Its average $\langle x_5 \rangle = \frac{2}{7}$. Similarly, calculate $q^p_{u,d}(x)$, plot it in Fig. 56b, find $\langle x_1 \rangle \frac{1}{7}$.

Hadronization in terms of diffraction dissociation then will lead to approximate relations

$$x(\Lambda_c) \simeq x_u + x_d + x_c$$

$$x(\bar{D}) \simeq x_u + x_{\bar{c}}$$

They imply $\langle x_{\Lambda_c} \rangle = \frac{4}{7}$, $\langle x_{\bar{D}} \rangle = \frac{3}{7}$, as schematically shown in Figs. 56c,d. Note then that this model predicts hard, higher-x Λ_c and $\bar{D}$ to emerge. The model also clearly prefers associated production $pp \to \Lambda_c \bar{D} + \ldots$ to pair production $pp \to \Lambda_c \bar{\Lambda}_c + \ldots$, $D^o\bar{D}^o + \ldots$. Lastly, the process is quasi-diffractive.

Is there a respectable theory to predict how much, if any, heavy flavor there is in such heavy Fock states? Bag model calculations[49] suggest a 1-2% admixture to the hadron wave function for Q = c, 0.1 - 0.2% for Q = b.

Is it reasonable to assume, in the face of the multiple gluon exchanges of the intrinsic $Q\bar{Q}$ system with the valence quarks, that these systems remain in the $J^P = 1^-$ state? Not really, and indeed peripheral production

$$pp \to pp\,\psi + \ldots$$

has not been prominently observed. Fritzsch suggests[50] that there may be an unexpectedly large η_c component as intrinsic charm, to be identified as a $J^P = 0^-$ $\bar{c}c$ part of the nucleon wave function. A specific prediction would then be that $\bar{c}c$ production proceeds via

$$pp \to (\eta' p) p_{diff} \to NN\ c\bar{c} \quad ,$$
$$\qquad\qquad\qquad\qquad\qquad\quad \downarrow \text{fragmentation}$$

a considerable production of η_c at high x values, little or no ψ in that kinematic regime.

It is logical to apply the original Drell-Yan also to the intrinsic charm component[51] (Fig. 57a). This configuration leaves additional two charmed particles in the final state, predicting

$$pp \to \psi + c\bar{c} + \ldots . \quad .$$

For $\psi \to 2\mu$, the typical Drell-Yan energy dependence ensues (Fig. 57b).

4.2.2 Peripheral Models

Regge Model: Early on in the charm physics game, Barger et al.[52] applied conventional Regge pole ideas to an evaluation of hadronic production cross-sections. The leading graph would thus (Fig. 58a) involve exchange of a D* vector trajectory. Assuming unit slope, $\alpha'_{D^*} = 1$, this trajectory has $\alpha_{D^*}(0) \simeq -2.3$. This leads to a suppression of charm production w.r.t. strangeness production (K* trajectory) by a factor of

$$\frac{\sigma(pp \to s\bar{s})}{\sigma(pp \to c\bar{c})} \sim s^{2\Delta\alpha} \qquad \text{with } \Delta\alpha = \alpha_{D^*}(0) - \alpha_{K^*}(0) = -2.6$$

For ISR energies, $\sqrt{s} = 60$, $s^{2\Delta\alpha} = 10^{-5}$, hardly an encouraging result!

The x dependence can be obtained from the triple Regge expansion

$\sigma(pp \to \Lambda_c + \ldots) = \text{disc}$ 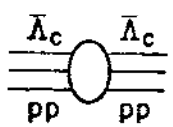

$=$ 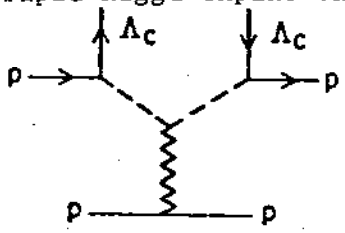

It leads to a steep dependence on $x, \sim(1-x)^5$, not in agreement with the data.

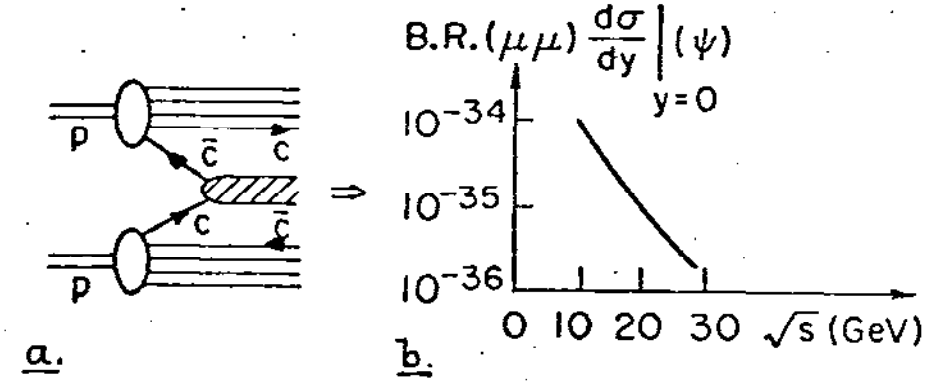

Figure 57. a) Drell-Yan process based on intrinsic charm component.
b) Energy dependence of ψ production by process a.

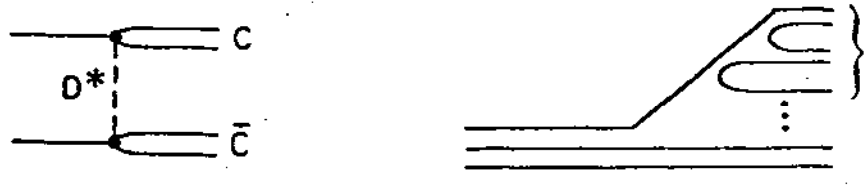

Figure 58. Soft hadronic processes: a) basic Regge graph for charm production, D* trajectory exchange; b) Fragmentation cascade.

Recombination Model:[53] The basic tenet of this idea is that the valence quarks before and after an interaction be the same, that they simply recombine in different configurations. This model predicts for the fast ($x > 0.5$) single-particle spectra in x

$$\frac{d\sigma}{dx} = \int_{x_1,x_2} \frac{dx_1}{x_1}\frac{dx_2}{x_2} \underbrace{F(x_1,x_2)}_{q_1(x)\ \bar{q}_2(x)} R(x_1,x_2,x),$$

where R is the recombination function. Clearly, this idea can be made to apply in the presence of an intrinsic $Q\bar{Q}$ component. The difficulty is, however, that R, like all fragmentation functions, cannot be calculated but must be extracted pragmatically from existing data. In the charm case, the predictive power of the model is clearly small.

Fragmentation Model:[54] This strictly non-perturbative model approach views the $Q\bar{Q}$ hadroproduction process as diffractive excitation; fragmentation into final-state hadrons is analogous to leptoproduction and e^+e^- annihilation. The fragmentation cascade (Fig. 58b) is then equivalent to tunneling in a linear color potential, and the emergence of a $Q\bar{Q}$ pair is proportional to

$$P(Q\bar{Q}) \propto e^{-\frac{\pi}{\kappa}m_\perp^2},$$

with κ the appropriate string constant. The model then predicts a suppression of Q(c, ...) vs. q(u,d,s) presence in the fragmentation products of

$$\frac{P(Q\bar{Q})}{P(u\bar{u})} \approx e^{-\pi(m_c^2-m_u^2)}, \text{ etc.}$$

For currently accepted quark mass values, we find quark ratios

$$u : d : s : c = 1 : 1 : \frac{1}{3} : 10^{-10}.$$

Statistical models lead to similarly discouraging results, and we will not describe them here. Rather, we will turn to the data for confirmation or rejection of the ideas advanced in this section.

4.3 Experimental Evidence:

How do we tune our experiments to look for hadronic charm and beauty (bottom) production? Hidden charm (ψ) and beauty (Υ) are most easily seen by their di-lepton decay modes. Open charm and open beauty were first observed in hadronic interaction via "direct lepton" production, both charged and uncharged, in fixed-target and storage ring (ISR) experiments.

This is a difficult business as far as a clean signal and a clean interpretation are concerned. Thick target (beam dump) experiments can offer high luminosities, but hold little precise information.

More informative experiments take advantage of prompt muons (or electrons) from Q or $\bar{Q}$ decay for tagging of a $Q\bar{Q}$ final state, then look for invariant-mass distribution signals that are due to the other open-Q hadron. This method, difficult due to the confusing presence of "non-prompt" leptons (from π,K decay) and to fierce combinatoric problems for higher multiplicities, has recently led to many indicative results, and we will concentrate on them. Recent data are due to fixed-target and storage-ring experiments, and show signals for Q = c and Q = b.

Finally, the precision vertex chamber and emulsion techniques mentioned in Section 3.3 have been gaining ground. For recent results in hadron beams using these techniques, we refer to C. Dionisi's presentation.[39]

4.3.1 Hidden $Q\bar{Q}$ Production

Hadronic production of ψ and T with subsequent decay into $\mu^+\mu^-$ shows, in the spirit of section 4.2.1, successful fits due to the GGF mechanism, but the empirical factor F varies from process to process: Fig. 59 gives data from pN scattering at 225 and 400 GeV, plus $\bar{p}$N data at 225 GeV; the F factors vary from $\frac{1}{9}$ to $\frac{1}{12}$.[55] The decisive input is the x distribution for the gluons inside the nucleon; it is seen to fully coincide with the form observed in photoproduction: Fig. 60 shows comparisons of the fits xg(x) extracted from both processes to coincide as a function of x. For meson-nucleon scattering, where the beam contains an antiquark valence component, we expect a different behavior; and indeed, data from π- and K-induced ψ production give fits to the gluon distribution of the form

$$g_{\pi,K}(x) \sim x^{-1}(1-x)^3$$

in agreement with hard-scattering counting rules (Fig. 61).

We had previously shown the need for the GGF mechanism for a fit to ψ production, which could not be accounted for by $q\bar{q}$ annihilation, in Fig. 53. The same argument is repeated, for T($\rightarrow\mu\mu$) production, in Fig. 62. Note that the fit here yields $F = \frac{1}{18}$.

The vexing empirical factors F account, among other phenomena, for the fact that some of the ψ, T production proceeds <u>via</u> inelastic mechanisms. It is well-known[56] that gluon-gluon fusion cannot directly lead to a vector ψ or T state; rather, production will proceed by way of (Fig. 63) χ production, where one of the 0^- states ($^3P_{0,1,2}$) subsequently decays via photon or gluon emission into the ($^3S_1$) ground states. By inserting appropriate wave functions, Rückl and Baier[57] were able to calculate the process in accordance with the data; the effect is expected

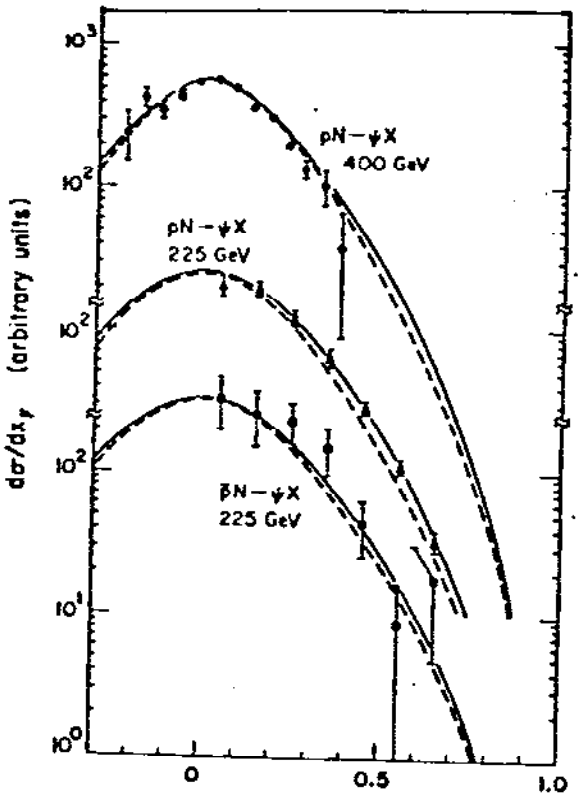

Figure 59. ψ production data from pN, $\bar{p}$N collisions at 225, pN at 400 GeV, with GGF fit.[80]

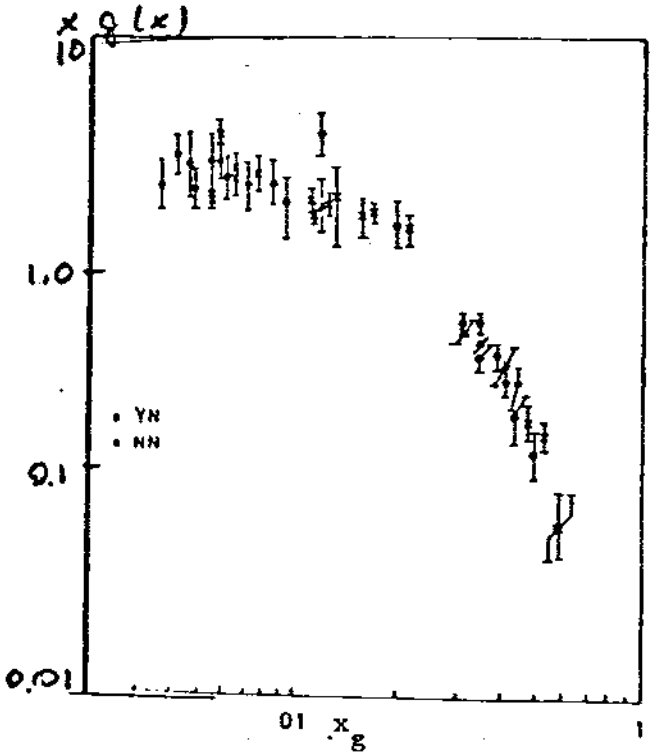

Figure 60. Comparison of gluon distribution functions extracted from photon- and hadron-initiated (γGF, GGF) data.[80]

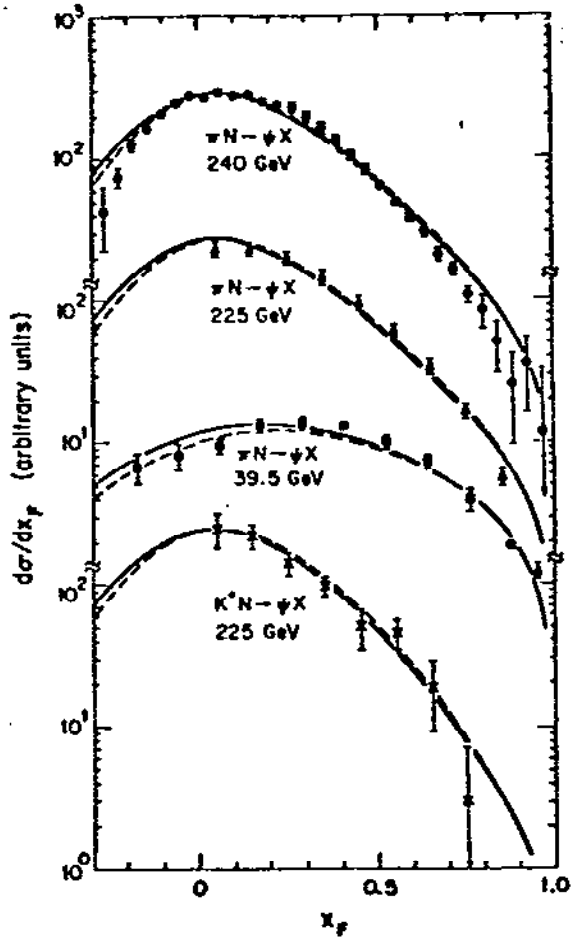

Figure 61. Longitudinal momentum dependence of meson-nucleon production of ψ at 39.5 and 225, 240 GeV; GGF fits.[80]

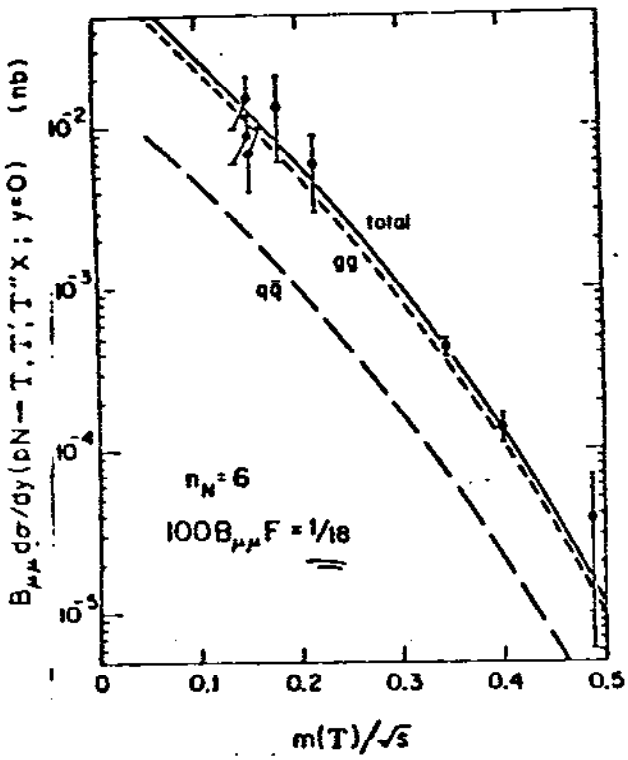

Figure 62. T ($\to\mu\mu$) production, like ψ production, cannot be explained by $q\bar{q}$ annihilation (dashed line). GGF fit is successful, but empirical factor F is now 1/18.[80]

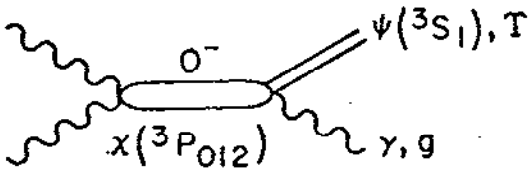

Figure 63. Two-gluon amalgamation produces $c\bar{c}$ pairs in P state (χ states), which then decay by gluon or photon emission: "inelastic ψ production."

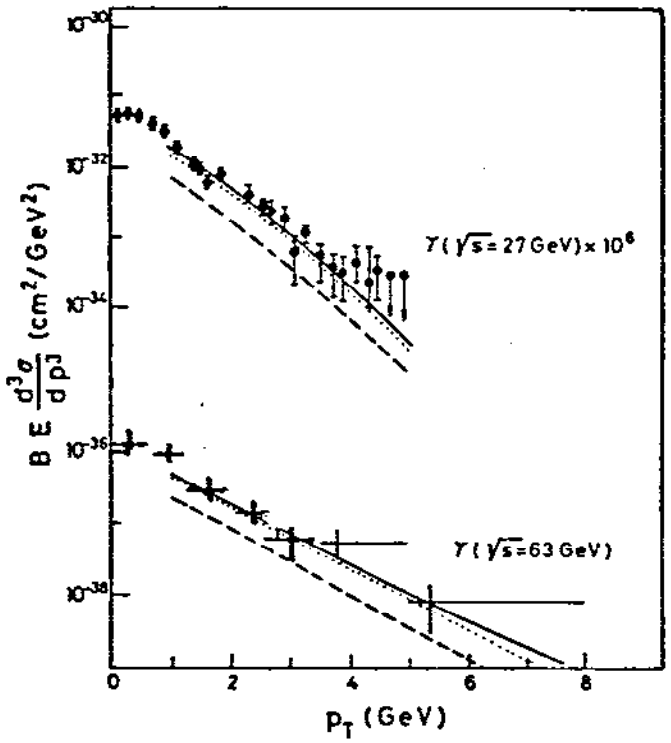

Figure 64. Experimental support for the importance of the graph in Fig. 63: T production with fit due to "elastic" graph only (dashed line), inelastic plus elastic (full curve). From Ref. 57.

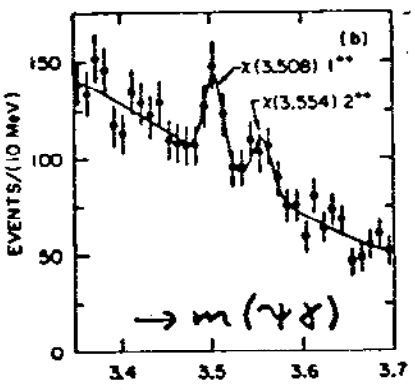

Figure 65. Direct experimental certification of mechanism of Fig. 63: two χ states appear resolved in WA-11 data from CERN.

to become more pronounced with increasing $p_\perp$, and is demonstrated in Fig. 64. Production via the P states is clearly needed to account for the data. Direct evidence for this process comes from the WA11 collaboration at CERN;[58] Fig. 65 shows the mass spectrum of $\psi\gamma$, with clear indications for the 1^{++} and 2^{++} χ states at 3.508 and 3.554 GeV, respectively. The needed ratio of χ vs ψ production is found to be

$$\frac{\sigma(\chi)\,B.R.(\chi\to\psi\gamma)}{\sigma(\psi)} \approx 0.3 - 0.4.$$

These observations (and, for the photoproduction case, those of Berger and Jones[59]) put the GGF mechanism on much more solid ground as a quantitative theory, to explain hidden-$Q\bar{Q}$ data.

4.3.2 Open $Q\bar{Q}$ Data: Direct Leptons, Beam Dump Experiments

The first undisputed evidence for hadronic heavy-flavor production came from fixed-target and ISR "direct-lepton" experiments where, for $p_\perp$ values > 0.3 GeV/c, e/π and μ/π ratios of 10^{-4} were observed. At smaller $p_\perp$, the data remained inconclusive, rising possibly to 10^{-3}. These inclusive lepton yields were ascribed to

$$pN \to D\bar{D} + \ldots \;(\to \ell + \ldots \;;\; \to \bar{\ell} + \ldots) \quad ; \quad pN \to \Lambda_c \bar{D} \;(\to \ell + \ldots) \quad ; \quad pN \to \Lambda_c \bar{\Lambda}_c \;(\to \ell + \ldots),$$

but translation into cross-sections was problematical due to the generic experimental information: as in the case of lepto-production of $Q\bar{Q}$, production models, decay branching fractions, acceptance modelling bring considerable uncertainties into all conclusions. Most analyses agree that, at $\sqrt{s}$ = 60 GeV

$$(pN \to D\bar{D}) \approx 20 - 30\ \mu b,$$

and that a central production mechanism is favored. A number of thick-target experiments have recently investigated prompt lepton production: Prompt electrons were observed in BEBC[60] with a track-sensitive target (liquid He) surrounded by a heavy H-Ne mix. Backgrounds from $\pi \to \mu \to e$ decays have to be evaluated; production and acceptance modelling then lead, on the basis of five events, to

$$\sigma(\pi^- p_{70\ GeV} \to C\bar{C}) = (19 \pm 11)\mu b.$$

Prompt muons and neutrinos have been looked for in beam dump experiments. The basic scheme is simple-minded (Fig. 66a): a thick target/absorber leaves only decay leptons (μ,ν) to interact in massive downstream detectors. All CERN neutrino experimental setups[61] were employed for such "prompt-ν" signal searches, as indicated in Fig. 66b: without commenting on experimental limitations,[62] let us mention that for high-energy (> 100 GeV) neutrinos emitted into a small forward cone ($\sim \pm 1.8$ mrad) the different detectors will be sensitive to these final-state features:

$\overset{(-)}{\nu}_\mu$ interactions, charged current $\to \mu^\pm$ in final state

$\overset{(-)}{\nu}_e$ interactions, charged current $\to$ showers for e^+, e^-

$(\nu_e+\bar{\nu}_e)$ interactions, all μ-less events - neutral current events (normalized to μ events).

To extract the true "direct-lepton" yield, i.e., the yield due to $Q,\bar{Q}$ decays, either of two methods is used: Yields taken with two different target densities are extrapolated to infinite density (Fig. 67), or a calculated contribution from K,π decays prior to the hadrons' absorption is subtracted from the data. Fig. 68 illustrates that the methods lead to tolerable agreement.[63]

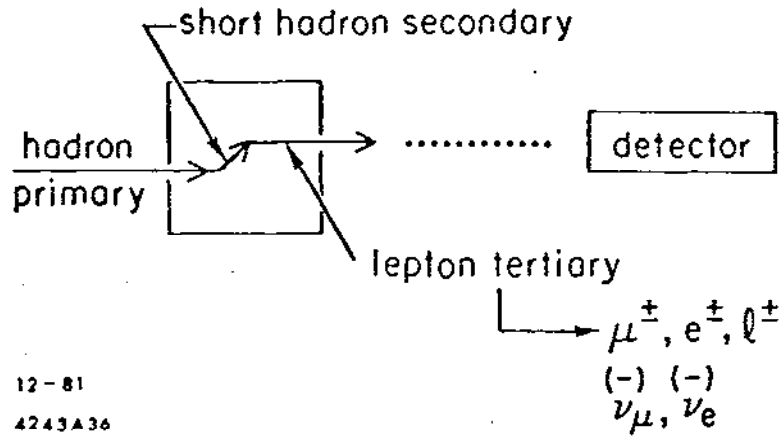

Figure 66. a) Principle of beam-dump experiments.

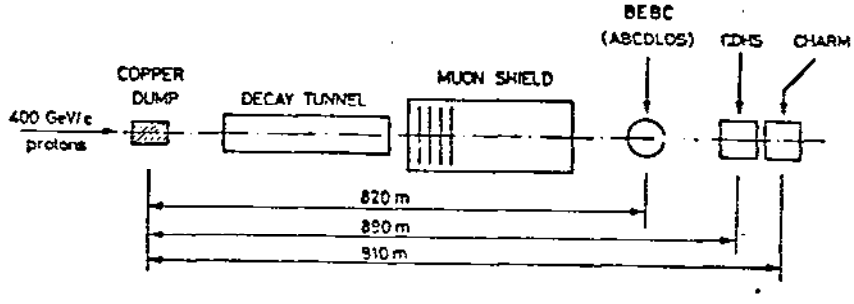

Figure 66. b) Basic arrangement for beam-dump experiments at the CERN SPS: all ν experimental facilities participate in the program.

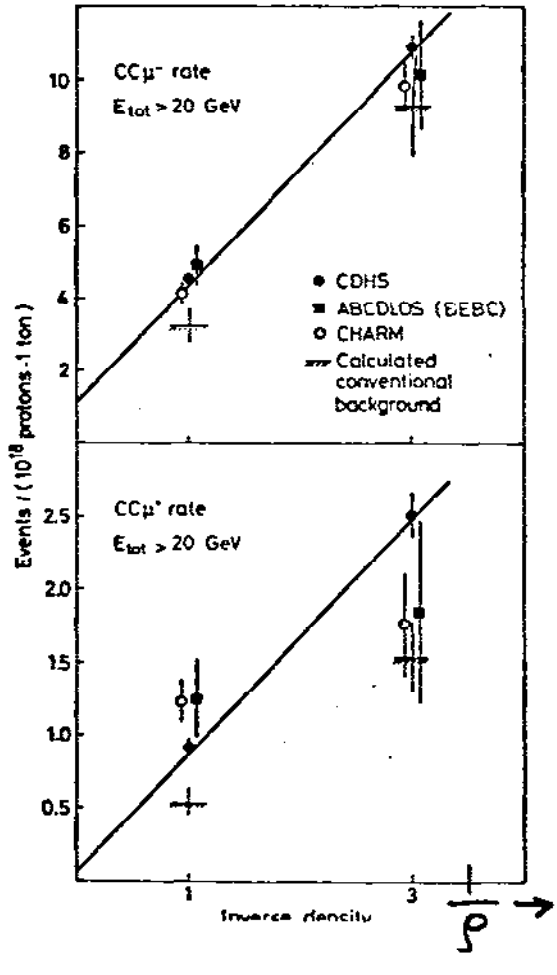

Figure 67. Extrapolation to infinite density for three CERN beam dump experiments: based on charged-current interactions of $\overset{(-)}{\nu}_\mu$ by observation of (a) μ^+, (b) μ^- event rate as a function of target density.

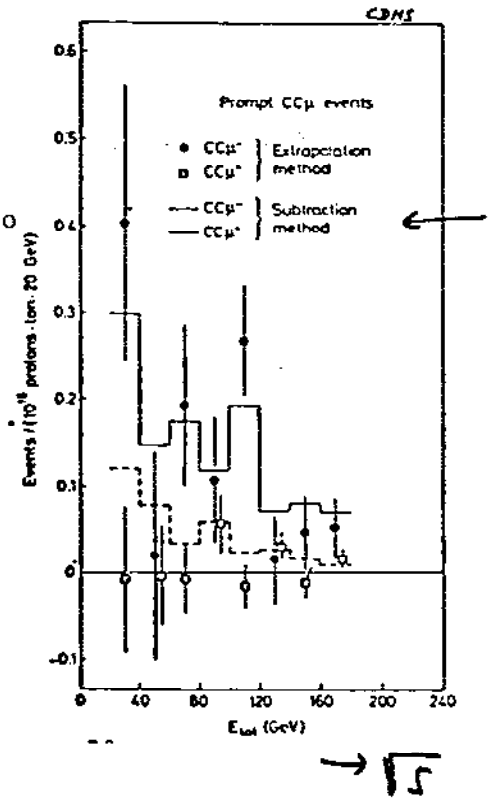

Figure 68. Comparison of two methods to evaluate prompt-ν signal: extrapolations to $\rho \to \infty$ are represented by points with error bars, calculated K,π decay backgrounds lead to full histogram (for μ^-), dashed histogram (for μ^+). Agreement is marginal.

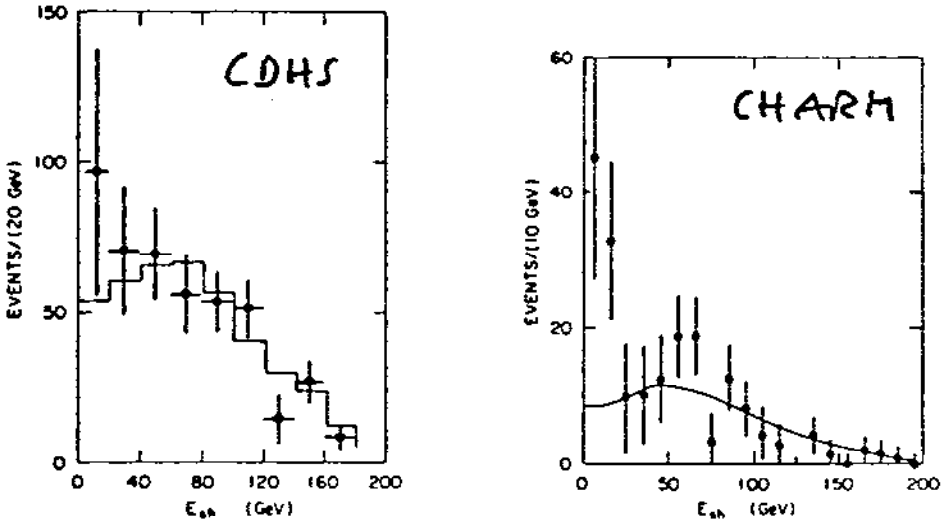

Figure 69. Hadronic shower distribution for no-μ events from a) CDHS; b) CHARM Collaborations. Lines correspond to signal expected from centrally produced $D,\bar{D}$ pairs. The excess at small energies may be significant, if proven on better confidence level.

These very inclusive experiments yielded several surprises:

a) $\frac{\nu_e}{\nu_\mu} \neq 1$. But, for charm (bottom) decay, we expect

$$\text{B.R.}(e) = \text{B.R.}(\mu)$$

$$\approx 0.6$$

b) $\nu_\mu \neq \bar{\nu}_\mu$ This indicates the influence of associated $\Lambda_c \bar{D}$ production rather than $D\bar{D}$ pair production.

The cross-section can be extracted via the assumption $\sigma(A) = A\sigma(N)$ and the model form

$$D \frac{d^3\sigma}{dp^3} \alpha(1-x)^4 \exp(2p_T).$$

Upon integration, this yields

c) $\sigma(pN \to D\bar{D} + \ldots) = 10$ to 20 μb.

In addition, the CDHS and CHARM Collaborations observe unexpectedly large low-energy neutrino events (Fig. 69a,b),

At Fermilab, a beam dump experiment[64] using an expandable iron target (Fig. 69) looked for prompt muons in a toroidal muon spectrometer. After appropriate background subtractions, the experimenters found a signal that indicated

a) $\frac{\mu^-}{\mu^+} = 1.3 \pm 0.3$, compatible with $D\bar{D}$ production origins (and unlike b) above)

b) a muon spectrum that prefers a central production mechanism (like GGF)

c) a model-dependent cross-section of $\sigma(pN \to D\bar{D} + \ldots) = 22 \pm 9$ μb/nucleon.

4.3.3 Open-Charm, Bump-Hunting with Fixed Target

Even prior to the J/ψ discovery, Glashow's suggestion[65] of the necessity of new heavy constituent quarks triggered the search for selective experimental criteria that would show the existence of such states.[66] The first dedicated experiment to search for hadronically produced charm states was performed by the Santa Cruz/SLAC Collaboration[67] in the summer of 1974; they used a 2m streamer chamber to search for signals due to $C\bar{C}$ production close to threshold by a 15 GeV π^+ beam according to

$$\pi^+ p \rightarrow C\,\bar{C} + \ldots$$
$$\qquad\quad \downarrow \quad \hookrightarrow K^0 + \ldots, \Lambda^0 + \ldots$$
$$\qquad\quad \hookrightarrow \mu + \ldots$$

The telltale muon was easily identified, but was contaminated by K-, π-decay muons. A sensitivity of 10 nb/event probed for effects at the 1 μb level in mass plots for all possible $K^0\pi$ ..., $\Lambda^0\pi$ ... combinations that were measured in the streamer chamber. We show a typical mass plot of this negative-result search in Fig. 70 to indicate that, in such searches, it is important to carefully evaluate the statistical significance of enhancements in invariant-mass plots: each cut applied to the data increases the number of bins studied significantly. The inset of Fig. 70a shows that a large number of bins will populate the 4-5 S.D. area in such searches, just as observed in the (blown-up) upper mass region of Fig. 70b. The usefulness of these observations will be seen below.

Overall, out of a large number of experiments completed or still active, only few have yielded indicative results; some of these are still quoted as preliminary. Experimental difficulties are due to problems with particle identification (for strange-particle content), with mass calibration due to insufficiently precise knowledge of magnetic

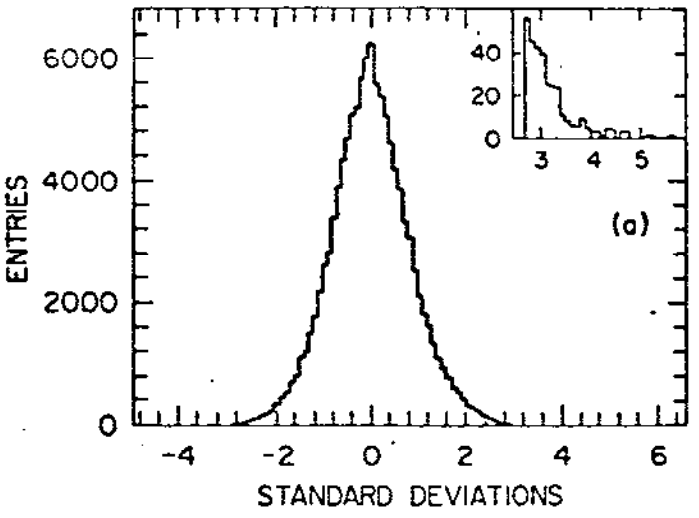

Figure 70. a) Caveat bump-hunter: Monte-Carlo simulation of invariant-mass distributions demonstrates that population of outlying bins in S.D. plot depends solely on total effective number of bins considered. Each cut or selection criterion increases this number significantly.[67]

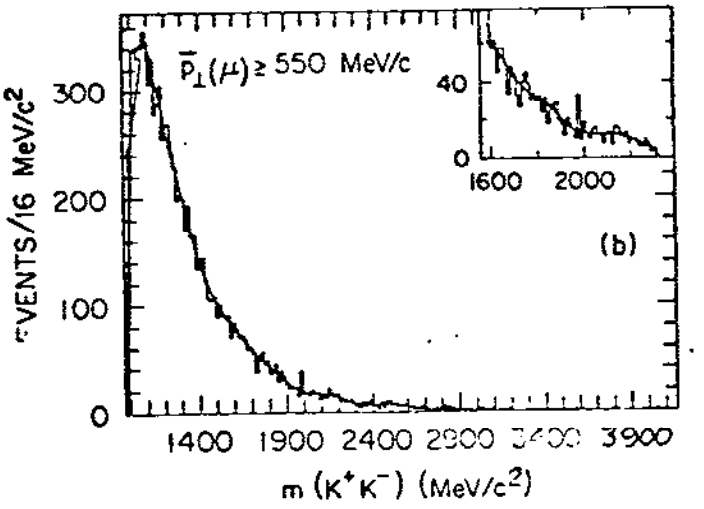

b) Typical result of Santa Cruz/SLAC Streamer chamber experiment: invariant-mass plot. Inset: blown-up view of statistical enhancement.[67]

fields of analyzing devices like the SFM at the CERN ISR. This also impacts on the mass resolution of observed peaks: are they really compatible with apparatus width (i.e., origin from weak decays)? High total multiplicities lead to often stifling combinatorics, and cuts inspired by production and decay modelling may severely eat into the statistical meaningfulness of any observed effect.

With these caveats in mind, let us look at the results of a few recent searches (where we can by no means be complete). An Illinois-FNAL-Harvard-Oxford-Tufts Collaboration[68] at Fermilab used the Chicago Cyclotron Magnet in conjunction with a large downstream spectrometer (Fig. 71) to look for charm signals according to a scheme similar to the above, in a 217 GeV π^- beam impinging on a liquid H_2 target:

$$\pi^- p \to (X^-) + p - \text{slow recoil}$$
$$\quad \to D\,\bar{D} + \ldots$$
$$\qquad \to \mu^+ + \ldots$$
$$\qquad \to \text{charged hadrons}.$$

Given a ratio of branching fractions into muons,

$$\frac{B\,(D^{\pm} \to \mu + \ldots)}{B\,(\overset{(-)}{D}{}^0 \to \mu + \ldots)} \approx 4.3,$$

this experiment is sensitive to $X^- = (D^+D^- + \ldots)^-$ rather than $(D^0\bar{D}^0 + \ldots)^-$, as illustrated by the mass plots in Fig. 72; the small enhancement in the $K\pi\pi$ system, after some modelling assuming $\frac{d\sigma}{dp_\perp} \sim \exp(-1.7p_\perp^2)$, yields

$$\sigma_\pi(D^+D^- + \ldots) \approx (10 \pm 4)\mu b$$

for an incomplete analysis. An ambitious two-arm spectrometer project at Fermilab including elaborate particle identification schemes (Fig. 73) for $\pi/K/p$ separation looked for D^{*+} decays into $D^0\pi^+$, where the π^+, almost

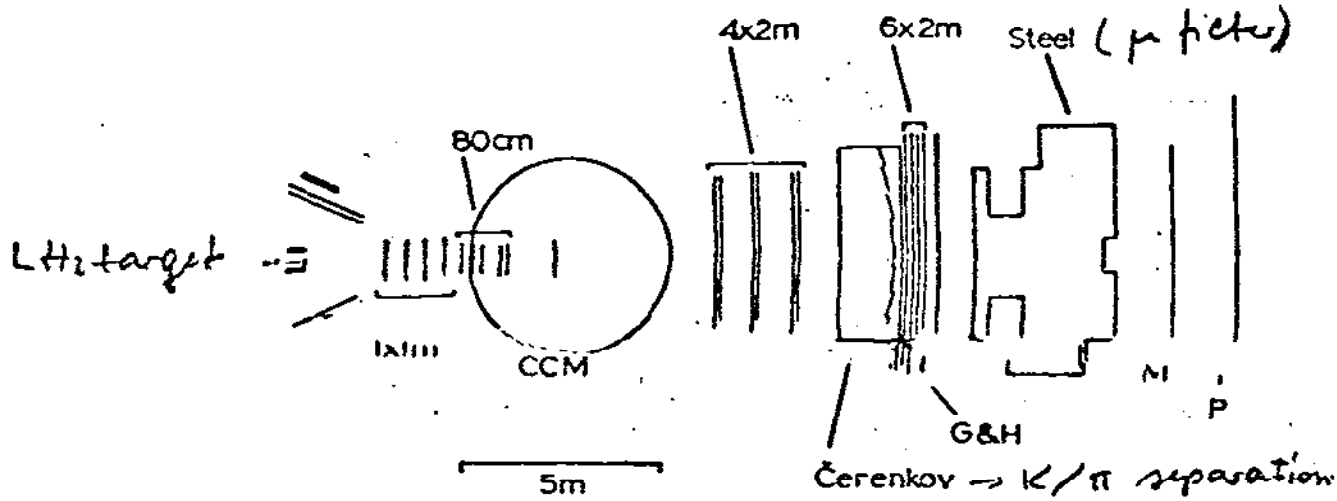

Figure 71. Schematic view of Illinois-Fermilab-Harvard-Oxford-Tufts charm search at FNAL, using the Chicago Cyclotron Magnet.[68]

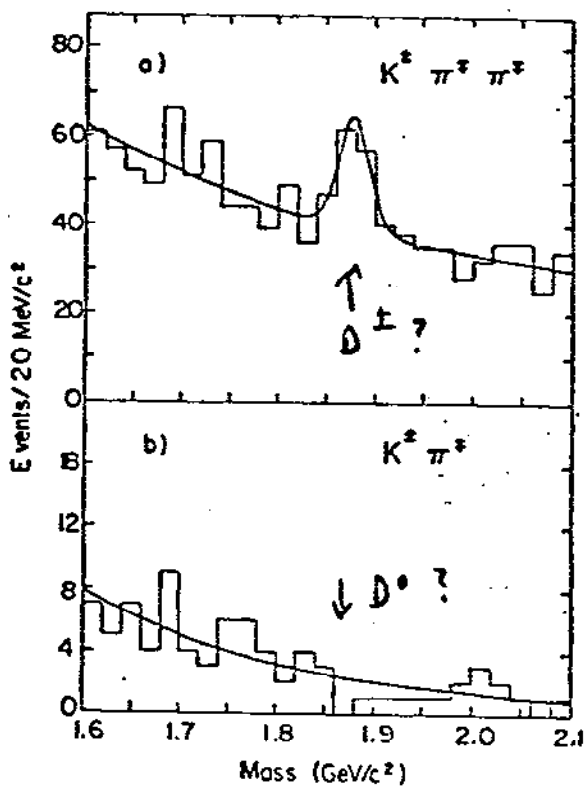

Figure 72. Preliminary data of IFHOT Collaboration on D meson production. A signal is indicated in Kππ mode.[68]

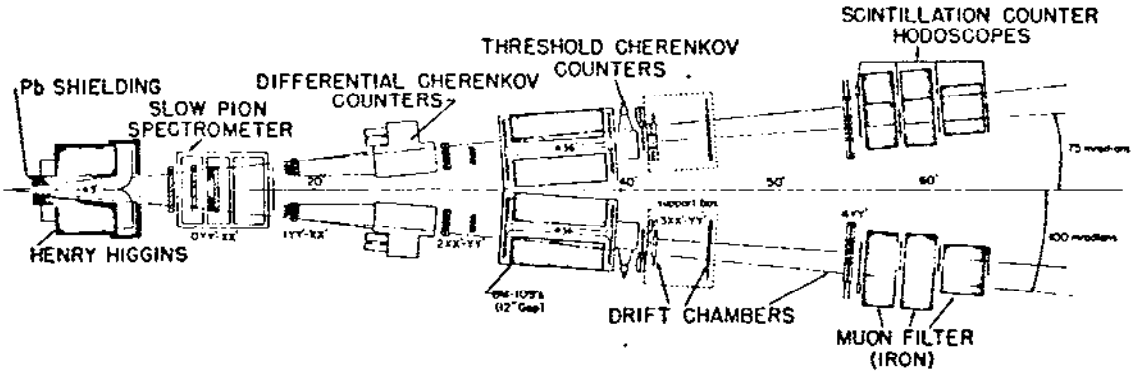

Figure 73. Princeton-Saclay-Torino-BNL setup at Fermilab. Elaborate 2-arm double spectrometer also has slow-pion detector close to target.[69]

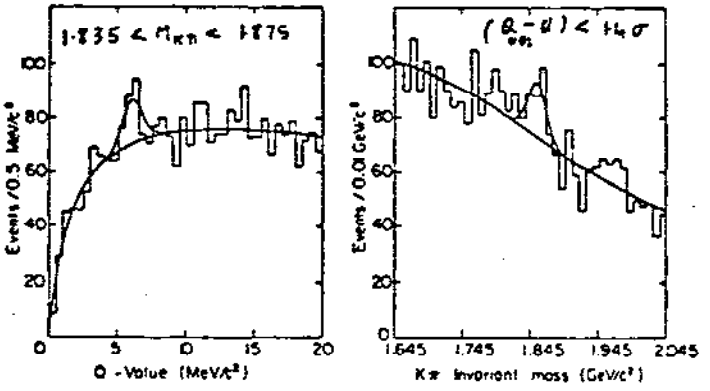

Figure 74. a) "Q value" of the slow pion associated with a Kπ signal in D mass band shows a possible enhancement at ~ 6 MeV. b) Cutting the data on this Q value yields a Kπ invariant mass plot as indicated. D signal candidate is indicated.[69]

at rest in the CMS of the D*, is observed in a separate "slow-π spectrometer." The experimenters from Princeton/Saclay/Torino/BNL[68] show marginal indications for structure in the "Q-value" of the slow π associated with a $K\pi$ signal in a mass band around the D^0 mass (Fig. 74a). Cuts on this Q value enhancement produce the invariant mass plot shown in Fig. 74b for the $K\pi$ system emitted forward. Assuming a production process according to

$$E\frac{d^3\sigma}{dp^3} \propto (1-x)^3 \exp(-1.1\ p_\perp^2)$$

and branching fractions $B.R.(D^{*+} \to D^0\pi^+) = 0.64$, $B.R.(D^0 \to K^-\pi^+) = 0.026$, the authors quote a cross-section

$$\sigma(\pi^- p \to D^* + \ldots) = \frac{1}{2}\left[\sigma(D^{*+}) + \sigma(D^{*-})\right]$$
$$= (4.2 \pm 1.4)\mu b \quad .$$

These results, although roughly compatible with beam-dump indications, point up the difficulties of the methods employed; but they do appear compatible with central production mechanisms, specifically the gluon-gluon fusion QCD graph. Similar estimates come from such efforts as FNAL Exp. 515 which looks for $e^{\pm}\mu^{\mp}$ correlations in the final state of π^-Be interactions. Other, very promising, experiments using vertex detectors (streamer chambers, special bubble chambers, emulsions) do not have the statistics to make statements on prevailing cross-sections at this stage.

4.3.4 Open-Charm: Bump Hunting at the ISR

The final-state recognition schemes explored above present much different experimental challenges when applied to $C\bar{C}$ production at the Intersecting pp Storage Rings at CERN. At CM energies much above those available in the experiments mentioned in the previous section, up to $\sqrt{s} \geq 60$ GeV, the detection of secondaries emanating from collisions that

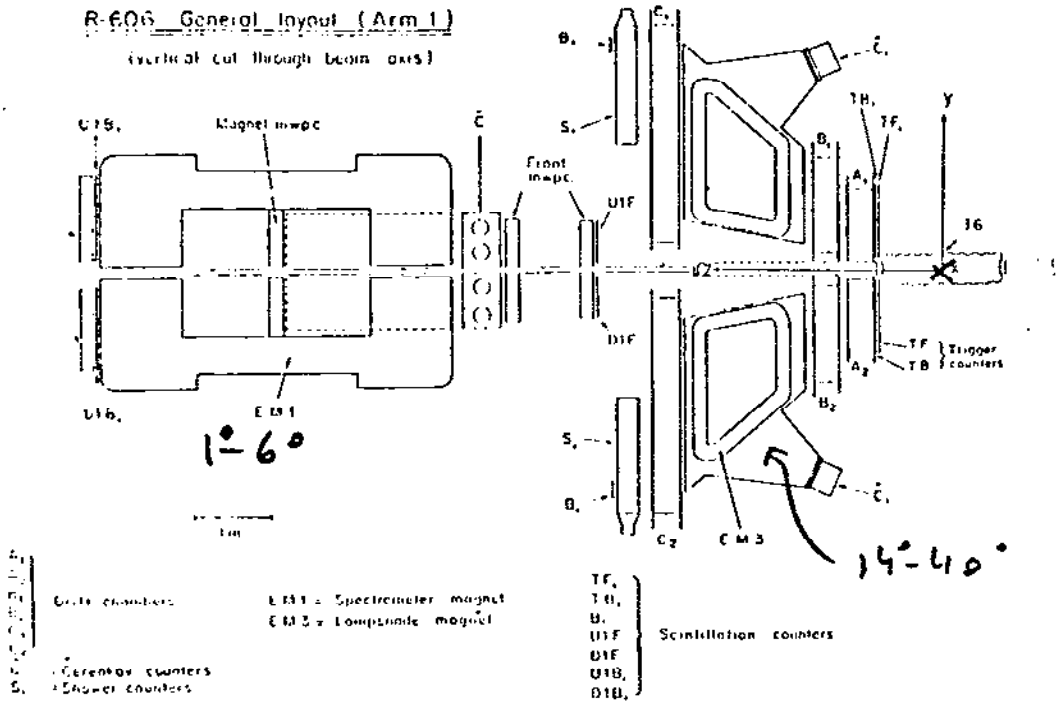

Figure 75. Basic layout for one arm of R-606 at the ISR. There are Cherenkov counters both in the "Lampshade Magnet" (LSM) and in the small-angle magnet.

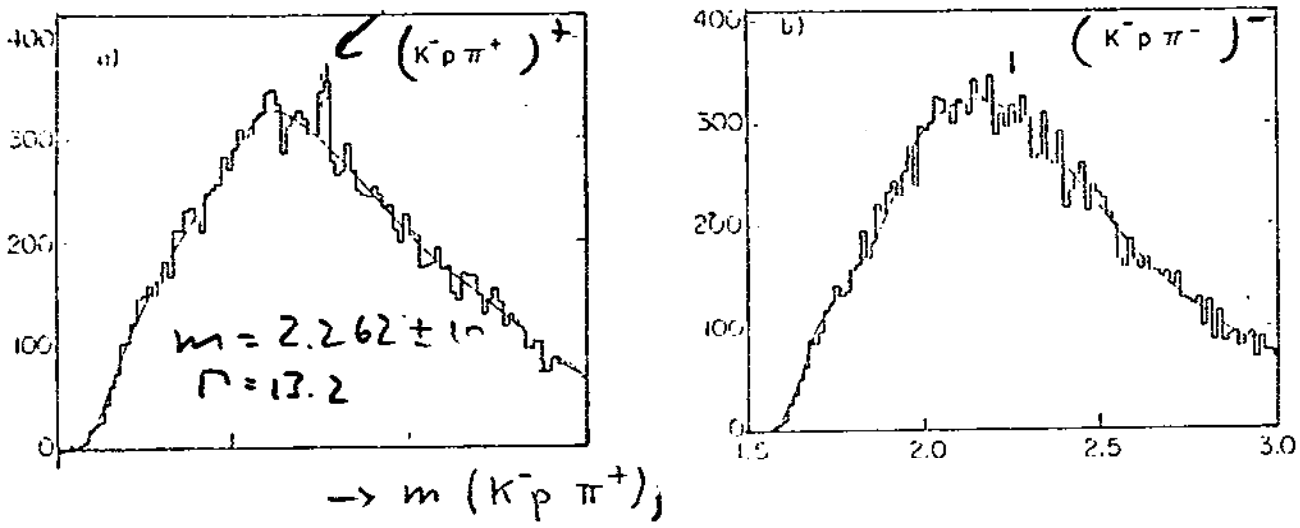

Figure 76. a) $K^- p \pi^+$ mass plot from first LSM experiment ("K^- trigger"). A candidate for Λ_c^+ signal is indicated.[70]

b) Same experiment: "wrong-charge $Kp\pi$ combinations show no enhancement.

occur almost head-on, measurement of their momenta, and their identification, present a considerable task to bump-hunters. Undaunted, four different collaborations have come up with results either published or circulated in preprint form that, if accepted at face value, upset the cohesive if imprecise picture which emerged up to this point.

a) The Aachen-CERN-Harvard-Munich-Northwestern-Riverside Collaboration used a two-arm spectrometer in I-6 including notably the "Lampshade Magnet" (LSM), which permits definition of a "prompt electron" trigger in the range $25^0 < \theta_c < 35^0$, and for $p_t^e > 0.4$ GeV/c. In a first experiment,[70] a forward proton trigger was provided by a septum magnet spectrometer covering the range $1^o < \theta_p < 6^0$, which also served to identify K and p in one arm, in coincidence with a signal with $x > 0.5$ from a small system in the other arm. To enrich this sample in events of the type

$$pp \to pX \qquad X \to \Lambda_c \bar{D} \ ,$$

a multiplicity of $n_{ch^-} \geq 6$ is demanded in the first arm, among which there is an identified K^-; the invariant-mass spectrum for $K^-p\pi^+$ combinations is shown in Fig. 76. The mass enhancement at $(2.262 \pm .01)$ GeV/c^2, not seen in the $K^-p\pi^-$ combination, is identified by the authors as Λ_c^+. For this diffractive region, $x(\Lambda_c) = 0.5 - 0.8$, the cross-section is quoted as $\Delta\sigma/\Delta x = 240 \pm 120\mu b$, based on a branching fraction $(\Lambda_c \to K^-p\pi^+)/(\Lambda_c \to \text{all})$ of 2.2%. After relaxation of the p trigger requirement, a search for $D,\bar{D}$ signals in the $K\pi$ and $K\pi\pi$ channels led to nothing but a generous upper limit in the 100μb range.

In a subsequent experiment[71], the same collaboration used the LSM to define an electron trigger for selection of semileptonic charm decays.

$$pp \to \Lambda_c \bar{C} + \ldots \quad \text{with } C,\bar{C} \text{ hadronic systems with } C = \pm 1$$
$$\hookrightarrow e^- + \ldots$$
$$\to \bar{\Lambda}_c C + \ldots$$
$$\hookrightarrow e^+ + \ldots$$

The resulting spectra show possible enhancements of a width consistent with apparatus resolution in Fig. 77, with comparable signals in the Λ_c and $\bar{\Lambda}_c$ candidate bins.

The translation of such mass enhancements into production cross-sections is clearly very model dependent. The result of the second experiment, taken at face value, favors production of $\Lambda_c\bar{\Lambda}_c$ pairs--not at all an expected result. The distribution in x is shown in Fig. 78--the poor statistics and large errors bars make it hard to conclude that any of the production models

$$\frac{d^2\sigma}{dx dp_\perp^2} \sim \exp(-bp_\perp^2) \qquad \text{(flat in x)}$$

$$\frac{d^2\sigma}{dy dp_\perp^2} \sim \exp(-bp_\perp^2) \qquad \text{(flat in y)}$$

$$E\frac{d^2\sigma}{dx dp_\perp^2} \sim \exp(1-x^3)\exp(-bp_\perp^2) \qquad \text{(central)}$$

is reproduced by the data. Note, however, that the trigger definitely favors the large-x region. A translation of data such as these into cross-sections depends on a number of assumptions beyond the choice of a production mechanism: does the $e^\pm$ originate from meson or baryon decay? What are the semileptonic branching fractions involved? What are they for the observed hadronic charmed decays? What are the overall detection and reconstruction efficiencies? Acceptance modelling is then hard to judge

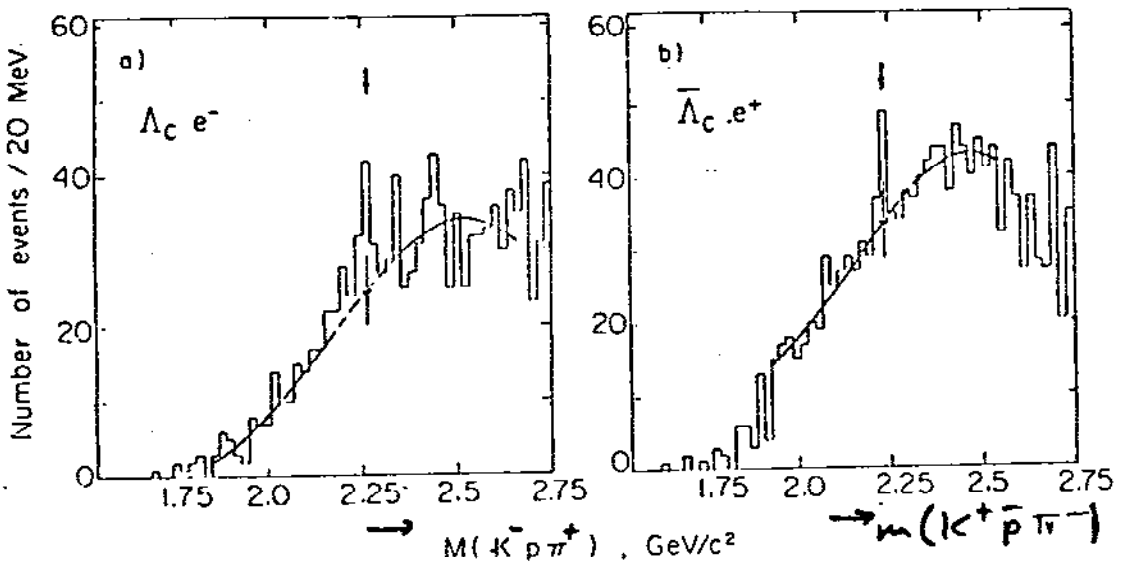

Figure 77. Results of electron trigger data with LSM array: a) $m(Kp\pi^+)$ plot with e^- trigger; b) $m(K^+\bar{p}\pi^-)$ with e^+ trigger. Data with wrong sign electrons (e^+ for a, e^- for b) do not show signal candidates at $\Lambda_c^{(-)}$ location.[71]

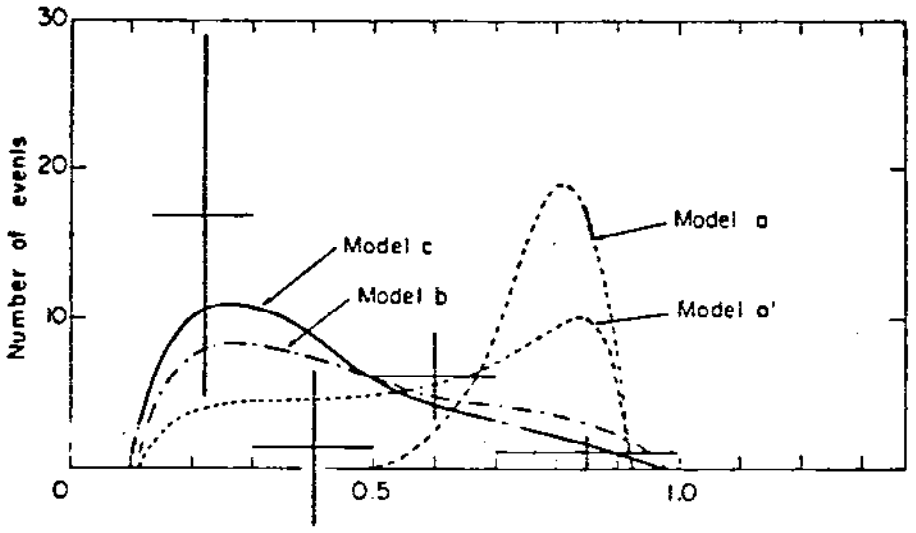

Figure 78. Longitudinal momentum distribution of Λ_c signals observed by LSM experiment compared to various production models (see text).[63]

between one experiment and another. Nevertheless, let us look at the other ISR experiments before quoting cross-sections extracted.

b) The UCLA-Saclay Collaboration (R-603),[72] sharing the intersection region with the previously mentioned groups, also used the small-angle (1^0-6^0) septum magnet in the relatively simple array shown in Fig. 79, using a single-arm inclusive trigger. For an enrichment of likely charmed baryon candidates, Λ^0 were identified by a secondary vertex > 150 mm from the primary one, with appropriate invariant mass values. Figs. 80a,b,c display the data for invariant mass distributions of $K^-p\pi^+$ and $\Lambda\pi^+\pi^+\pi^-$ systems, all from a narrow window in x ($0.75 \leq x \leq 0.9$); there is an indication of narrow structure in both channels.

It is clear that the proper charge combination prevails in both cases (a,b), and gives the added signal (c). The mass, however, is higher than reported above,

$$m(\Lambda_c) = (2290 \pm 15)\ \text{MeV}/c^2.$$

For the limited x-range covered here, this Collaboration quotes a cross-section comparable to that, simultaneously measured, for Λ production(!):

$$\frac{\Delta\sigma}{\Delta x} = (700 \pm 90)\ \mu\text{b}.$$

It is presently engaged in a new experiment (R-608) which has greatly enhanced sensitivity and accuracy.

c) The Split-Field Magnet Facility (SFM) has been exploited independently by two groups. The CERN-Collège de France-Heidelberg-Karlsruhe Collaboration (CCHK)[73] used the SFM (Fig. 81) with a negative-particle trigger at ~ 8^o, with $p_\perp > 0.5$ GeV/c (at $\sqrt{s} = 53$ GeV), coincidence with a K^- candidate (from Cherenkov signal) with $0.3 \leq x_K \leq 0.6$ (Exp. R407/8). Demanding that a $K\pi$ system be in the K* band ($m(K\pi) \simeq m(K^*)$),

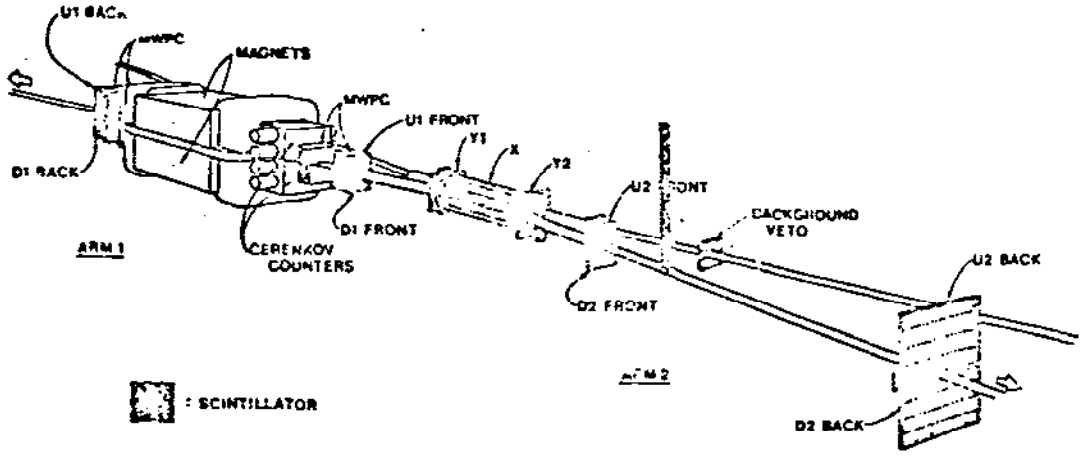

Figure 79. Setup of UCLA-Saclay experiment at ISR.

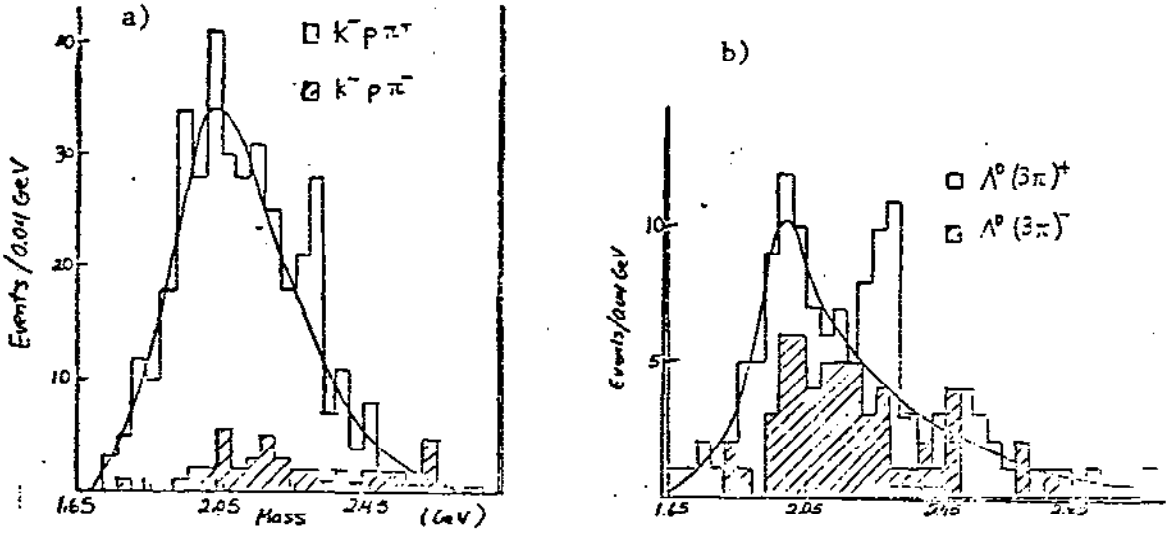

Figure 80. Mass plots for a) $K^-p\pi^\pm$ and b) $\Lambda^0\pi^+\pi^-\pi^\pm$ systems from 603 experiment. c) Sum over "right charge states" from both plots.[72]

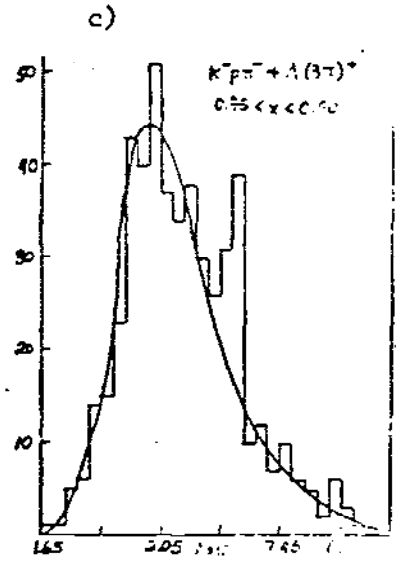

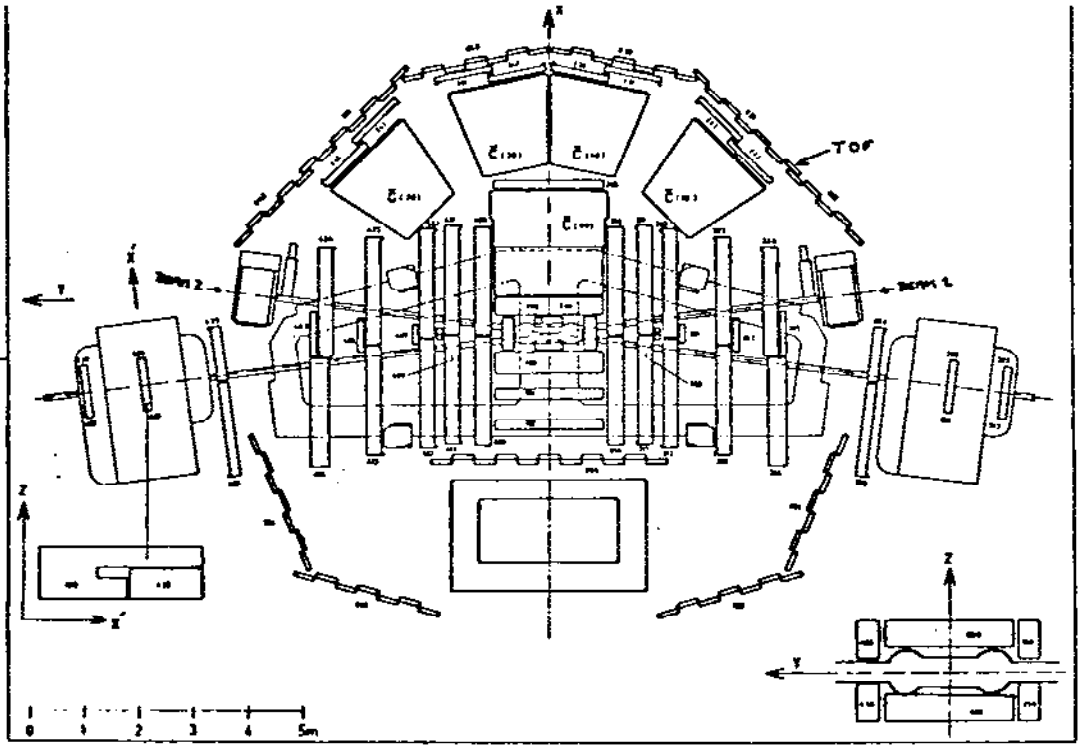

Figure 81. Split-Field Magnet facility at the ISR: General layout. For details of instrumentation, refer to individual experiment references.

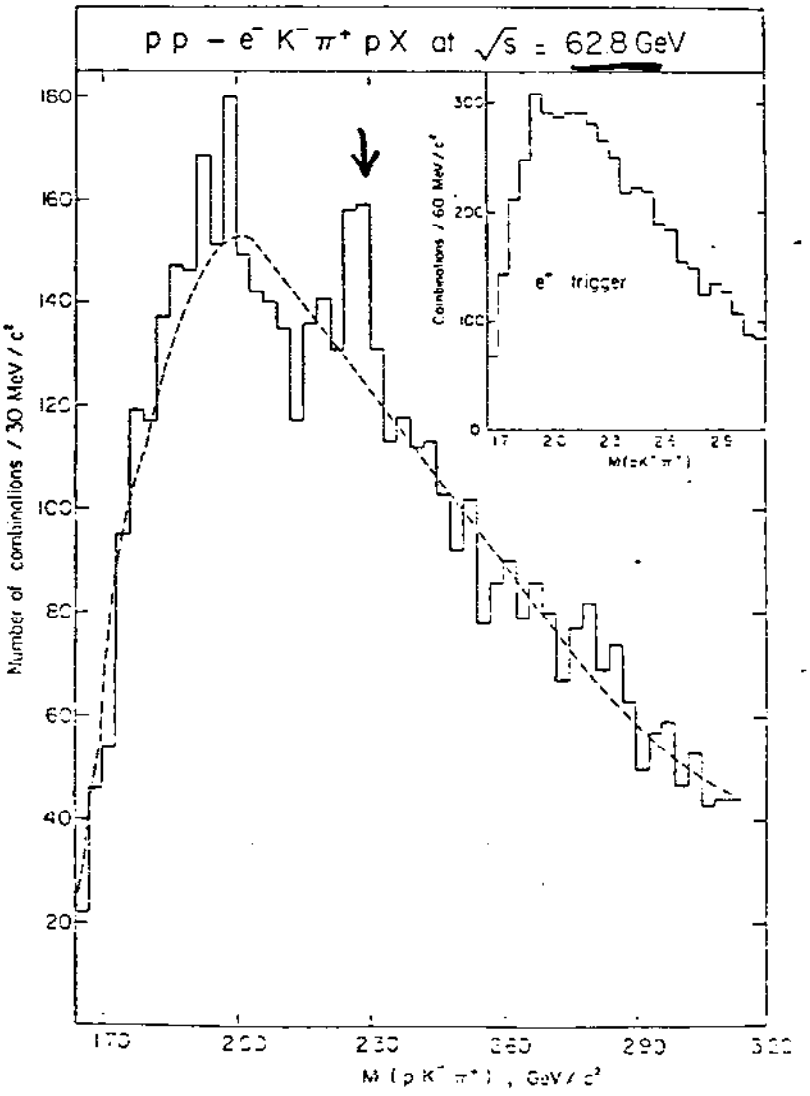

Figure 82. $m(K^-p\pi^+)$ plot for e^- triggered events, with signal candidate. Insert: e^+ trigger should not lead to charm signal in $K^-p\pi^+$ channel, and does not.

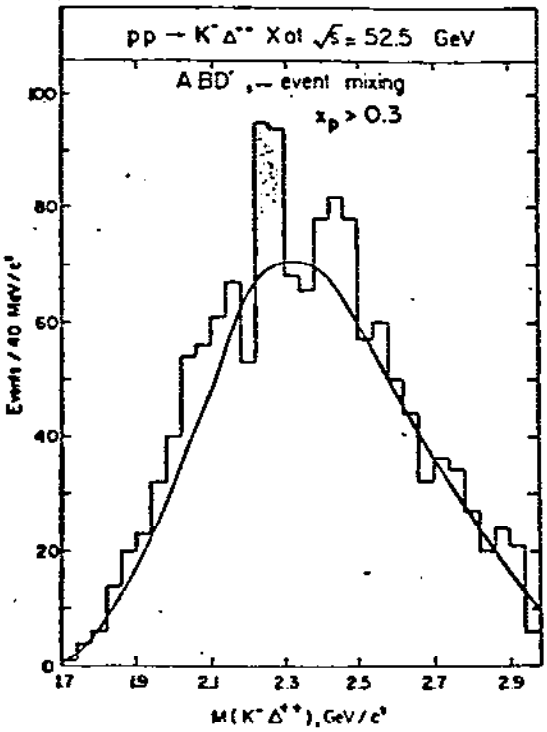

Figure 83. Resonance production enhances charm signal: $m(K^-p\pi^+)$ plot with $m(p\pi^+) \approx m(\Delta^{++})$ requirement.[74]

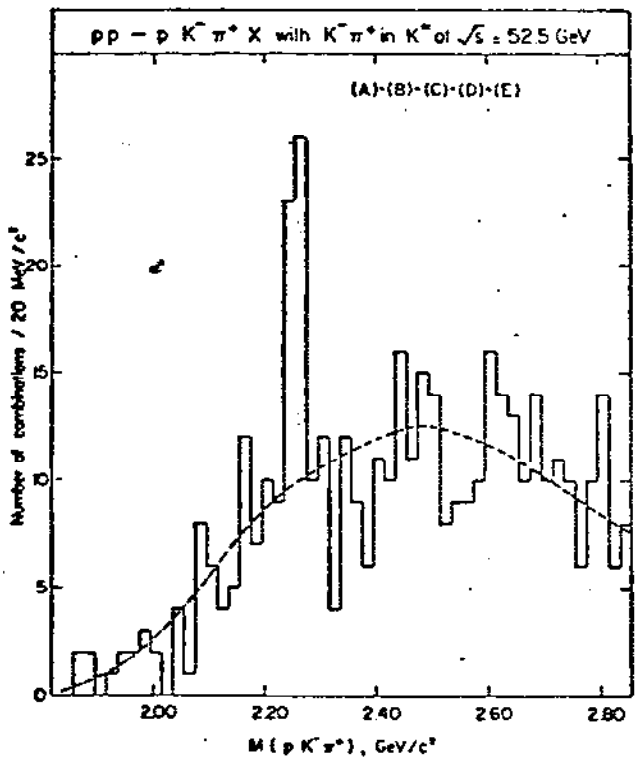

Figure 84. More resonance production in charm signal data on $m(K^-p\pi^+)$ for $m(K^-\pi^+) \approx m(K^{*0})$.[74]

Fig. 82 shows their suggestive mass plot for $M(pK^{*o})$; an enhancement also appears when $m(p\pi^+) = m(\Delta^{++})$ is demanded (cf. Fig. 83). In a subsequent experiment (R416),[74] the somewhat expanded Collaboration (now ACCDHW) used an electron/positron trigger (but without shower counter) for background suppression (by a factor $\sim 10^3$) in a more heavily instrumented SFM facility to produce, at $\sqrt{s} = 63$, the $(pK^-\pi^+)$ mass plot of Fig. 84. With an e^+ trigger, there should be no enhancement corresponding to the Λ_c state: the insert of Fig. 84 shows this to be true. This experiment is sensitive to low-x events, $0 \leq |x| < 0.3$, and quotes production cross-sections varying from 290 to 1460 (± 60%) μb depending on assumed production laws.

d) The Bologna-CERN-Frascati Collaboration also used the SFM facility, but added shower counters for better e^+ definition and energy measurement. In a series of recent papers,[75-78] the group investigates many features of the interaction based on data that span the range $0.3 < |x| < 1$ and demand an opposite leading system for the trigger. Demanding $p_\perp (e^+) > 0.5$ GeV/c, calling a positive track with $\alpha > 0.3$ a proton, a negative that, by time-of-flight, is not π^- or $\bar{p}$, a K^-, the spectra of Fig. 85 are produced: a peak is indicated in the $K^-p\pi^+$ data with e^- trigger, none for the e^+ trigger case (but: mass enhancement is at 2330 GeV/c^2!).

Fig. 85c specifically shows the effect of the cut on the rapidity observed in the opposite hemisphere: Σx_i(opp.) > 0.5 produces a better signal-to-background ratio, indicating high-mass diffraction.

BCF also found that the resonant subsystems Δ^{++} and K* tend to depress the combinatorial background.[76] Specifically, they quote

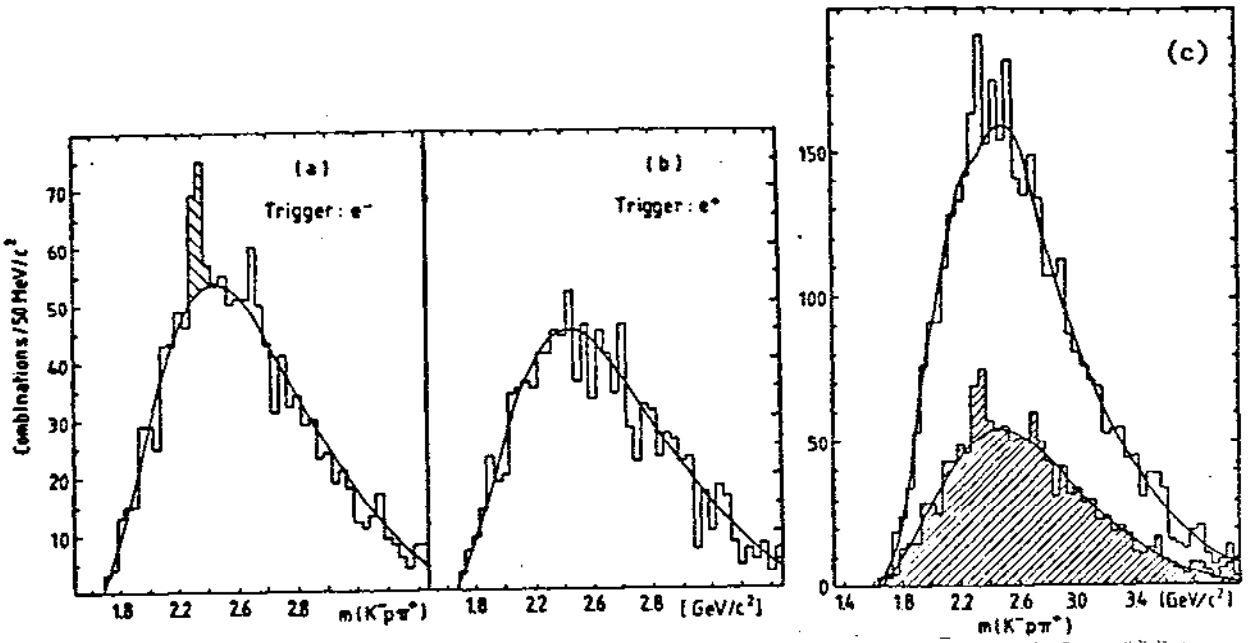

Figure 85. BCF data from SFM facility, with improved time-of-flight system and added shower counter array: a) $m(K^-p\pi^+)$ plot for right-sign electron trigger; b) same, wrong-sign electron; c) effect of cut on opposite leading system: shaded area has cut on $\sum_{opp} x_i > 0.5$ (or > 0.1 for escape in beam pipe).

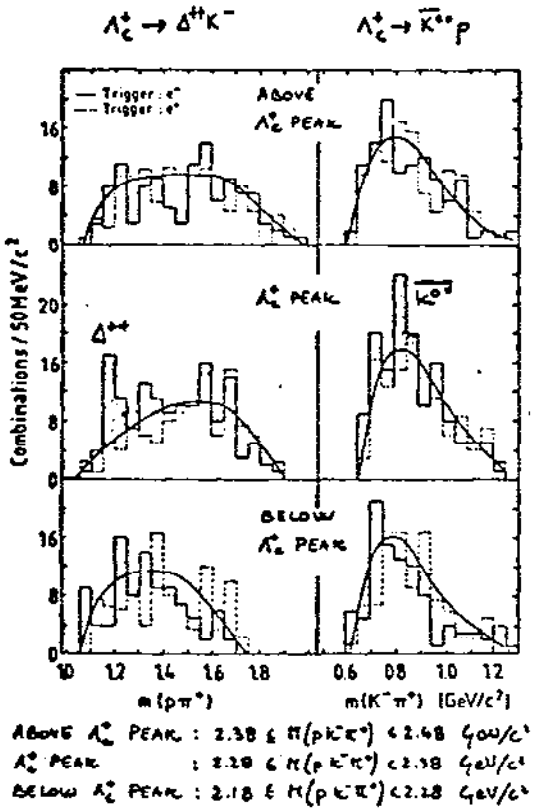

Figure 86. Presence of resonance production in BCF data: Δ^{++} and K^{*0} production are prominent only in Λ_c mass band.

$$\frac{\Lambda_c^+ \to \overline{K^{*0}}p}{\Lambda_c^+ \to pK^-\pi^+} = 0.28 \pm 0.16 ,$$

$$\frac{\Lambda_c^+ \to \Delta^{++}K^-}{\Lambda_c^+ \to pK^-\pi^+} = 0.40 \pm 0.17 .$$

Fig. 86 demonstrates the effect as a function of $m(K^-p\pi^+)$; there is little if any resonance production outside the Λ_c band. In an interesting study,[77] the x dependence of Λ_c^+ production is studied and compared with Λ^0 and $\overline{\Lambda^0}$ production. For the range covered (Fig. 87), Λ_c^+ production is much flatter in longitudinal momentum than $\overline{\Lambda^0}$ production, strongly mitigating against a "central" production mechanism. Λ^0 and Λ_c production may follow similar patterns; this is the strongest support for an intrinsic heavy flavor component in the nucleon.

BCF also presented data on D production[78] in both the $K\pi\pi$ and $K\pi$ systems, by demanding a K^- signal from time-of-flight information, in coincidence with the electron trigger. The results are shown in Fig. 88; the $K^-\pi^+\pi^+$ system shows an enhancement with the e^- trigger, none with e^+. The $K^-\pi^+$ mass plot shows analogous behavior (Fig. 88c). The D^+D^- cross-section at $\sqrt{s}$ = 62 GeV is quoted as ~ 300 μb, assuming central production. This assumption is plausibly supported by the x distributions for D^0 and D^+, given in Fig. 89; they are strongly peaked at small x values. For completeness, we also give, from the same study, the $p_\perp$ distributions for D^0 and D^+, adequately fitted by (cf. Fig. 90)

$$\frac{1}{p_\perp}\frac{dn}{dp_\perp} \propto e^{-2.5p_\perp} .$$

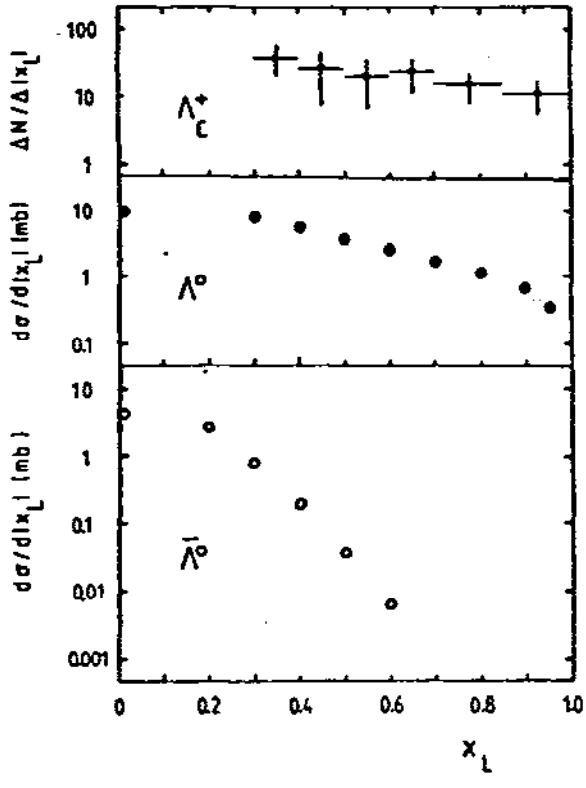

Figure 87.

a) Longitudinal momentum distributions for Λ_c^+ from BCF data[77] compared with those for Λ^0 and $\bar{\Lambda}^0$: Λ^0 and Λ_c^+ are compatible and flat, $\bar{\Lambda}^0$ is concentrated at lower x values.

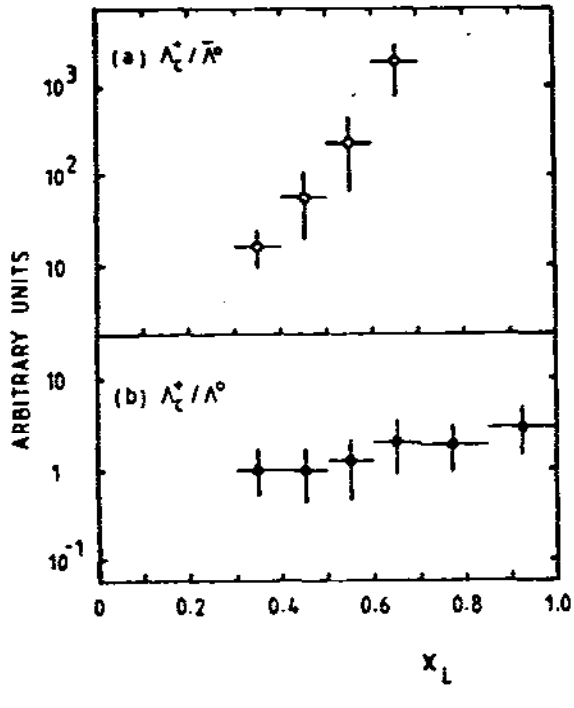

b) Ratio of Λ_c^+ to Λ^0, $\bar{\Lambda}^0$ as a function of longitudinal momentum.

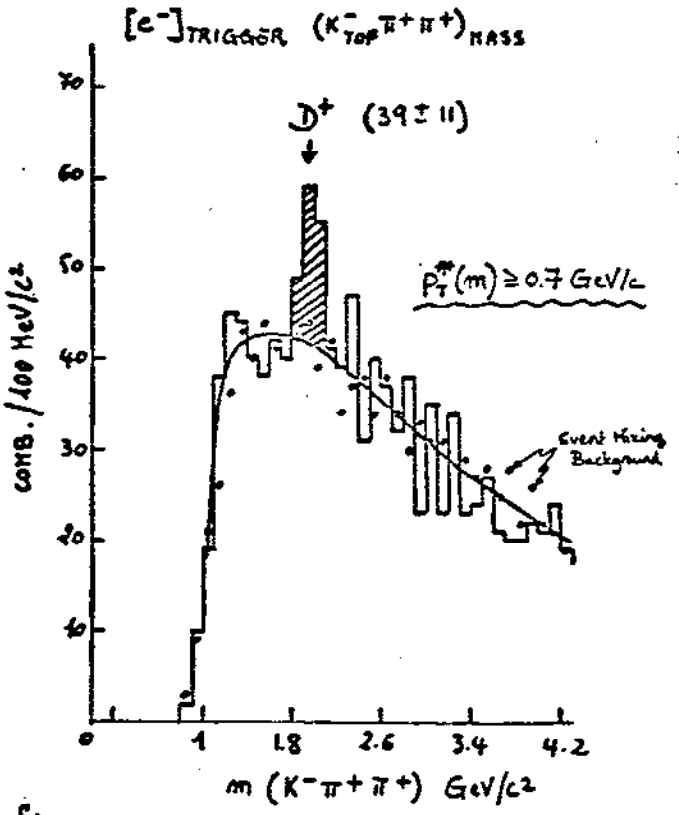

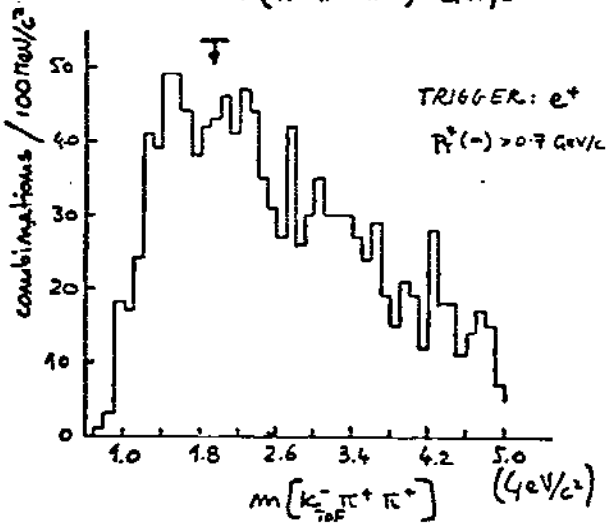

Figure 88.
$D^{+,o}$ production in BCF data:

a) signal is seen in e^- trigger data for $K^-\pi^+\pi^+$ channel

b) none for e^+ trigger.

c) $m(K^-\pi^+)$ plot also leads to a solid D^0 candidate.[78]

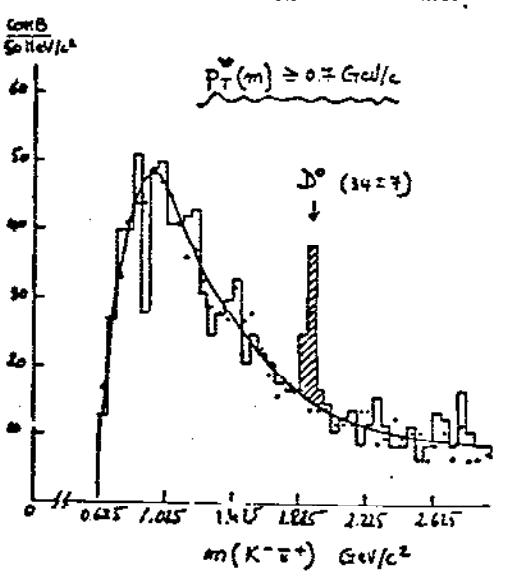

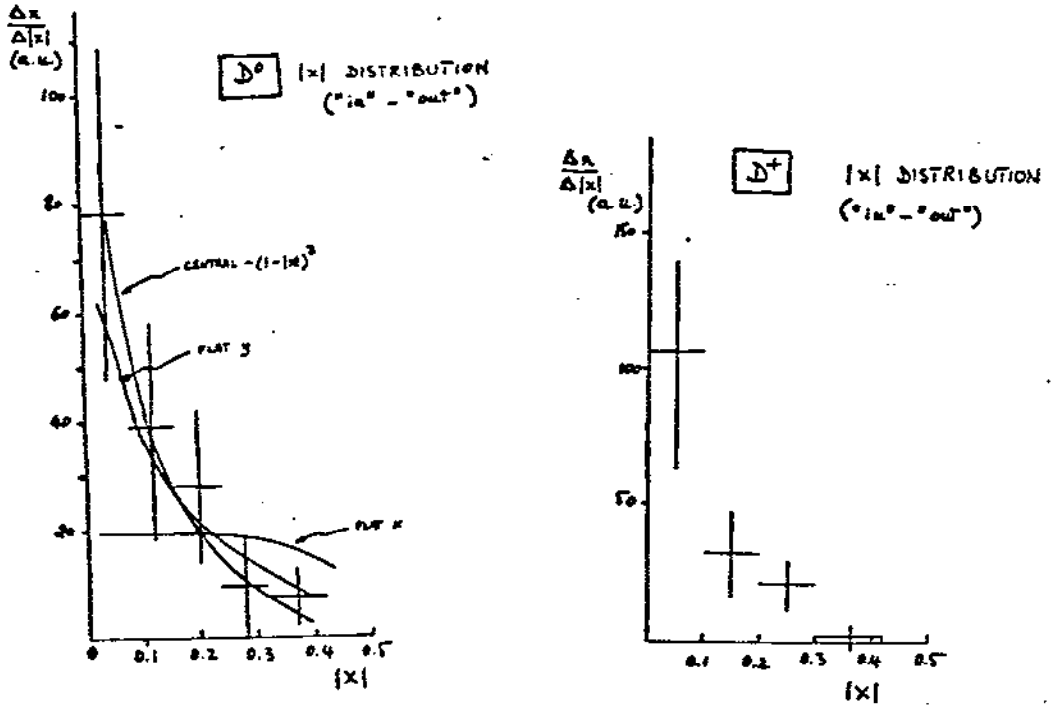

Figure 89. Longitudinal momentum distribution for D production clearly indicates central production, fit curve is $\sim (1-x)^{3.78}$

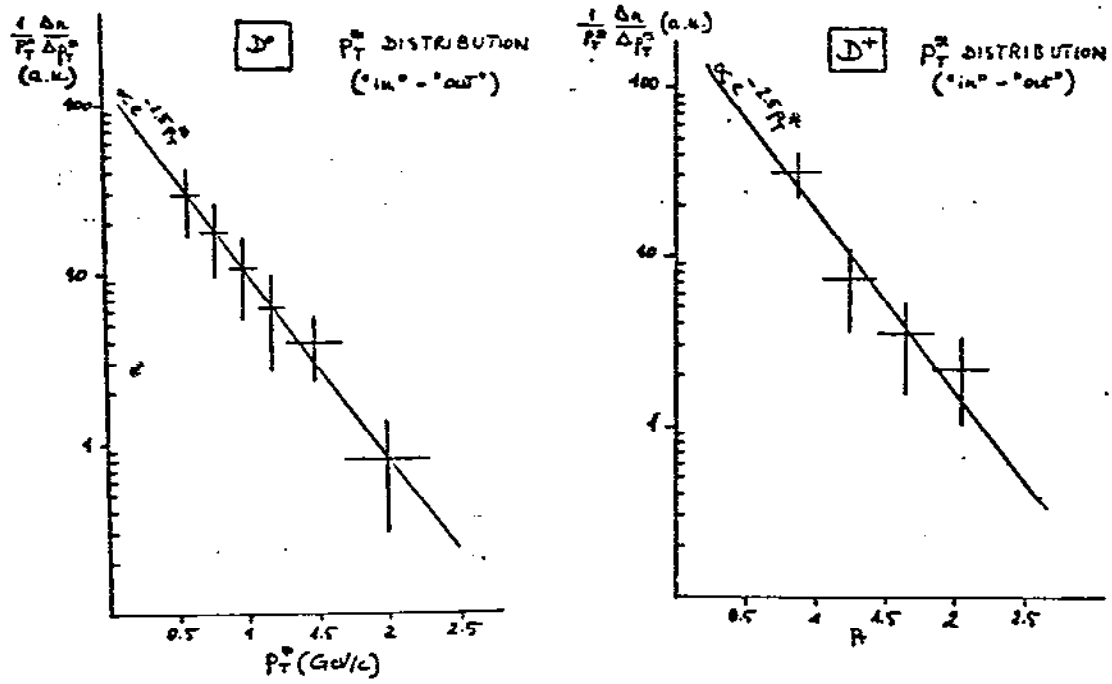

Figure 90. Transverse momentum distribution for D production by BCF Collaboration. $e^{-2.5p_T^2}$ fit satisfies both D^0 and D^+ cases.

4.3.5 Wrap-up of ISR Open-Charm Production

What do we make of all this information? Clearly, the accumulation of indicative evidence from four experiments is highly suggestive. But a pervasive feeling of uneasiness is based on the lack of clearly compelling evidence from any one experiment. Further, there is the lack of agreement on what production mechanism is to be favored; this leads to the widely disparate cross-section results seen in Tables 4.1 and 4.2, for Λ_c and $D^{0,+}$, respectively.[79]

Features particularly worth noting are these:

1. Λ_c production, not observed at lower energies, appears prominent at ISR energies.
2. $pp \to \bar{\Lambda}_c \Lambda_c + \ldots$ may have a cross-section similar to $pp \to \bar{D}\Lambda_c$.
3. Λ_c's are produced almost <u>flat in x</u>. Central production is excluded as the principal mechanism.
4. For $\overset{(-)}{D}$, on the other hand, $pp \to \bar{D}D + \ldots$ clearly proceeds according to a central production process.
5. With accepted branching ratios, the results from the four experiments are roughly compatible (Figs. 91, 92).[63]
6. These cross-sections, at face value, appear remarkably high. D and Λ_c production rates are comparable.
7. With 200-400 μb each for D^0, D^+ and Λ_c production, σ(charm) $\simeq$ 1 mb. This would imply, for given ISR conditions, $\frac{e}{\pi}$-ratios of $\sim 10^{-3}$, some 4-5 times those previously measured. This is a model-dependent figure, and could be even larger.
8. Neither the statistical significance nor the mass and width definitions are overwhelming for any single one of these

Table 4-1

ISR Cross Sections for $pp \to D\bar{D}X$ ($D^+ \to K^-\pi^+\pi^+$ or $D^0 \to K^-\pi^+$)
(Compilation by F. Muller.)[63]

	Trigger	Part.	Assumed D and $\bar{D}$ production law			x-range
			Central	$d\sigma/dy = c^t$	$d\sigma/dx = e^t$	
SFM (CCHK)	Forward K^-	D^+	1100 (±60%)	390	210	$.2 < \|x\| < .8$
LSM	Diffractive	D^+	(< 300)			$.2 < x < .45$
		D^0	(< 160)			$.2 < x < .65$
SFM (ACCDHW)	90° e^-	D^0	245 (±60%)	395	890	$0 < \|x\| < 0.3$
LSM	30° e^-	D^+	< 530 (±30%)	< 340	< 280	$.14 < x < .9$
SFM (BCF)	90° e^-	D^+, D^0	∿ 500	∿ 1000		$0 < \|x\| < .4$

Table 4-2

ISR Cross Sections for $pp \to \Lambda_c \bar{D}X(\Lambda_c \to K^-p\pi^+)$
(Compilation by F. Muller.)[63c]

	Trigger	Assumed Λ_c production law			x-range
		$d\sigma/dx$ = const.		$d\sigma/dy = c^t$	
SFM (CCHK)	Forward K^-	300 (±40%)		610	$.4 < \|x\| < .8$
LSM	Diffractive	(240 ± 120)			$.5 < x < .8$
UCLA-SAC	Inclusive	(700 ± 90)			$.75 < x < .9$
SFM (ACCDHW)	90° e^-	290 (±60%)	1460	430	$0 < \|x\| < .3$
LSM	30° e^-	840 (±50%)	1220	1650	$.14 < x < .94$
SFM (BCF)	90° e^-	184 (±40%)	1125	750	$.3 < \|x\| < 1$
		Central	Flat x	Flat y	
		Assumed $\bar{D}$ production law			

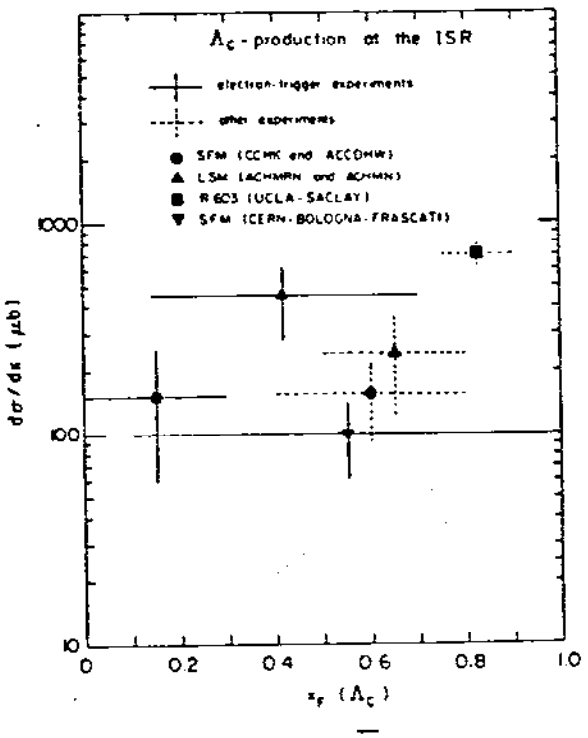

Figure 91. Longitudinal momentum dependence for Λ_c candidate signals from four collaborations at the ISR.[63]

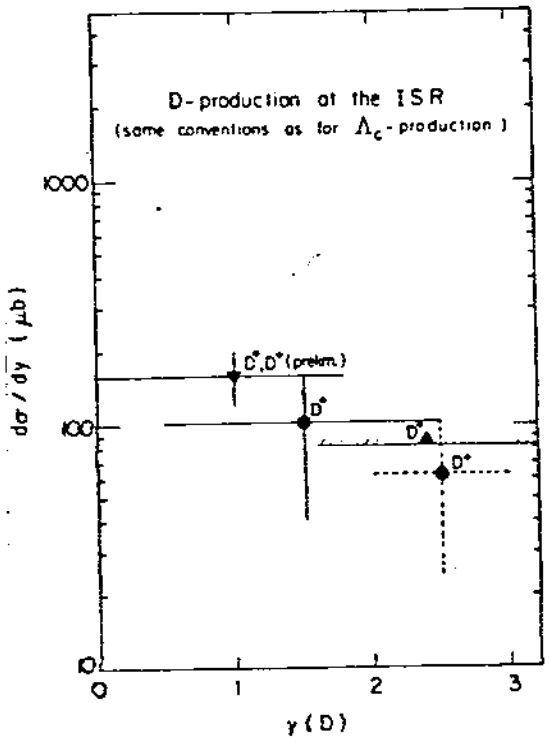

Figure 92. Rapidity distribution for D signals observed at ISR.

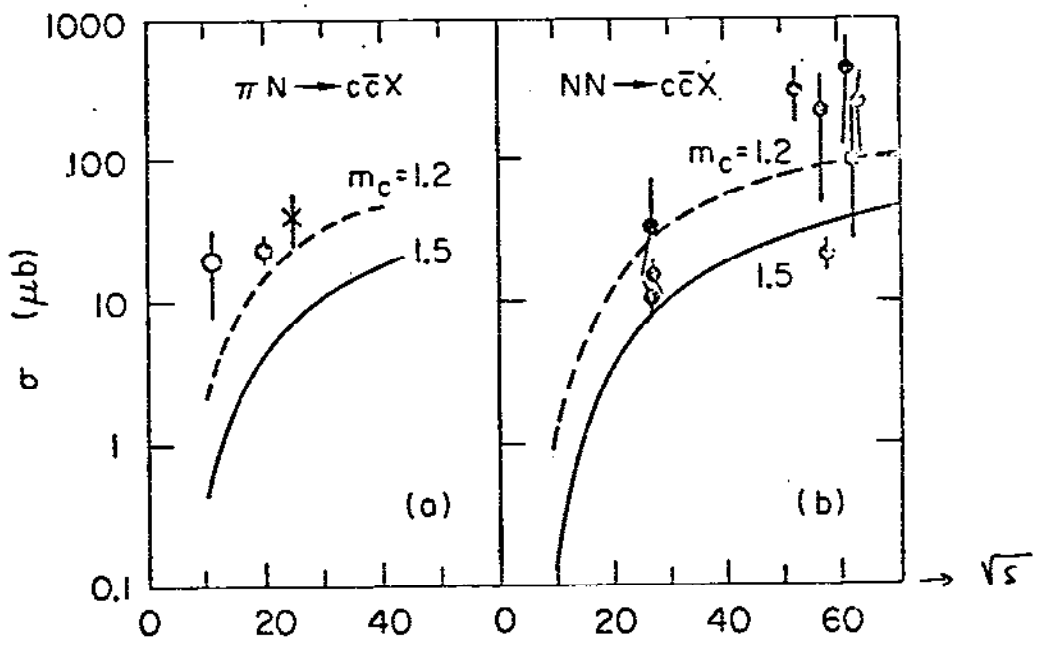

Figure 93. Conventional $q\bar{q}$ and gg amalgamation graphs give approximately adequate trend for $\pi N \rightarrow c\bar{c}x$ (a), but not for $NN \rightarrow c\bar{c}X$ (b). An additional component is needed.[80]

experiments. It cannot be excluded, at this point, that there is at least partial confusion with some hyperon state; several Y* indications could be substitute candidates.

For the time being, however, let us take these cross-sections at face value. We can then say with certainty that the GGF graph can no longer do as our phenomenological guiderail unless we do a quick -- and somewhat disreputable -- fix-up by changing the charmed quark mass.[80] This remedy is simply based on the steep m_Q dependence of the GGF pair production graph: $m_c = 1.2$ GeV/c^2 will do the job, but will destroy the good fits obtained by the γGF model in photo- and lepto-production. It will also ignore some highly successful notions of $Q\bar{Q}$ spectroscopy.

If we reject this fix-up, acceptance of the data fairly constrains us to resort to the intrinsic charm notion (section 421) for relief. This is tantamount to adding to the amalgamation graphs $q\bar{q} \to Q\bar{Q}$, $gg \to Q\bar{Q}$, which cannot alone account for the data observed (Fig. 93), the flavor excitation processes predicted on the presence of the heavy-quark Fock states in the nucleon wave function (cf. Fig. 55b),

$$qQ \to qQ$$

$$q\bar{Q} \to q\bar{Q}$$

as illustrated in Figs. 51e-h to order α_s^2. In this fashion, it is possible to perturbatively calculate[81] the entire production process: $Q,\bar{Q}$ are so heavy that even diffractive processes are expected to be tractable in this fashion. Without going into great detail, we can make an order-of-magnitude argument that a 1% $c\bar{c}$ Fock component will lead to

$$\sigma_{c\bar{c}}^{diff} \simeq 0.01\ \sigma_{el} \simeq 0.5 \text{ mb.}$$

This looks quite compatible with the ISR data. The x_{Λ_c} distribution is

also reasonably interpreted in these terms, as expected from Fig. 56 and shown with the data in Fig. 94.[82]

A problem remains, the lack of observation of diffractive ψ (or η_c) production at SPS and ISR energies. At 200 GeV, πN experiments[83] give only 100 nb cross-sections for ψ production, but 20 μb for open charm, with an x distribution compatible with central production. A suppression factor of 5×10^{-5} is needed to explain the data: Peterson[81] manages to find this factor by invoking

$$\begin{aligned} \text{color suppression for a factor } & \frac{1}{9} , \\ \text{flavor suppression for a factor } & \frac{1}{4} , \\ \text{mass suppression for a factor } & \frac{1}{100} , \\ \text{channel suppression for a factor } & \frac{1}{3} . \end{aligned}$$

The first two of these are self-explanatory; the third is due to the requirement that the color-singlet $c\bar{c}$ system be below $D\bar{D}$ threshold to emerge bound; Fig. 95 illustrates that this is true for a small fraction of $c\bar{c}$ pairs only. The last factor takes the presence of χ and η_c, etc., into account. These, however, are much harder to observe experimentally. No data exist on these channels.

4.3.6 Open-Beauty Searches

Bump hunting in pursuit of quark decay heavier than c becomes even more trying due to the increased multiplicity of daughter hadrons. Special signatures are therefore at a premium. One of these was suggested by Fritzsch,[84] who estimated possible signals for open-botton mesons B decaying, according to Fig. 96, into the final state $B \to \psi\bar{K}\pi$ with a branching fraction of several percent. A CERN SPS experiment[85] promptly produced data that appeared to have a mass enhancement (Fig. 97) in a mass range (5.3 GeV/c^2) appropriate for B mesons, corresponding to $\sigma(\pi N \to B\bar{B}) \approx 200$ nb. Better

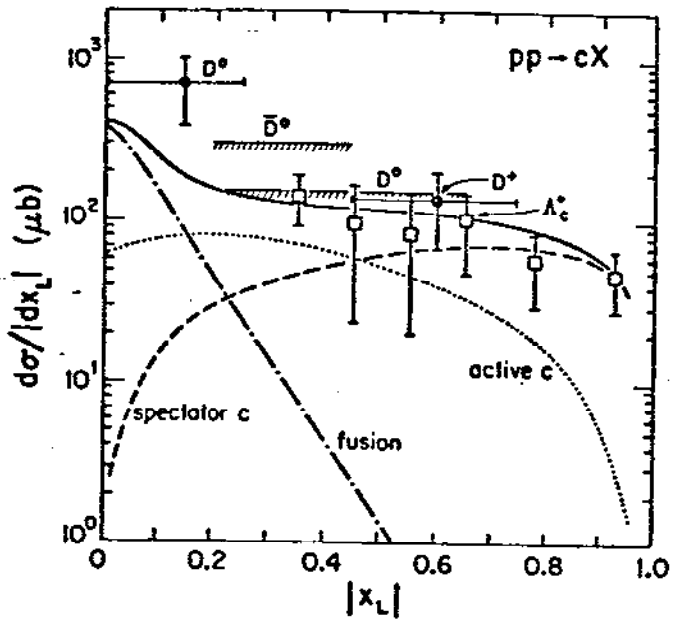

Figure 94. A combination of central processes and intrinsic-charm component is seen to adequately reproduce the x dependence of charm production at the ISR.[82]

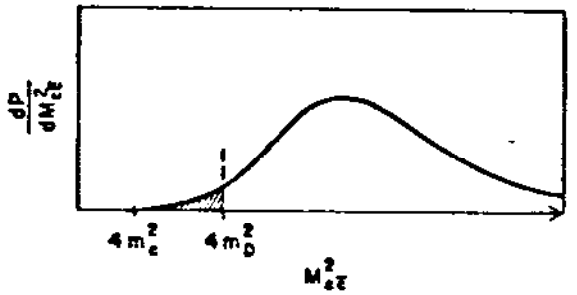

Figure 95. The probability that a $c\bar{c}$ pair is produced below open-charm threshold is so small that it seriously suppresses ψ production in diffractive pp interactions.

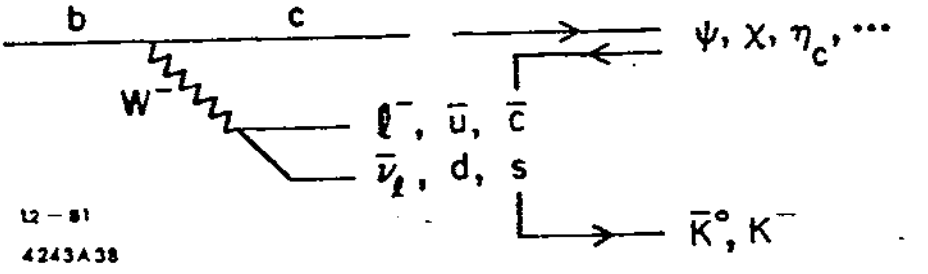

Figure 96. Signature suggested by Fritzsch[84] for B-meson decay searches. The $\psi(\rightarrow 2\mu)$ and $\bar{K}^0$ signals are relatively easy to identify.

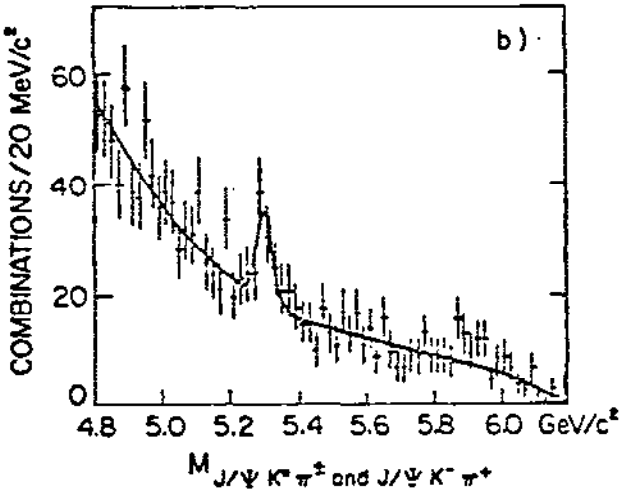

Figure 97. Potential signal in $m(\psi K^0\pi^{\pm}) + m(\chi K^{-}\pi^{+})$ combinations as observed at CERN.[85] Later accumulation of more statistics did not corroborate the interpretation of this bump as an open-beauty meson.

statistics have since obliterated that indication, and the B meson remains to be discovered.

Open-b baryons will, if the intrinsic charm notions are correct, be accessible to high-energy pp experimentation at the ISR. Brodsky et al. predict a $b\bar{b}$ Fock component at a level some 20 times below the $c\bar{c}$ analog. The BCF group at the CERN ISR consequently attempted[86] to use the same scheme that appeared so successful for Λ_c detection. Fig. 98 gives the decay chain which is expected to yield an enriched sample: if one b decay provides a high-$p_\perp$ (> 0.8 GeV/c) trigger electron, the other may decay hadronically into $pD^0\pi^-$, with leading particle characteristics (x(p) > 0.3). Good e^+ identification is given by threshold Cherenkov and shower counters. D decays into $K\pi$ may be recognizable by time-of-flight particle identification up to 2 GeV/c. Fig. 99a gives the mass plot for all $pK^-\pi^+\pi^-$ systems, which, upon a cut on $m(K^-\pi^+) \simeq m(D)$, becomes somewhat suggestive of a meaningful effect (Fig. 99b). After checking that, in the Λ_B candidate band, the D signal is prominent (c), the $K\pi$ cut is tightened to $m_D \pm 75$ MeV/c^2, resulting in the signal shown in (d).

The interpretation is that of observation of a state Λ_B with

$$m(\Lambda^0_B) = (5.425 \begin{smallmatrix} + .175 \\ - .075 \end{smallmatrix}) \text{ GeV/c}^2,$$

with a "partial cross section" quoted as $\Delta\sigma = (3.8 \pm 1.2)10^{-35}$ cm^2. In a later paper,[87] the group makes model-dependent estimates of the cross-section and the (unknown) branching fraction B.R.$(\Lambda^0_B \to pD^0\pi^-)$. Resulting cross-sections are quoted as

$$\sigma \times \text{B.R.}(\Lambda^0_B \to pD^0\pi^-) \simeq 3 - 30 \ \mu\text{b};$$

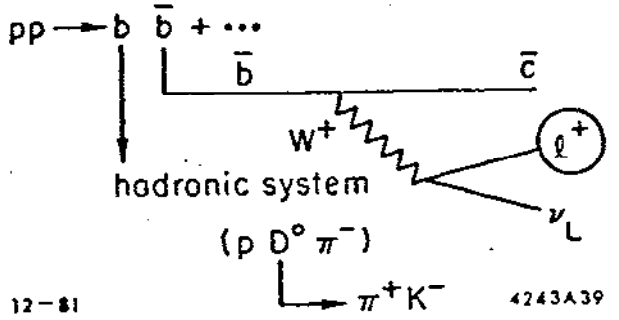

Figure 98. Signature graph for open-beauty baryon (Λ_B) search analogous to Λ_c search in SFM facility by the BCF Collaboration.

Figure 99. Results of BCF search for open-beauty baryons:[86]

a) mass plot for $pK^-\pi^+\pi^-$ system.

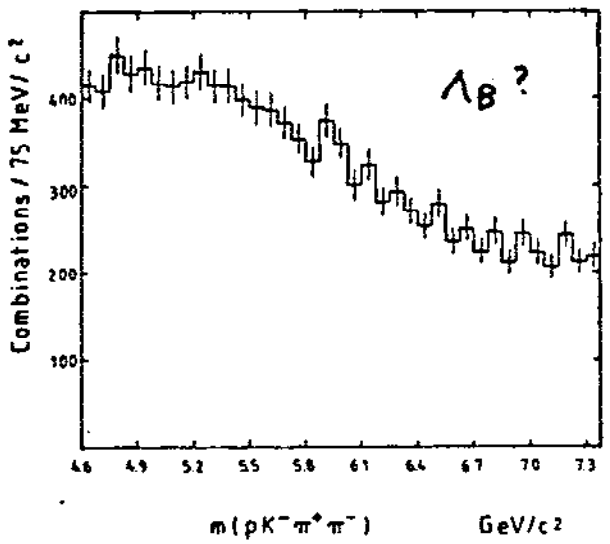

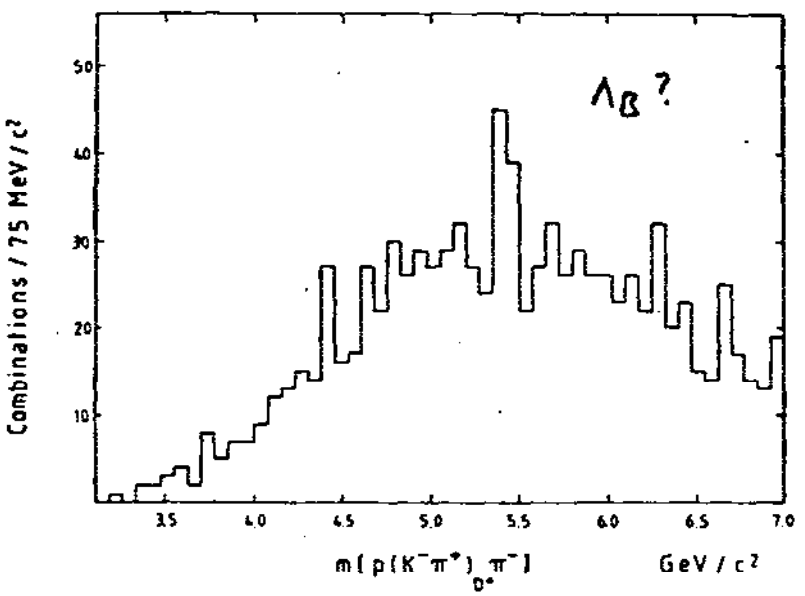

b) same, but with the requirement that the $K^-\pi^+$ system be in the D^0 mass band.

Figure 99.

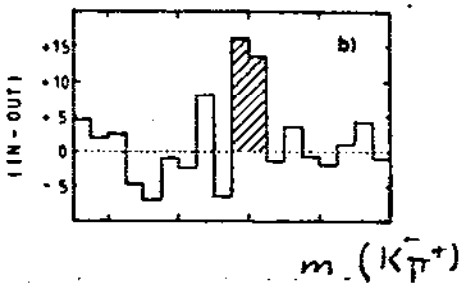

c) Difference of $K^-\pi^+$ mass distributions inside and outside candidate mass band for Λ_b.

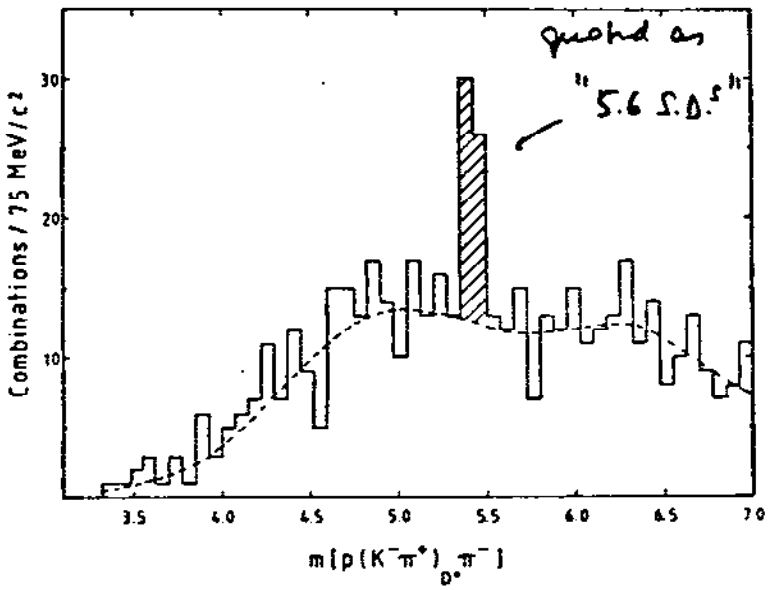

d) Final candidate sample for Λ_b, after $K^-\pi^+$ mass cut has been tightened (cf. text).

within reasonable ranges of the value for the branching fraction, this is compatible with "intrinsic-beauty" expectations.

What are the caveats for this spectacular result? (1) the statistical meaningfulness of what is quoted as a 5.6 S.D. effect (Fig. 99d) is dependent on the total number of bins considered; (2) the cross-section appears large, and may lead to serious trouble with accepted $\frac{e}{\pi}$ ratios; (3) a closer look at the total number of candidate events and the quoted signal of some 30 events appears to have little if any room for backgrounds, efficiencies, and smaller values for the unknown branching fractions.

Clearly, this result should be followed up with further confirming searches;[88] should the signal display similar longitudinal momentum characteristics as Λ_c production in the same reaction, this will further add to the credibility of the intrinsic heavy flavor notion.

4.4 What Have We Learned From Hadron Production of Heavy Flavors?

This field has evolved very slowly; notwithstanding the very high luminosities available, it took a number of years before the original discoveries of hidden-$Q\bar{Q}$ at Brookhaven and Fermilab and early open-$Q(\bar{Q})$ indications due to inclusive-prompt-lepton signals were followed up with the first hints at explicit open-charm events. To date, not a single contribution to open-charm spectroscopy has been made by data owed to a hadron-initiated reaction.

So, the first thing we learned is that life is hard for the experimentalist attempting to study open heavy flavors with hadron beams. High final-state multiplicities and small branching fractions make bump-hunting in invariant-mass plots a tedious as well as risky proposition. This picture may be about to change significantly:

1. The perfection of highly resolving vertex detectors gives a powerful new handle to the experimentalist investigating long-lived ($\tau \geq 10^{-13}$ sec) states. Streamer chambers and small bubble chambers are rapidly developing the techniques necessary to exploit this feature. Together with downstream spectrometers, they will no doubt yield important results.

2. For flavors beyond charm, small cross-sections and steep energy dependences of some production processes put high luminosities and high energies at a premium. pp collisions yield the highest available values for both of these parameters: this is illustrated by the reported first open-beauty signal from the ISR.[86,87]

3. The advent of $\bar{p}p$ colliders puts hadronic initial states in competition with e^+e^- machines for annihilation processes. The higher available energies are somewhat detracted from by low luminosities and the large amount of non-annihilation interactions from which data have to be disentangled.

In the meantime, we have gleaned the following information from hadron-hadron $\rightarrow Q\bar{Q}$ reactions:

Expected QCD graphs are adequate to describe most of the generic data. The gluon-gluon fusion graph gives characteristic features well reproduced by data up to FNAL/SPS energies.

At ISR energies, forward production of heavy baryons appears prominent. Its acceptance in the face of some experimental and interpretative uncertainties makes the presence of an additional component unavoidable. Explanations in terms of more conventional diffraction excitation have numerical difficulties[89] and lead necessarily to forward $\bar{D}$ ... etc. production, which is not seen.

The possible emergence of a long-lived heavy component of the nucleon wave function -- and, by implication, of other hadronic wave-functions, including that of the hadronic photon -- has important implications, both for our basic understanding of hadronic matter and for future experimentation in search of heavier quarks. The characteristic mass-dependence $\frac{1}{m_Q^2}$ puts diffractive $Q,\bar{Q}$ excitation in the realm of observability for b, t ... quarks at ISABELLE energies.

Independent confirmation of the relative importance of expected QCD graphs and those involving heavier $Q\bar{Q}$ components is urgently needed: an evaluation of μN scattering data at x values sensitive to the latter (i.e., at $0.3 \leq x \leq 0.8$)[90] presently involves too many assumptions to yield compelling results.[91,92] It remains to be seen whether telling signatures for the presence of long-lived $Q\bar{Q}$ components can be defined in other accessible processes.

5. Conclusion

As we progressed in these lectures from simple, local probes of hadronic matter to more complicated, structured incident systems, we have seen important features emerge that add significant information to the vital body of knowledge on $Q\bar{Q}$ systems as well as open-$(\bar{Q})$ states accumulated by e^+e^- and, to a lesser degree, by νN experimentation. Healthy controversies over the emergence of open-b hadrons and of a new component to stable-hadron wave functions attest to the rapidly evolving body of knowledge and understanding. Many experimental projects are presently in a stage of active progress toward presentation of new data, but could not yet be included in these lectures. A new realm is just opening up at the CERN SPS $\bar{p}p$ collider. The real conclusion to these lectures will therefore best be left to the review speakers of future sessions of this Institute.

6. Acknowledgments

I owe gratitude to many colleagues who shared their knowledge of data and of theoretical notions with me. This applies particularly to S. Brodsky and C. Peterson. The latter and P. Zerwas were kind enough to give the manuscript a critical reading and make helpful comments. I particularly thank Georgia Hamel for the patience she showed during the painstaking job of assembling this manuscript.

1. There are many excellent recent reviews, e.g.,
P. Duinker, Proc. 1981 Int. Conf. on High Energy Physics, Lisbon (1981);
H. Meyer, U. Wuppertal preprint 81-0574 (1981);
M. Derrick, ANL preprint ANL-HEP-CP-81-33 (1981).

2. E. Fisk, Proc. 1981 Int. Symp. on Lepton and Photon Interactions at High Energies, Bonn (1981).

3. E. Bloom, these Proceedings;
N. Isgur, Proc. Particles & Fields 1981, ed. C.A. Heusch, W.T. Kirk, AIP Conf. Proc., NY (1981);
K. Berkelman, High Energy Physics-1980, p. 1500, AIP Conference Proc. No. 68, N.Y. (1981).

4. S.W. Herb et al., PRL 39, 252 (1977).

5. R.P. Feynman, Photon-Hadron Interactions, Benjamin, Reading, Mass. (1972).

6. R.D. Field, R.P. Feynman, PR D15, 2590 (1977);
NP B136, 1 (1978).

7. L. Jones, H. Wyld, PR D17, 759, 1782, 2332 (1978);
M. Glück, E. Reya, PL 79B, 453 (1978); 83B, 98 (1979);
H. Fritzsch, K. Streng, PL 72B, 404 (1978);
M. Shifman, A. Vainshtein, V. Zacharov, NP B136, 157 (1978);
J.P. Leveille, T. Weiler, NP B147, 147 (1979).

8. G. Altarelli, G. Parisi, NP B126, 298 (1977);
G. Altarelli, Nota Interna 714, INFN Rome (1978).

9. H. Bledsoe et al., UCSC 79/076 (unpublished).

10. D.C. Allkofer et al., NA-9 proposal, CERN (1978).

11. A.R. Clark et al., PRL 43, 187 (1979).

12. D. Allkofer et al., N.I.M. 179, 445 (1981).

13. D. Bollini et al., Proc. 1979 Int. Symp. on Lepton and Photon Interactions at High Energies, FNAL, (1979).

14. J.P. Leveille, T. Weiler, Ref. 7.

15. M. Strovink, LBL-1347 (1981) Proc. of 1981 Int. Symp. on Lepton and Photon Interactions at High Energies, Bonn, Germany.

16. J.P. Leveille, T. Weiler, Northeastern Univ. preprint, NUB2479 (1980).

17. W.H. Smith, Ph.D. Thesis, LBL-12789 (1981).

18. M. Strovink, Proc. 1980 SLAC Summer Inst. on Particle Physics, ed. A. Mosher (1981).

19. C.H. Best, Proc. XVIth Rencontre de Moriond, ed. J. Tran Thanh Van (1981).

20. See Refs. 17 and 18.

21. V. Ganapathi, J. Smith, PR D23, 75 (1981);
V. Barger, T. Gottschalk, R.J.N. Phillips, PR D19, 92 (1979).

22. B. Margolis, PR D17, 1310 (1978);
D. Horn, PL 73B, 199 (1978).

23. J.J. Aubert et al., PL 105B, 315 (1981).

24. G.D. Gollin et al., PR D24, 559 (1981).

25. B. Knapp et al., PRL 34, 1040 (1975); 34, 1044 (1975).

26. W.Y. Lee, Proc. 1975 Int. Symp. on Lepton and Photon Interactions at High Energies, ed. W.T. Kirk (1975).

27. S.J. Brodsky, SLAC-PUB-2747 (1981).

28. J.J. Sakurai, D. Schildkuecht, PL 40B, 121 (1972).

29. D.O. Caldwell et al., PRL 40, 1222 (1978).

30. A.M. Breakstone et al., PRL 47, 1778 (1981).

31. U. Camerini et al., PRL 35, 483 (1975);
R.L. Anderson et al., PRL 38, 263 (1977).

32. D. Aston et al., PL 94B, 113 (1980).

33. M.S. Atiya et al., PRL 43, 414 (1979).

34. P. Avery et al., PRL 44, 1309 (1980).

35. D. Aston et al., PL 100B, 91 (1981).

36. D. Aston et al., NP B189, 205 (1981).

37. B. Knapp et al., PRL 37, 882 (1976).

38. J.J. Russell et al., PRL 46, 799 (1981).

39. C. Dionisi, these Proceedings.

40. J. Brau, these Proceedings.

41. A. Fiorino et al., N.C. Letters 30, 166 (1981).

42. K. Abe et al., SHF Collaboration, paper submitted to EPS Conference, Lisbon (1981).

43. As these lectures go to print, increased statistics put the ratio $\tau(D^{\pm})/\tau(D^{0})$ at 1.2 (K. Moffeit, private communication of preliminary results).

45. A. Soni, NP B168, 147 (1980).

46. S.D. Drell, T.M. Yan, PRL 25, 316 (1970);
Ann. Phys. (N.Y.), 66, 578 (1971).

47. H. Fritzsch, K.H. Streng, PL 78B, 447 (1978).

48. S.J. Brodsky, C. Peterson, N. Sakai, PR D23, 2745 (1981) and
Ref. 44.

49. J.F. Donoghue, E. Golovich, PR D15, 3421 (1977).

50. H. Fritzsch, Proc. IXth Int. Winter Meeting on Fundamental
Physics, Siguenza (1981).

51. B.A. Campbell, U. Toronto preprint (1981).

52. V. Barger, R.J.N. Phillips, PR D12, 2623 (1975).

53. K.P. Das, R.C. Hwa, PL 68B, 459 (1977).

54. B. Anderson, G. Gustafson, C. Peterson, PL 71B, 337 (1977).

55. V. Barger, W.Y. Keung, R.J.N. Phillips, PL 91B, 253 (1980);
92B, 179 (1980).

56. C.E. Carlson, R. Suaya, PR D18, 760 (1978).

57. R. Baier, R. Rückl, PL 102B, 364 (1981).

58. R. Barate et al., High Energy Physics 1980, ed. L. Durand,
L.G. Pondrom, AIP 1980 (p. 197).

59. E.L. Berger, D. Jones, PR D23, 1521 (1981).

60. R. Barloutaud et al., NP B172, 25 (1980).

61. cf. Report to 1980 Int. Conf. on High Energy Physics, Madison,
Wis.: K. Kleinknecht, High Energy Physics 1980, p. 237;
F. Niebergall, ibidem, p. 242; P.O. Hulth, ibidem, p. 247.

62. S. Wojcicki, High Energy Physics 1980, ed. L. Durand,
L.G. Pondrom, Madison (1980) p.

63. F. Muller, Inv. Talk at IVth Warsaw Symp. on Elementary Particle
Physics, CERN/EP/0475R/RM/ed (1981).

64. J. Ritchie et al., PRL 44, 230 (1980), see also Ref. 62.

65. S.L. Glashow in: Experimental Meson Spectroscopy, AIP Conf.
Proc. 21, ed. D. Garelick, N.Y. (1974).

66. C.A. Heusch in: Lepton and Hadron Structure, ed. A. Zichichi,
Academic Press, N.Y. (1975).

67. K. Bunnell et al., PRL 37, 85 (1976).

69. V.L. Fitch et al., PRL 46, 761 (1981).

70. K.L. Giboni et al., PL 85B, 437 (1979).

71. J. Irion et al., PL 99B, 495 (1981).

72. W. Lockman et al., PL 85B, 443 (1979).

73. D. Drijard et al., PL 85B, 452 (1979).

74. G. Sajot, High Energy Physics 1980, ed. L. Durand, L.G. Pondrom, p. 192 (1980).

75. M. Basile et al., N.C. 63A, 230 (1981).

76. M. Basile et al., N.C. 62A, 14 (1981).

77. M. Basile et al., N.C. Letters 30, 487 (1981).

78. M. Basile et al., CERN EP/81-125.

79. These tables are reproduced from F. Muller, Ref. 63.

80. R.J.N. Phillips, High Energy Physics 1980, ed. L. Durand, L.G. Pondrom, p. 1470 (1981), and references therein.

81. C. Peterson, Inv. Talk at XIIIth Int. Symp. on Multiparticle Dynamics, South Bend (1981). SLAC-PUB 2775.

82. V. Barger, F. Halzen, W.Y. Keung, U. Wisconsin preprint DOE-ER/00881-215 (1981).

83. J. Badier et al., Proc. 1979 Int. Symp. on Lepton and Photon Interactions at High Energies, Fermilab (1979) p. 161.

84. H. Fritzsch, Proc. Workshop on New Flavors, Paris (1979); PL 86B, 343 (1979).

85. R. Barate et al., Saclay preprint DPhPE 79-17 (1979).

86. M. Basile et al., N.C. Letters 31, 97 (1981).

87. M. Basile et al., CERN EP/81-75 (1981).

88. D. Treille (Rapporteur's talk at the EPS Int. Conf. on High Energy Physics, Lisbon 1981; to be published in the Proceedings) discusses possibly controversial evidence between BCF and the R416 Collaboration.

89. The cross-section projection for diffraction excitation to ISR energies by G. Gustafson and C. Peterson (PL 67B, 81 (1977)) is probably too high by a factor of 2-4 due to an overestimate of the fraction of Λ production due to diffractive processes in existing data. C. Peterson, private communication.

90. See the tentative insert in Fig. 24a.

91. S.J. Brodsky and C. Peterson, SLAC Informal Note, October 1981.

92. J.J. Aubert et al., CERN-EP/81-161 (submitted to PL).